Ch 292

# ACTA POLYTECHNICA SCANDINAVICA

CHEMICAL TECHNOLOGY SERIES No: 292

## A Thermodynamic Analysis of the System Fe-Cr-Ni-C-O

Rauno Luoma

Helsinki University of Technology
Department of Materials Science and Rock Engineering
Laboratory of Metallurgy
FIN-02015 HUT, Finland

Current address:
OMG Harjavalta Nickel Oy
Teollisuuskatu 1
FIN-29200 Harjavalta, Finland

Dissertation for the degree of Doctor of Technology to be presented with due permission for public examination and debate in Auditorium V1 at Helsinki University of Technology (Espoo, Finland) on the 5th of December, 2002, at 12 o'clock noon.

Luoma, R., **A Thermodynamic Analysis of the System Fe-Cr-Ni-C-O**. Acta Polytechnica Scandinavica, Chemical Technology Series No. 292, Helsinki 2002, 91 pp. Published by the Finnish Academies of Technology. ISBN 951-666-615-9, ISSN 1239-0518.

**Keywords:** C-Cr-Fe-Ni-O-system, phase diagrams, activities, thermodynamic modelling

## ABSTRACT

A thermodynamic database for the system Fe-Cr-Ni-C-O has been built using previously assessed binary and ternary systems. Six ternary systems, Fe-Cr-O, Fe-C-O, Fe-Ni-O, Cr-Ni-O, Cr-C-O, and Ni-C-O, have been assessed. Quaternary and quinary systems were calculated using only interpolation models. This method of building a database is known as the Calphad method and it is widely used in modern thermodynamics.

An associated solution model with a non-ideally interacting species, namely 'Fe', 'Cr', 'Ni', 'C', 'FeO', '$FeO_{1.5}$', '$Cr_{2/3}O$', and 'NiO' was used for the liquid phase. The solid metallic phases were described using the sublattice model with carbon and oxygen on the second sublattice, and solid oxide phases were described using the compound energy model. The carbide phases were treated as stoichiometric or semistoichiometric phases. The optimisation was performed using the Parrot module included in the Thermo-Calc program.

The model parameters for the liquid phase in metal-oxygen systems were transformed from the parameters optimised with the ionic liquid model by other authors. Because of the new assessments of the binary systems, all the ternary systems including oxygen were optimised. Only in the Ni-C-O system could the parameters not reproduce the experimental data.

The calculated quaternary systems are in good agreement with the experimental data without using any quaternary parameters. The model parameters assessed in this work describe the system Fe-Cr-Ni-C-O well according to the experimental information from its sub systems.

The complete Gibbs energy expressions for the alloy phases were presented, allowing the calculation of the phase diagrams and thermodynamic mixing properties of the mixture phases.

## PREFACE

This work was carried out in the Laboratory of Metallurgy at Helsinki University of Technology, Outokumpu Research Oy, Outokumpu Harjavalta Metals Oy, and OMG Harjavalta Nickel Oy during the years 1993-2002.

I would like to express my deep gratitude to my supervisor, Professor Lauri Holappa, for his invaluable encouragement and interest in my work.

I want to thank all the co-workers I have had during these years for the encouraging working environment they helped to create.

Special thanks are due to Professor Mats Hillert, Professor Bo Sundman, and Larry Kaufman PhD, for their valuable advice and skill in thermodynamics.

I want to thank Outokumpu Research Oy and Docent Pekka Taskinen for the opportunity to use the Thermo-Calc program.

I want to thank OMG Harjavalta Nickel Oy for the opportunity they gave me to finish this work.

I would like to express my thanks to all those innumerable people who have helped me collect all the papers for this work.

Pori, November 2002 Rauno Luoma

# CONTENTS

## LIST OF SYMBOLS

| | |
|---|---|
| A | Anion specie |
| a, b, c, d, $a_0$, $a_1$, $a_n$ and q | Parameters of thermodynamic functions |
| B | Neutral specie |
| C | Cation specie |
| $C_p$ | Heat capacity |
| f | Activity coefficient |
| G | Gibbs energy |
| $G^{magn}$ | Gibbs energy of magnetic term |
| °G | Gibbs energy of pure specie |
| $^{id}G$ | Gibbs energy of ideal mixing |
| $^{ex}G$ | Excess Gibbs energy |
| H | Enthalpy |
| $L_n$ | Interaction parameter |
| n | Amount of moles |
| $N^s$ | Total number of sites on sublattices |
| p | Pressure |
| p | Structure-dependent parameter of magnetic ordering |
| P | Number of sites on cation sublattice |
| Q | Number of sites on anion sublattice |
| R | Gas constant, 8.3145 J/K mol |
| S | Entropy |
| SER | Stable element reference state |
| T | Temperature unit (in K) |
| $T_c$ | Curie temperature |
| Va | Vacancy |
| Wp | Number of permutations |
| x | Mole fraction |
| y | Site fraction |
| β | Magnetic momentum |
| τ | $T/T_c$ |

# 1 INTRODUCTION

Phase diagrams are commonly used to represent the thermodynamic properties of multicomponent, multiphase systems. They have become the most important tool especially for chemists, physical metallurgists etc. Phase diagrams of complex thermodynamic systems also provide a means of understanding the phenomena that occur in several pyrometallurgical processes, helping those working in the field of extractive metallurgy.

Thermodynamic calculations in multicomponent systems are very complex. Even though the basic equations are simple, they are almost impossible without the aid of computers. This has led to large computerised databank systems that contain thermodynamic information for multicomponent systems in the form of mathematical functions. Using such an expert system, it is possible to calculate any phase diagram for the systems included in the databank and also make predictive calculations and other useful diagrams in order to solve a specific problem.

During the last decade thermodynamic assessments of many oxide systems have been carried out. These works were mainly concerned with slag chemistry and therefore they did not include carbon. Metal melts are still described using simple models for dilute systems, which, in most cases, they are. In the production of ferrochromium or stainless steels melts contain so many components other than iron that the systems can no longer be treated as dilute systems. Therefore there is a need for a databank that deals comprehensively with such metals systems.

The present work deals with the system Fe-Cr-Ni-C-O which is a basic system in describing stainless steels. The system is described using models that allow calculating thermodynamic properties over whole concentration range. The database does not include slag-forming components as silica or calcium oxide and therefore calculated diagrams does not represent situations where there is slag as stable phase. The main application for this database will be in steel making processes at high temperatures and therefore the low temperature behaviours are not taken account. Nevertheless, this database is a full description of the five-component system and can be used at any concentrations. While using this database in other areas, one should notice that the uncertainty of the description is much greater in the areas where no experimental information is available.

# 2 THERMODYNAMIC BACKGROUND

The thermodynamic description of equilibrium can be made using several functions of state. For multicomponent systems it is practical to use a model that allows the system to be described unambiguously and as a whole. This can be done most simply by choosing the Gibbs energy as the fundamental property function.

## 2.1 Gibbs energy

The Gibbs energy of a phase is defined as a function of temperature, pressure and amounts of species in the phase as:

$$G = G(T, p, n_i) \quad (1)$$

or by mole fractions as:

$$G = G(T, p, x_i) \quad (2)$$

These definitions are satisfactory in cases that they do not include surface phases or changes in strong electromagnetic fields /1/.

The definition

$$G = H - T * S \quad (3)$$

where H is enthalpy
T is temperature
S is entropy

is valid for all equilibria, chemical reactions and changes between equilibria /2/.

The temperature dependence of Gibbs energy can be described using the heat capacity, which is often described using an empirical formula, such as:

$$C_p = a + bT + \frac{c}{T^2} + dT^2 \quad (4)$$

Enthalpy and entropy can be calculated from heat capacity by:

$$C_p = \frac{\partial H}{\partial T} \quad (5)$$

$$\frac{C_p}{T} = \frac{\partial S}{\partial T} \quad (6)$$

According to the equations 3-6, the Gibbs energy for a pure element, compound or mixture phase as a function of temperature is:

$$G = a_0 - a_1 T + aT(1 - \ln T) - b\frac{T^2}{2} - \frac{c}{2T} - d\frac{T^3}{6} \qquad (7)$$

where a,b,c,d are the same constants as in equation ( 4)
$a_0$ and $a_1$ are constants that can be calculated from the constants a,b,c and d and standard values H(298) and S(298)

Equation 7 is an adequate description for stoichiometric compounds and elements if pressure dependence and magnetic ordering are not taken into account. For ferromagnetic phases the magnetic ordering will give additional terms for the Gibbs energy for pure elements and constituents:

$$G^{mag} = RT\ln(1+\beta)f(\tau) \qquad (8)$$

where $\tau = T/T_c$
$\beta$ is the average magnetic momentum in Bohr magnetons
$f(\tau)$ is structure-dependent and given, based on the modelling of the $c_p$ function by Inden /3/ and Hillert /4/ as

for $\tau < 1$
$$f(\tau) = 1 - \frac{\frac{79\tau^{-1}}{140p} + \frac{474}{497}\left(\frac{1}{p} - 1\right)\left(\frac{\tau^3}{6} + \frac{\tau^9}{135} + \frac{\tau^{15}}{600}\right)}{A}$$

for $\tau > 1$
$$f(\tau) = -\frac{\frac{\tau^{-5}}{10} + \frac{\tau^{-15}}{315} + \frac{\tau^{-25}}{1500}}{A} \qquad (9)$$

where
$$A = \frac{518}{1125} + \frac{11692}{15975}\left(\frac{1}{p} - 1\right)$$

p is a structure dependent parameter: for fcc and hcp metals p=0.28 and for bcc metals p=0.4

## 2.2 Description of mixture phases

The Gibbs energy for a mixture phase can be expressed as:

$$G = \sum n_i G_i \qquad (10)$$

where G is the Gibbs energy of the phase
$n_i$ is the amount of specie i
$G_i$ is the partial Gibbs energy of species i

The Gibbs energy for a species in a mixture phase can be divided in three parts as:

$$G_i = {}^{0}G_i + {}^{id}G_i + {}^{ex}G_i \quad (11)$$

where ${}^{\circ}G_i$ is the partial Gibbs energy for pure species i
${}^{id}G_i$ is the partial Gibbs energy of ideal mixing
${}^{ex}G_i$ is the excess Gibbs energy

Combining these two equations, the Gibbs energy for a mixture phase will be:

$$G = \sum_i n_i \, {}^{0}G_i + \sum_i n_i \, {}^{id}G_i + \sum_i n_i \, {}^{ex}G_i \quad (12)$$

Descriptions for the Gibbs energy of ideal mixing and the excess Gibbs energy are different for each model used in calculation.

### *2.2.1 Random substitutional solution models*

The random substitutional solution model is a pure mathematical model widely used for many simple systems.

For a species in a random substitutional solution the Gibbs energy is expressed as:

$$G_i = {}^{0}G_i + RT \ln x_i + RT \ln f_i \quad (13)$$

where $x_i$ is the mole fraction of component i
$f_i$ is the activity coefficient of component i
R is the gas constant
T is the temperature

For a phase we will get, according to equations 12 and 13

$$G = \sum_i x_i \, {}^{0}G_i + RT \sum_i x_i \ln x_i + {}^{Ex}G \quad (14)$$

where ${}^{Ex}G$ is the excess Gibbs energy for the phase

The excess Gibbs energy is described using polynomial functions. In the simplest case Margules polynomials /5/ are used, which are, for a specie in binary phase:

$$\ln f_i = \sum_k a_k x_i^k \quad (15)$$

Using the Gibbs-Duhem relation, it can be seen that parameters $a_0$ and $a_1$ are zero. For a binary phase the following function can then be expressed:

$${}^{Ex}G = RTx_i x_j \sum_k q_k x_j^k \quad (16)$$

where $q_k$ are parameters that can be calculated from expressions for the activity coefficients of components

The problem with these Margules polynomials is that the parameters are not transformed directly to higher order systems.

The Redlich-Kister polynomials /6/, which are mathematically more efficient and can be easily enlarged to higher order systems, are widely used nowadays. These polynomials do not have an identical form for each term, which was also a problem for the Margules polynomials. The general polynomial for the binary mixture phase is:

$$^{Ex}G = x_i x_j \sum_{k=0}^{n} {}^{k}L_{ij}\left(x_i - x_j\right)^k \qquad (17)$$

where $^{k}L_{i,j}$ is a pressure- and temperature-dependent parameter

Partial excess Gibbs energies for the binary mixture phase are then defined as /7/:

$$^{Ex}G_i = RT \ln f_i = x_j^2\left[{}^{0}L_{ij} + \sum_{k=1}^{n} {}^{k}L_{ij}\left(x_i - x_j\right)^{k-1}\left((2k+1)x_i - x_j\right)\right]$$

$$^{Ex}G_j = RT \ln f_j = x_i^2\left[{}^{0}L_{ij} + \sum_{k=1}^{n} {}^{k}L_{ij}\left(x_i - x_j\right)^{k-1}\left(x_i - (2k+1)x_j\right)\right] \qquad (18)$$

For multicomponent systems these functions can be calculated similarly. If there is a need to define a ternary interaction, it can be expressed by the equation:

$$^{Ex}G = x_i x_j x_k\left(V_i\,{}^{0}L + V_j\,{}^{1}L + V_k\,{}^{2}L\right) \qquad (19)$$

where

$$V_i = x_i + \frac{1 - x_i - x_j - x_k}{3}$$

$$V_j = x_j + \frac{1 - x_i - x_j - x_k}{3}$$

$$V_k = x_k + \frac{1 - x_i - x_j - x_k}{3}$$

### *2.2.2 Sublattice model*

For solid phases that have an internal structure it is better to use a model that can describe the structure more specifically. In the sublattice model the elements of the phase are divided into separate lattices according to the crystallographic structure of the phase /8/. For example, in a simple body-centred cubic structure sites at the body's centre and in corner positions can be described as different "sublattices", as presented is Figure 1.

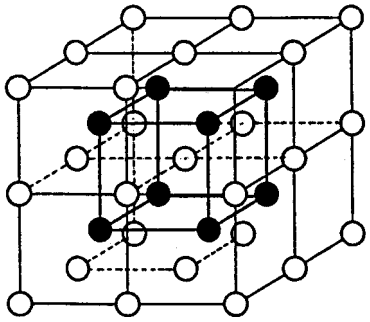

Figure 1. Simple body-centred structure.

In the sublattice model, instead of the overall composition $x_i$, the site-fraction $y_i$ is used as a coefficient when defining the Gibbs energy of the phase. The site-fraction is defined as the fractional site occupation of each of the components on the specific sublattice /8/, i.e.

$$y_i^S = \frac{n_i^S}{\sum n_j^S} \tag{20}$$

where $n^S_i$ is the number of atoms of component i on sublattice S
summation j is performed for all components on sublattice S

If there are vacancies on the sublattice they are taken into account as components. The overall composition given in mole fractions is directly related to site fractions by the following relationship /9/:

$$x_i = \frac{\sum_S N^S y_i^S}{\sum_S N^S \left(1 - y_{Va}^S\right)} \tag{21}$$

where $N^S$ is the total number of sites on sublattice S
$y^S_{Va}$ is the number of vacancies on sublattice S

The ideal entropy of mixing is made up of the configurational contributions by components mixing on each of the sublattices. The number of permutations that are possible, assuming ideal interchanges within each sublattice, is given by the equation /9/:

$$W_P = \prod_S \frac{N^S!}{\prod_i n_i^S!} \tag{22}$$

and the molar Gibbs energy of ideal mixing is /8/:

$${}^{id}G = -T\,{}^{id}S = RT \sum_S N^S \sum_i y_i^S \ln y_i^S \tag{23}$$

The ‘end members’ generated when only pure components exist on the sublattice, effectively define the Gibbs energy reference state. For a sublattice phase with the following formula $(A,B)_1(C,D)_1$ it is possible for four points of ‘complete occupation’ to exist where pure A exists on sublattice 1 and either pure C or D on sublattice 2 or, conversely, pure B exists on sublattice 1 with either C or D on sublattice 2. The composition space of the phase can then be considered in Figure 2. below as consisting of four compounds, the so-called ‘end members’, at the corners of the square. The composition of the phase is then encompassed in the space between the four ‘end-member’ compounds and the reference energy surface will look like Figure 2.

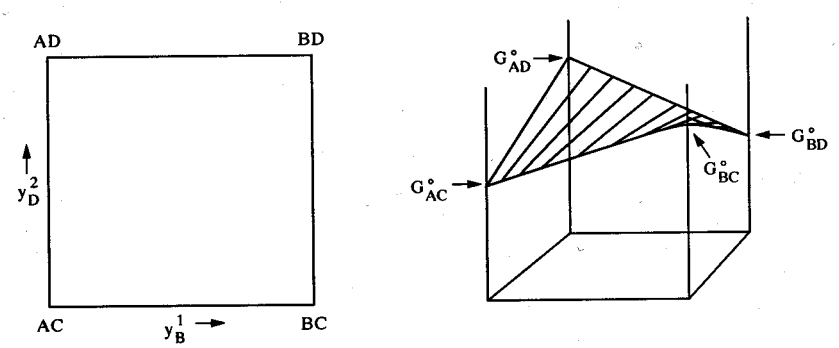


Figure 2. Composition space encompassed by the system $(A,B)_1(C,D)_1$ /9/.

The surface in Figure 2 can be represented by the equation

$$^{ref}G = y_A y_C {}^\circ G_{AC} + y_B y_C {}^\circ G_{BC} + y_A y_D {}^\circ G_{AD} + y_B y_D {}^\circ G_{BD} \qquad (24)$$

Using the same sublattice phase $(A,B)_1(C,D)_1$ as an example, the Gibbs excess energy of mixing is defined as the A-B and C-D interactions inside the sublattices. The parameters can usually have Redlich-Kister-type polynomials for composition dependence. Thus the excess Gibbs energy for this phase can be represented by the equation /8/:

$$^{Ex}G = y_A^1 y_B^1 y_C^2 \sum_{k=0}^{n} {}^k L_{A,B:C}(y_A^1 - y_B^1)^k + y_A^1 y_B^1 y_D^2 \sum_{k=0}^{n} {}^k L_{A,B:D}(y_A^1 - y_B^1)^k +$$

$$y_A^1 y_C^2 y_D^2 \sum_{k=0}^{n} {}^k L_{A:C,D}(y_C^2 - y_D^2)^k + y_B^1 y_C^2 y_D^2 \sum_{k=0}^{n} {}^k L_{B:C,D}(y_C^2 - y_D^2)^k \qquad (25)$$

### *2.2.3 Compound energy model*

Solid oxide phases can be defined using the sublattice model if ionic constituents are defined as being on the sublattices. In that case the model is known as the Compound Energy Model (CEM) /10/. If all the ‘end-members’ are neutral, the parameters and definitions are identical with the sublattice model. In cases where there are many charged ‘end members’, the model easily becomes very complex and is difficult to get balanced. The model can be most simply presented through examples.

If we have a phase that is formed from two compounds, AX and BY, where A and B are cations and X and Y are anions, all possible compounds can be described by means of an exchange reaction:

$$AX + BY = AY + BX \qquad (26)$$

Whose Gibbs energy change is expressed as:

$$\Delta^0 G_{AX:BY} = {}^0G_{AY} + {}^0G_{BX} - {}^0G_{AX} - {}^0 G_{BY} \qquad (27)$$

If there is a need for more parameters to define the system, the anion-anion and cation-cation interactions can be used /10/.

In cases where the charges of anions or cations are not the same, some of the 'end members' are charged. For example, in the system iron-oxygen the wüstite phase (FeO) can be defined with two sublattices, with cations $Fe^{2+}$ and $Fe^{3+}$ and vacancies on the first sublattice and oxygen anions on the second sublattice i.e. with a halite structure /18/, formulated as:

$$(Fe^{2+},Fe^{3+},Va)_1(O^{2-})_1 \qquad (28)$$

The 'end members' are then FeO, $FeO^+$, and $O^{2-}$, of which only the first one is neutral. The structure can be represented as a constitutional triangle, as shown in Figure 3. Each corner of the triangle represents one 'end member'. Only the solid line trough the triangle has physical significance, as it represents the neutral combinations of $Fe^{3+}$ and Va.

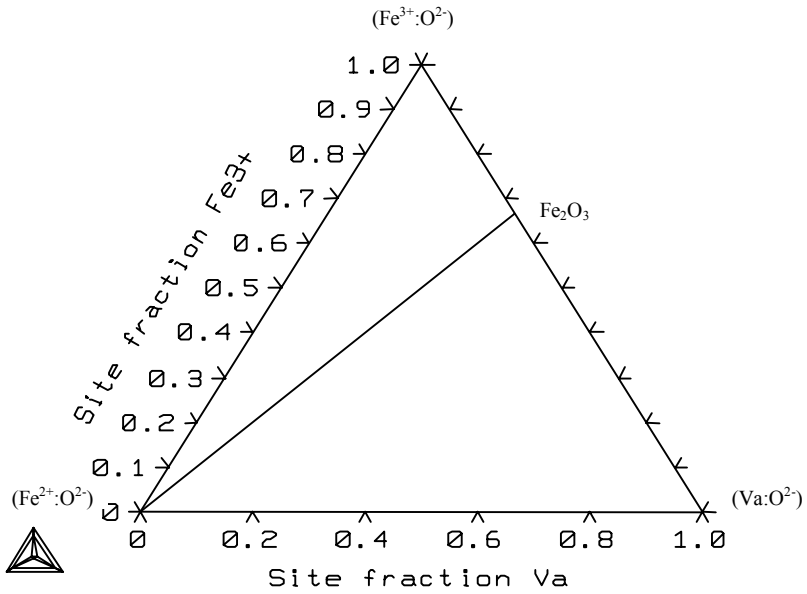


Figure 3. Structural model of wüstite /18/.

The compound energy model gives the following expression for the Gibbs energy:

$$\begin{aligned}\Delta_{mix}G = {} & y_2\,{}^\circ G_{2:O} + y_3\,{}^\circ G_{3:O} + y_{Va}\,{}^\circ G_{Va:O} \\ & + RT\left(y_2 \ln y_2 + y_3 \ln y_3 + y_{Va} \ln y_{Va}\right) + {}^{Ex}G\end{aligned} \qquad (29)$$

where the variables $y_2$ and $y_3$ are the site-fractions of divalent and trivalent iron respectively, and $y_{Va}$ is the site-fraction of a vacancy.

The three °G terms describe the Gibbs energies of the three 'end members' in Figure 3. Because two end members have a net charge, it is possible to evaluate only a neutral combination of these. The parameter $^{\circ}G_{VaO}$ represents the halite phase with only oxygen, and this parameter will be used in other oxygen systems where halite is also stable. Therefore it is convenient to set it to zero as $^{\circ}G_{VaO}=0$. The term preceded by RT is the ideal entropy of mixing on the metallic sublattice. The sublattice with oxygen has no entropy of mixing, as it is completely filled with $O^{2-}$ /18/.

The excess Gibbs energy, $\Delta_{mix}G^{ex}$, for the wüstite can be described with Redlich-Kister expressions as:

$$\begin{aligned} {}^{Ex}G &= y_2 y_3 \left[ {}^{0}L_{2,3:O} + \sum_i (y_2 - y_3)^i \, {}^{i}L_{2,3:O} \right] \\ &+ y_2 y_V \left[ {}^{0}L_{2,Va:O} + \sum_j (y_2 - y_{Va})^j \, {}^{j}L_{2,Va:O} \right] \\ &+ y_3 y_V \left[ {}^{0}L_{3,Va:O} + \sum_k (y_3 - y_{Va})^k \, {}^{k}L_{3,Va:O} \right] \end{aligned} \qquad (30)$$

There are sets of Redlich-Kister terms in each side of the triangle in Figure 3. However, as the vacancies are needed only to maintain electroneutrality, the parameters involving vacancies should be set to zero. One may otherwise have problems when combining assessments of halite phases from different subsystems because the same parameter will appear in other systems /18/.

A more complicated phase structure is used to describe the spinel phase. In the Fe-O system the magnetite has a spinel structure, with oxygen ions on the fcc sublattice and divalent and trivalent metallic ions on the octahedral and tetrahedral interstitial sublattices. A normal spinel has the trivalent ions on the octahedral sites and the divalent ions on the tetrahedral sites. However, at low temperatures, magnetite is an inverse spinel, with the tetrahedral sites filled with $Fe^{3+}$ -ions and the octahedral sites filled with both $Fe^{2+}$ and $Fe^{3+}$ -ions. At higher temperatures magnetite transforms gradually into a normal spinel, and before melting, it is almost random. The structure of the stoichiometric magnetite is thus /10/:

$$(Fe^{3+},Fe^{2+})_1(Fe^{3+},Fe^{2+})_2(O^{2-})_4 \qquad (31)$$

Only one of the 'end members' is also neutral in this case. This is a normal spinel. Figure 4 shows the constitutional diagram for a stoichiometric spinel, including the neutral line. On the neutral line all points have the same composition, but only one point is a stable compound and defines the degree on inversion.

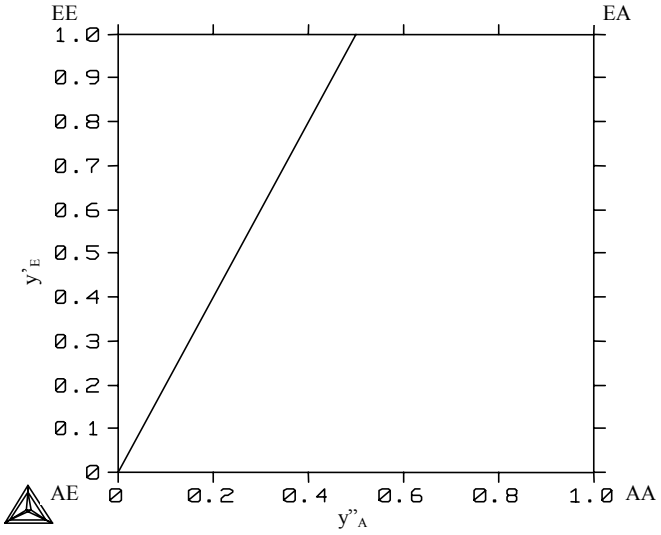


Figure 4. Constitutional diagram of spinel /10/.

The Gibbs energy for a normal spinel is defined as:

$$G_n = {}^0G_{Fe^{2+}:Fe^{3+}} \tag{32}$$

At the other end of the neutral line the Gibbs energy for an inverse spinel is:

$$G_i = 0.5\ {}^0G_{Fe^{3+}:Fe^{3+}} + 0.5\ {}^0G_{Fe^{3+}:Fe^{2+}} - 2RT\ln 2 + 0.25\ L_{Fe^{3+}:Fe^{2+},Fe^{3+}} \tag{33}$$

In this case, the phase is defined by eight parameters:

$$\begin{array}{cccc} {}^0G_{Fe^{2+}:Fe^{3+}} & {}^0G_{Fe^{3+}:Fe^{2+}} & {}^0G_{Fe^{2+}:Fe^{2+}} & {}^0G_{Fe^{3+}:Fe^{3+}} \\ L_{Fe^{2+},Fe^{3+}:Fe^{2+}} & L_{Fe^{2+},Fe^{3+}:Fe^{3+}} & L_{Fe^{2+}:Fe^{2+},Fe^{3+}} & L_{Fe^{3+}:Fe^{2+},Fe^{3+}} \end{array}$$

A condition of electroneutrality binds these parameters so that on the neutral line there are only four independent parameters, which can be expressed as:

$$\begin{array}{ll} G_n & G_i \\ \left(\Delta^\circ G + 0.5\ L_{Fe^{3+}:Fe^{2+},Fe^{3+}} - 2\ L_{Fe^{2+},Fe^{3+}:Fe^{3+}} - L_{Fe^{2+}:Fe^{2+},Fe^{3+}}\right) & \\ \left(2\ L_{Fe^{2+},Fe^{3+}:Fe^{3+}} - 2\ L_{Fe^{2+},Fe^{3+}:Fe^{2+}} - L_{Fe^{3+}:Fe^{2+},Fe^{3+}} + L_{Fe^{2+}:Fe^{2+},Fe^{3+}}\right) & \end{array}$$

Δ°G is the Gibbs energy for the exchange reaction and can be defined as being zero. The model can also be used by defining the interaction parameters as zero. Hence, there are only two parameters to be optimised. The dependence for the other parameters is then:

$$\begin{aligned} {}^\circ G_{Fe^{2+}:Fe^{3+}} &= G_n \\ {}^\circ G_{Fe^{2+}:Fe^{3+}} + {}^\circ G_{Fe^{3+}:Fe^{3+}} &= 2\ G_i + 4RT\ln 2 \\ {}^\circ G_{Fe^{2+}:Fe^{2+}} + 2\ {}^\circ G_{Fe^{3+}:Fe^{3+}} &= G_n + 2\ G_i + 4RT\ln 2 \\ {}^\circ G_{Fe^{3+}:Fe^{3+}} &= {}^\circ G_{Fe^{3+}:Fe^{3+}} \end{aligned} \tag{34}$$

The last equation is the definition for the standard state for charged components and therefore the value for $°G_{Fe^{3+}:Fe^{3+}}$ can be set to any numerical value, including zero.

If the phase is formed from two components, which have a common divalent cation, such as a solution of magnetite, $Fe_3O_4$, and chromite, $FeCr_2O_4$, the structure of the phase is /10/:

$$(Fe^{2+},Fe^{3+},Cr^{3+})_1(Fe^{2+},Fe^{3+},Cr^{3+})_2(O^{2-})_4 \qquad (35)$$

The constitutional diagram for this phase is shown in Figure 5. The number of 'end members' is seven and two of them are neutral. The neutral plane defines all compositions between $Fe_3O_4$ and $FeCr_2O_4$ and also all possible degrees of inversion. The Gibbs energy of this phase will be defined in the same way as earlier defined for a simple spinel and it can be expressed using four independent parameters /18/.

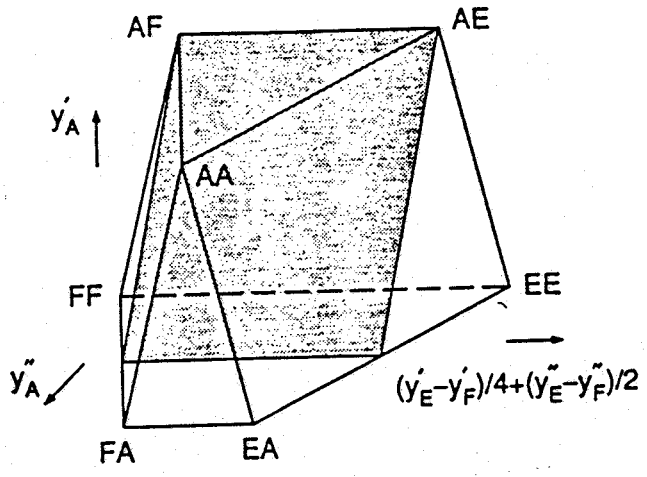


Figure 5. Constitutional diagram for the solution of two spinels. Corners AF and AE describe two normal spinels and the shaded plane is the neutral plane /10/.

Magnetite also has a considerable deviation from its ideal stoichiometry at higher oxygen potentials and temperatures. This can easily be accommodated in the structure by allowing an excess of $Fe^{3+}$ on the octahedral sites and at the same time introducing vacancies to maintain electroneutrality. The experimental methods used have not shown whether the vacancies are on octahedral or tetrahedral sites. Finally, magnetite has a small deviation towards excess iron in equilibrium with wüstite and liquid at higher temperatures. This is due to some $Fe^{2+}$ entering as interstitials into the remaining octahedral sites, which are normally empty. To model this, we add one more sublattice with two sites that are mainly filled with vacancies. The final expression for magnetite will be /10/:

$$(Fe^{2+},Fe^{3+})_1(Fe^{2+},Fe^{3+},Va)_2(Fe^{2+},Va)_2(O^{2-})_4 \qquad (36)$$

This description will then have 12 °G functions but only four independent parameters, as presented by Sundman /18/.

Figure 6 shows the constitutional diagram for a spinel with the composition of $MgAl_2O_4$ and its neutral plane. The corners of the neutral plane are, in this case, the normal spinel $MgAl_2O_4$ and the metastable compounds $\gamma$-$Al_2O_3$, $\gamma$-MgO, and $AlMg_{2.5}O_4$. This phase can be defined using four independent parameters.

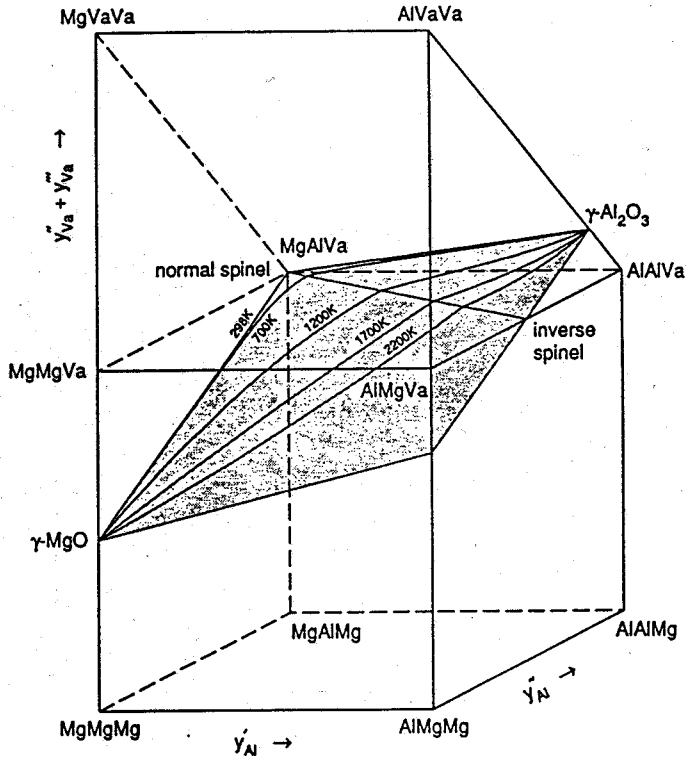


Figure 6. Constitutional diagram for the spinel MgO-$Al_2O_3$.

A phase comprising two non-stoichiometric spinels can be expressed with the formulas shown above. The final description of the phase will then have eight independent parameters /10/.

### *2.2.4 Partially ionic liquid*

The liquid phase can be treated as a random substitutional phase in many metallic systems. In cases where the phase includes oxygen, this necessitates the defining of thermodynamic functions for the phase more accurately in order to avoid a rather complicated set of parameters that do not have any physical meaning. One possibility is to use the sublattice model for the liquid phase. This model is also known as a partially ionic liquid model /11/.

In this model we have two sublattices, with cation constituents on the first sublattice and anion and neutral constituents and vacancies on the second. The sublattice formula for the model can then be written as:

$$\left(C_i^{+\nu_i}\right)_P \left(A_j^{-\nu_j}, Va, B_k^0\right)_Q$$

where C represents a cation
A an anion
Va a hypothetical cation
B neutrals

The charge of an ion is denoted by $\nu_i$ and the indices i, j, and k are used to denote specific constituents. The number of sites on the sublattices is varied, so that electroneutrality is maintained, and the values of P and Q are calculated from the equations:

$$\begin{aligned} P &= \sum_j \nu_j y_{A_j} + Q y_{Va} \\ Q &= \sum_i \nu_i y_{C_i} \end{aligned} \qquad (37)$$

Equation 37 simply means that P and Q are equal to the average charge on the opposite sublattice, with the hypothetical vacancies having an induced charge equal to Q. Mole fractions for the components can be defined as:

$$\begin{aligned} x_{C_i} &= \frac{P_{y_{C_i}}}{P + P(1 - y_{Va})} \\ x_{A_i} &= \frac{Q y_{A_i}}{P + Q(1 - y_{Va})} \end{aligned} \qquad (38)$$

where $C_i$ denotes a cation and $A_i$ an anion

The integral Gibbs energy for this model is then given by:

$$\begin{aligned} G = & \sum_i \sum_j y_{C_i} y_{A_j} {}^\circ G_{C_i:A_j} + Q y_{Va} \sum_i y_{C_i} {}^\circ G_{C_i} + Q \sum_k y_{B_k} {}^\circ G_{B_k} \\ & + RT\left( P \sum_i y_{C_i} \ln y_{C_i} + Q\left( \sum_j y_{A_j} \ln y_{A_j} + y_{Va} \ln y_{Va} + \sum_k y_{B_k} \ln y_{B_k} \right)\right) \\ & + \sum_{i_1} \sum_{i_2} \sum_j y_{i_1} y_{i_2} y_j L_{i_1 i_2:j} + \sum_{i_1} \sum_{i_2} y_{i_1} y_{i_2} y_{Va} L_{i_1 i_2:Va} \\ & + \sum_i \sum_{j_1} \sum_{j_2} y_i y_{j_1} y_{j_2} L_{i:j_1 j_2} + \sum_i \sum_j y_i y_j y_{Va} L_{i:jVa} \\ & + \sum_i \sum_j \sum_k y_i y_j y_k L_{i:jk} + \sum_i \sum_k y_i y_k y_{Va} L_{i:Vak} \\ & + \sum_{k_1} \sum_{k_2} y_{k_1} y_{k_2} L_{k_1 k_2} \end{aligned} \qquad (39)$$

where ${}^\circ G_{Ci:Aj}$ is the Gibbs energy of formation for $(\nu_1+\nu_2)$ moles of atoms of liquid $C_iA_j$ and ${}^\circ G_{Ci}$ and ${}^\circ G_{Bk}$ are the Gibbs energy of formation per mole of atoms of liquid C and B respectively. The first line represents the Gibbs energy reference state, the second line the configurational mixing term, and the last three lines the excess Gibbs energy of mixing. In some papers /12/ reciprocal terms are also used.

The model is certainly complex, but the terms have some physical meaning, representing different interactions in different parts of the system. Selleby /13/ suggests that the number of terms needed to describe a ternary system such as Fe-Mn-S is quite similar for both ionic sublattice liquid and associate models. The modelling of ionic liquids is complex and the advantages of the various techniques only become apparent as they become more commonly used.

There are a number of immediate advantages to the ionic sublattice model. The first is that it becomes identical to the more usual Redlich-Kister representation of metallic systems when the cation sublattice contains only vacancies. This immediately allows data from an assessed metallic system to be combined with data from an oxide system so that the full range of composition is covered. In binary cases the model can be made equivalent to an associate model. For example, the associate model would consider a substitutional solution of Cu, S and $Cu_2S$ in the system Cu-S. If an ionic sublattice model with a formula $(Cu^{+1})_P(S^{-2},Va,S)_Q$ is used, it is straightforward to derive parameters to give an identical result to the associate model /9/. However, it should be noted that the Gibbs energy of the two models does not remain equivalent if they are extended into ternary and higher-order systems /11/.

### *2.2.5 Associate model*

The liquid phase in oxide systems can also be treated as a substitutional solution of metals and oxides. In this case oxides are associates or complexes. The thermodynamic properties of the liquid phase then depend predominantly on the Gibbs energy of the formation of these associates instead of the interaction between the components. This gives rise to the enthalpy of mixing diagrams, which are characterised by sharp changes at critical compositions where associates exist, and also by markedly non-ideal mixing entropies.

The derivation of Sommer /14/ can be used as an example. This considers the formation of a single associate with the formula $A_iB_j$ within a binary system, A-B. It is assumed that the liquid contains $n_{Ai}$ and $n_{Bj}$ moles of free A and B in equilibrium with $n_{AiBj}$ moles of associate $A_iB_j$. The mole fractions of A, B, and $A_iB_j$ in a binary alloy containing 1 mole of A and B atoms are then given by the formula:

$$\begin{aligned} x_A &= n_A + i\, n_{A_iB_j} \\ x_B &= n_B + j\, n_{A_iB_j} \\ x_{A_iB_j} &= n_{A_iB_j} \end{aligned} \qquad (40)$$

The excess Gibbs energy of mixing is then given by the general formula:

$$G_{mix}^{Ex} = G^{ass} + G^{reg} \qquad (41)$$

where $G^{ass}$ is the Gibbs energy due to the formation of the associate defined as:

$$G^{ass} = n_{A_iB_j}\, {}^{\circ}G_{A_iB_j} \qquad (42)$$

Here ${}^{\circ}G_{AiBj}$ is the Gibbs energy of formation of one mole of the associate. $G^{reg}$ considers the Gibbs energy due to the interactions between the components A and B themselves and with the associate $A_iB_j$ such that:

$$G^{reg} = G_{A,B}^{reg}\frac{n_A n_B}{n_A + n_B + n_{A_iB_J}} + G_{A,A_iB_j}^{reg}\frac{n_A n_{A_iB_j}}{n_A + n_B + n_{A_iB_J}} + G_{B,A_iB_j}^{reg}\frac{n_B n_{A_iB_j}}{n_A + n_B + n_{A_iB_J}} \qquad (43)$$

The configurational entropy is given simply by:

$$S_{mix}^{conf} = -R\left(n_A \ln x_A + n_B \ln x_B + n_{A_iB_j} \ln x_{A_iB_j}\right) \qquad (44)$$

The model was applied to numerous ionic melts and good agreement was found with experimental results /14, 15/. One of the main criticisms of associate formalism has been that, although the concept considers associates or complexes to be diffuse in nature, mathematical formalism implies that distinct molecules exist, which is more difficult to justify. However, if this stringent view is relaxed, it can be seen that the model merely implies some underlying structure to the liquid, which is quite reasonable, and it does provide functions that allow a temperature dependence for the enthalpy of mixing. A more serious criticism is that some knowledge of the relevant associate is necessary before the model can be applied. The most appropriate associate can be selected by the fitting of experimental results for enthalpies of mixing, which is sufficient in a large number of cases. However, in some systems there may be a number of different associates and it is not always obvious which types actually exist. The main advantage of the associate model is that it allows a simple strategy to be adopted for optimisation. It is easy to further define ternary and higher-order associates and extend the model to multicomponent systems. This was shown by Rannikko /15/ in his study on the system Cu-O-CaO-$SiO_2$.

It is easy to show equivalence between the ionic sublattice model and the associate model, as demonstrated by Hillert /11/. For the system $(A^{+\nu_A})_P(B^{-\nu_B},Va^{-\nu_A},B^0)_Q$ where $+\nu_A=-\nu_B$ equation 39 can be simplified for one mole of atoms as:

$$G = \frac{y_B G^0_{\underset{+\nu A}{\underset{}{A_{-\nu B}B_1}}} + RT\left(y_B \ln y_B + y_b \ln y_b + y_{Va} \ln y_{Va}\right) + \dfrac{G^{Ex}_{mix}}{\nu_A}}{\left(1 - \dfrac{y_B \nu_B}{\nu_A}\right)} \qquad (45)$$

where $y_b$ is the site fraction occupation of the neutral $B^0$ on sublattice Q. Equations 42-44 will yield, for one mole of atoms:

$$G = \frac{x_{A_iB_j} G^{Ass} + RT\left(x_{A_iB_j} \ln x_{A_iB_j} + x_A \ln x_A + x_B \ln x_B\right) + G^{Reg}}{1 + x_{A_iB_j}(i + j - 1)} \qquad (46)$$

The two models become identical in the case where $i=j=\nu_A=-\nu_B=1$ and it is possible to show the following identities:

$$x_{AiBj} = y_B$$
$$x_B = y_b$$
$$x_A = y_{Va}$$

If $y_A = 1$ the $G^{ass}$ term has the following equivalence

$$x_{A_iB_j} G^{Ass} = y_A y_B G^0_{A^{+\nu A}:B^{-\nu B}} \qquad (47)$$

and the excess terms of the associate show the following equivalences

$$\begin{aligned} x_A x_B G^{reg}_{A,B} &= y_A y_{Va} y_B L_{A^{+\nu A}:B^0,Va^{-\nu A}} \\ x_A x_{A_iB_j} G^{reg}_{A,A_iB_j} &= y_A y_{Va} y_B L_{A^{+\nu A}:B^{-\nu B},Va} \\ x_B x_{A_iB_j} G^{reg}_{B,A_iB_j} &= y_A y_b y_B L_{A^{+\nu A}:B^{-\nu B},B^0} \end{aligned} \qquad (48)$$

They can also be made identical in a general case if the conditions $i = -\nu_B/\nu_A$ and $j = 1$. This has been used by Kowalski et al. /16/ for the systems Fe-O, Cr-O, and Ni-O. They selected the associates $CrO_{1.5}$, FeO, $FeO_{1.5}$, and NiO for the liquid phase. These associates correspond to the $(Cr^{+3})_{2/3}(O^{-2})_1$, $(Fe^{+2})_2(O^{-2})_2$, $(Fe^{+3})_{2/3}(O^{-2})_1$, and $(Ni^{+2})_2(O^{-2})_2$ phase compounds resulting from the ionic liquid description adopted by Taylor et al. /17/ for the Cr-O and Ni-O liquid and by Sundman /18/ for the Fe-O liquid. In the recent remodelling /19/ of the Fe-O liquid the $Fe^{+3}$ species, and in consequence the $(Fe^{+3})_2(O^{-2})_3$ phase compound, has been replaced by the neutral $FeO_{1.5}$ species. The numerical values for the Gibbs energy of formation for these associates can be calculated straight from the corresponding values for these phase compounds. Only the change in the number of atoms per associate should be taken into account. Similarly, the excess Gibbs energy can be transformed. Kowalski et al. reassessed the parameters to give a simpler model. The equivalence breaks down in ternary and higher-order systems, as there is the introduction of more compositional variables in the associate model than for the sublattice model /9,11/.

One problem arises when selecting the associates. For example, Kowalski et al. /16/ used the associate $CrO_{1.5}$ in the system Cr-O. In this case the activity coefficient of oxygen in infinite dilution does not have a defined value. This is due to the fact that the activity coefficient can be calculated from the equation:

$$Cr + 1.5O \rightleftharpoons CrO_{1.5} \qquad (49)$$

For this reaction the Gibbs energy change $\Delta G$ is defined. From this we can calculate the equilibrium constant K, which is defined as:

$$K = e^{\frac{-\Delta G}{RT}} = \frac{a_{CrO_{1.5}}}{a_{Cr}a_O^{1.5}} = \frac{f_{CrO_{1.5}}x_{CrO_{1.5}}}{f_{Cr}x_{Cr}f_O^{1.5}x_O^{1.5}} \qquad (50)$$

From this we can calculate:

$$f_O = \sqrt[1.5]{\frac{f_{CrO_{1.5}}x_{CrO_{1.5}}}{K\ f_{Cr}x_{Cr}x_O^{1.5}}} \qquad (51)$$

which does not have defined limiting value when $x_{CrO_{1.5}}$ goes to zero. But by selecting $Cr_{2/3}O$ as the associate we will get the reaction:

$$2/3\ Cr + O \rightleftharpoons Cr_{2/3}O \qquad (52)$$

and this will give the activity coefficient by the equation:

$$f_O = \frac{f_{Cr_{2/3}O}x_{Cr_{2/3}O}}{K\ f_{Cr}^{2/3}x_{Cr}^{2/3}x_O} \qquad (53)$$

which will have a defined value when $x_{Cr_{2/3}O}$ goes to zero and it is

$$f_O = \frac{f_{Cr_{2/3}O}}{K\ f_{Cr}^{2/3}x_{Cr}^{2/3}} \qquad (54)$$

For this reason associates should be selected so that the associate containing the least oxygen has stoichiometric number one for oxygen, as does associate FeO in the system Fe-O. This problem does not arise with the ionic sublattice model, when there is always oxygen on the anion sublattice in the form $O^{2-}$.

### *2.2.6 Interpolation models*

The molar excess Gibbs energy of a binary system using Redlich-Kister formalism with components 1 and 2 is expressed as:

$$^{Ex}G = x_1 x_2 \sum {}^{k}L_{12}(x_1 - x_2)^k \qquad (55)$$

where $x_1$ and $x_2$ are mole fractions and ${}^{k}L_{12}$ is the interaction parameter. When using these binary parameters to calculate ternary systems, several "geometric" models are proposed. In these models the excess Gibbs energy in a ternary solution at a composition point p is estimated from the excess Gibbs energies in three binary subsystems at points a, b, and c by the equation:

$$^{Ex}G = x_1 x_2 G_{12(a)} + x_2 x_3 G_{23(b)} + x_1 x_3 G_{13(c)} + (\textit{ternary terms}) \qquad (56)$$

where $G_{12(a)}$, $G_{23(b)}$, and $G_{13(c)}$ are the binary G-functions evaluated at points a, b and c. The ternary terms are polynomial terms and may be chosen in order to fit ternary experimental data. The differences between four models are shown in Figure 7 /20/.

The Kohler/Toop /21/ and Muggianu/Toop /22/ models are asymmetrical, as one component is singled out, whereas the Kohler /23/ and Muggianu /24/ models are symmetrical ones. For systems with strong interactions, the four models can give quite different results when binary $G^{ex}$ functions are composition-dependent.

Using Thermo-Calc as the optimisation program, the only available geometric models are Muggianu and Kohler, which are both symmetrical /36/. Most of the systems that are already optimised and available in databases were made using the Muggianu model. Therefore, it was obvious to select this model in the present work. However, a few words will be addressed to the choice between these models.

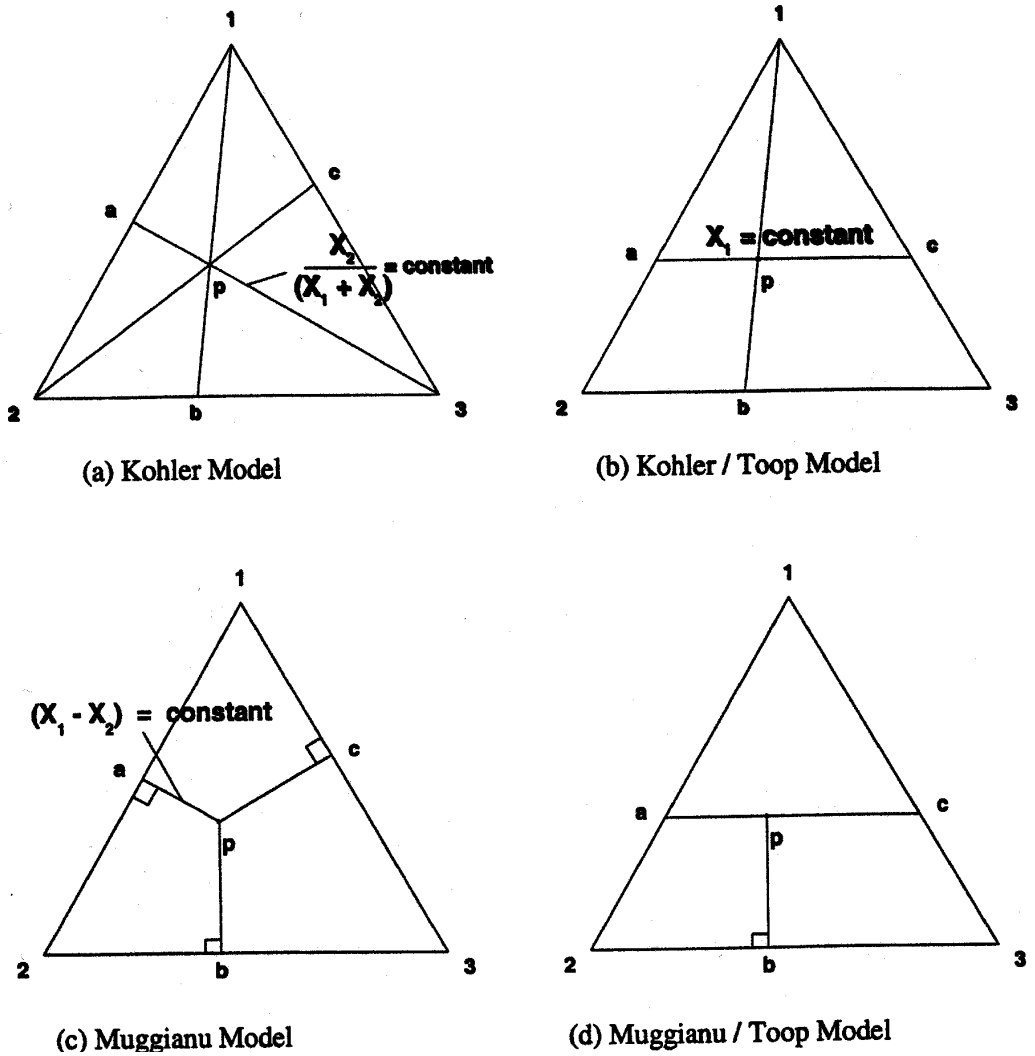


Figure 7. Geometric interpolation models for estimating ternary thermodynamic properties from optimised binary systems.

Suppose that the data for the three binaries of a ternary system have been optimised to give binary coefficients $G_{xy}$ in equation ( 56) and the $^{Ex}G$ is estimated in the ternary system using the Kohler model. Along the line a-3 in Figure 7(a) the ratio $x_2/(x_1+x_2)$ is constant and the ratio is equal to $x_2$ at point a. Therefore function $G_{12(a)}$ in equation ( 56) can be written as:

$$G_{12(a)} = \sum_k {}^k L_{12} \left( \frac{x_1 - x_2}{x_1 + x_2} \right)^k \qquad (57)$$

where $^kL_{12}$ are the binary coefficients. That is, $G_{12(a)}$ as given is constant along the line a-3. Similarly, the functions $G_{23(b)}$ and $G_{13(c)}$ may be written in terms of the ratios $x_3/(x_2+x_3)$ and $x_3/(x_1+x_3)$ /20/.

In the Muggianu model, we note that $(x_1-x_2)$ is constant along the line ap in Figure 7(c). Hence equation ( 55) can be substituted directly into equation ( 56) with no change. This difference means that the Kohler model assumes that the energy change of the pair exchange reaction is constant at a constant $x_1/x_2$ ratio, whereas the Muggianu model sets this energy as equal to its value at the geometrically closest binary composition. From a physical standpoint, the former assumption is perhaps more justifiable. Nevertheless, for more concentrated solutions, the Kohler and Muggianu models will give quite similar results /20/.

However, in dilute solutions, the Kohler model is to be preferred for the reason illustrated in Figure 8. In a ternary solution dilute, in component 1, the Kohler model estimates values $G_{12(a)}$ and $G_{13(c)}$ from the values in the binary systems at compositions that are also dilute in component 1, as seems reasonable. On the other hand, the Muggianu model uses values from binary systems at compositions that are far from dilute /20/.

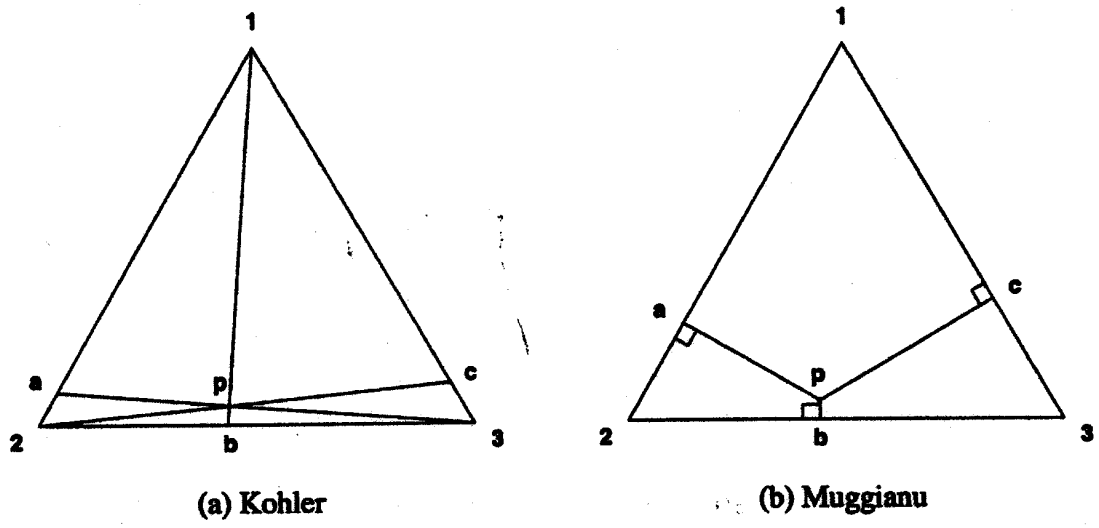


Figure 8. The Kohler (a) and Muggianu (b) models applied at a composition dilute in component 1.

In the asymmetrical models illustrated in Figure 7 (b) and (d), the energies of the 1-2 and 1-3 pair interactions are assumed to remain constant at constant $x_1$. An asymmetrical model is thus more physically reasonable than a symmetrical model if components 2 and 3 are chemically similar while component 1 is chemically different, as for example in metal-metal-oxygen systems /20/.

# 3 CALCULATION PRACTICE

## 3.1 Database programs

There are some programs that were developed to calculate chemical equilibrium in multicomponent systems. These programs calculate the equilibrium by minimising the Gibbs energy of a system. In multicomponent systems this minimisation is such a large calculation process that it cannot be done without modern computers. Therefore development in this area has been very heavily dependent on the improvement of computers' calculation capacity.

In this work the Thermo-Calc program is used. It was developed in Sweden, in Royal Institute of Technology (RIT). This program has an optimisation module called Parrot, which allows the using of different kinds of experimental thermodynamic data to assess parameters. The Thermo-Calc program can handle a large variety of models that are used to describe the thermodynamics of different types of solution phases. It also has a flexible interface that enables the user to calculate many different types of equilibria and diagrams of various types. The software can handle single equilibria, thermodynamic property diagrams or phase diagrams, with up to twenty elements or 200 species /25/.

The Thermo-Calc program can be used to calculate many kinds of stability diagrams, for example phase diagrams, species of phases, liquidus surfaces and thermodynamic property diagrams. Although this program is deliberately restricted to equilibrium calculations, it can also be used for simple non-equilibrium simulations, for example, solidification simulations based on the Scheil-Gulliver model. Thermo-Calc can also be used as a subroutine package in other models to calculate the socal equilibrium in some more complicated systems /26/.

Other programs that can be used for optimising the systems are BINGSS, MTDATA, F*A*C*T and Chemsage. BINGSS was developed by H. L. Lukas in Stuttgart and it is a very powerful optimiser for binary systems. It can easily use thousands of experimental values of different kinds. It does not include any database and its only purpose is the optimisation. Using a parameter file made by BINGSS one can calculate diagrams using the BINFKT program. H. L. Lukas has also created optimisation programs for ternary systems, called TERGSS, and quaternary systems, called QUAGSS, but those programs do not include very many solution models /27/.

MTDATA /28/ is a large database program, which has its own database. It can be used for many different calculations, particularly for multicomponent systems.

F*A*C*T /29/ and Chemsage /30/ have basically the same optimisation routine, because they are both based on developments by G. Eriksson. The latest versions of these programs are identical and called FactSage.

## 3.2 The Calphad principle

While building a database for multi-component systems it is essential to take into account some principles.

Unary systems (i.e. elements) must have the same standard state. A useful selection for the standard state is SER, in which the enthalpy of the most stable state of an element is zero at 25°C. The entropy of the most stable crystal structure at zero Kelvin is zero. The enthalpy and entropy of an element at any temperature can then be calculated using equations 5 and 6 and the Gibbs energy of an element using equation 3. Thermodynamic properties for all species are then calculated from the Gibbs energy of the formation of those species.

All calculated parameters must work with both higher order and lower order systems. This also means that if there is a phase in a ternary system that does not exist in binary systems as a stable phase but can mathematically be calculated as being able to exist, the parameters of that phase should be defined with values that keep the phase metastable.

These basic rules are also known as the Calphad method. The optimisation according to this method is described in Figure 9.

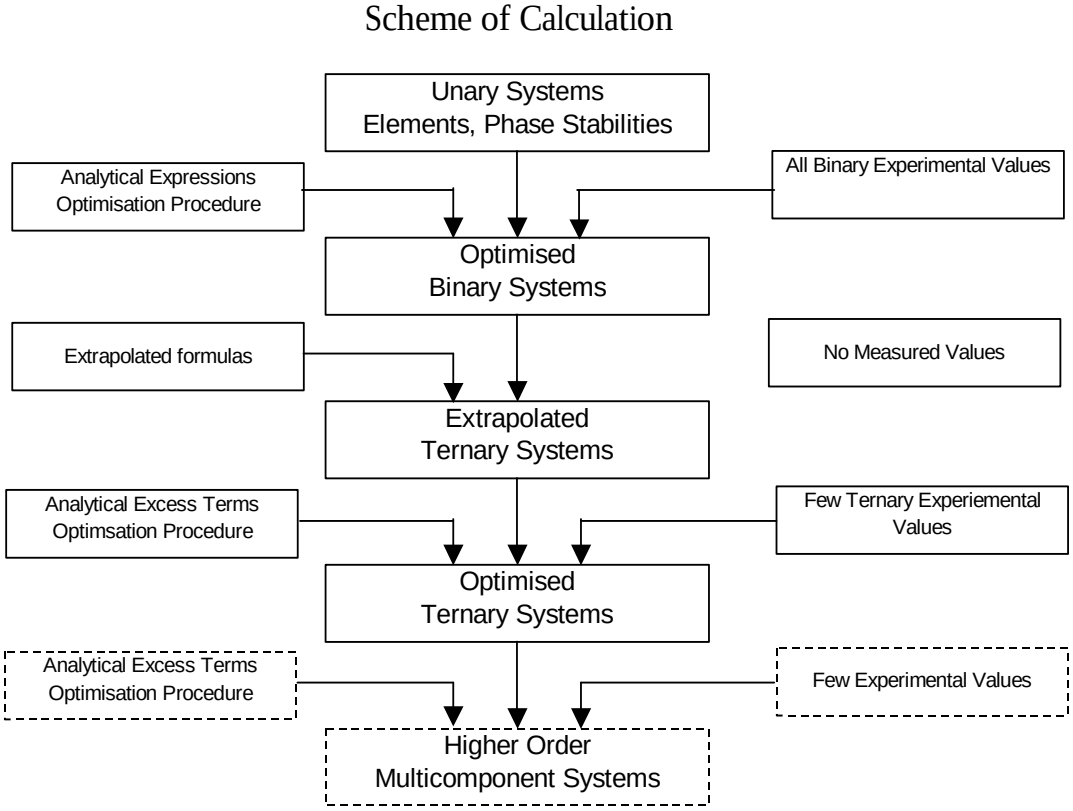


Figure 9. Schematic presentation of the Calphad method /31/.

## 3.3 Optimisation practice

The general practice of optimisation is performed through a process of trial-and-error combinations of the adjustable parameters. Optimisation programs, such as Parrot, reduce the error using mathematical algorithms, while a "manual" procedure means that the user changes these parameters according to their personal judgement. Although a mathematical least-squares-type approach might be considered ideal, a great deal of judgement is still required in this process, particularly when there is little experimental information available. It must also be noted that these mathematical programs do not take account of the physical meanings of parameters and therefore it is possible to find a combination of parameters that works with a binary system, but does not work in higher order systems.

The simplest way to explain the method of optimisation is to look at it with an example. The following shows a simplified optimisation procedure for the system Fe-Cr-O /53/.

To start with, a literature survey must be carried out. In the case of the example system the latest and largest literature survey was carried out by Raghavan /32/. The THERMET literature databank in Grenoble was also checked. All the data that were found were adopted for the optimisation. On the other hand, the Parrot program can not handle any number of experimental data. Besides, as there are hundreds of measured values for one phase they may give too much weight on one study. Therefore it was necessary to critically analyse the data and their errors before selecting the most consistent set from these data.

The optimisation of the ternary system Fe-Cr-O was performed using the Parrot module. It was started from solid oxide phases. First the thermodynamic parameters for chromite were calculated, using measured data of chromite-$Cr_2O_3$-metallic-phase equilibrium. The oxygen partial pressures in these equilibria were also used. The values used at the start of this optimisation were the values of the Gibbs energy of the formation of chromite that were found in the literature.

In the next step, the parameters of the spinel phase were optimised, using the oxygen pressures in this phase. Then the spinel phase parameters were optimised together with those of a sesquioxide phase ($Fe_2O_3$-$Cr_2O_3$), after fixing these parameters.

The parameters of wüstite were optimised using first only the measured oxygen potentials in different compositions and at different temperatures. Then they were optimised together with the parameters of the other solid phases.

After all the solid phase parameters were optimised the work with the liquid phase was started. First the parameters of the metal-rich liquid were optimised using measured oxygen concentrations and activities. After that they were optimised together using measured equilibria oxidic liquid.

When all the phases had been described separately, calculations were performed with all parameters and all experimental data. During this procedure the parameters did not change very much.

# 4 DESCRIPTION OF THE SYSTEM

The program used in this work, Thermo-Calc, allows the use of a different model for each phase. The reference state was chosen to be SER.

## 4.1 Gas phase

The gas phase is an ideal mixture phase. Its species are $O_2$, CO, and $CO_2$.

## 4.2 Liquid

The liquid phase is described with an associate model using Fe, Cr, Ni, C, FeO, $FeO_{3/2}$, $Cr_{2/3}O$, and NiO as associates. This description can handle both the metallic and oxide liquid.

## 4.3 Solid metallic phases

These phases are body-centred and face-centred cubic phases (bcc and fcc) for iron, chromium, and nickel. Carbon and oxygen are on interstitial sites, which gives the second sublattice for these phases. In the bcc and fcc phases the site numbers are 1:3 and 1:1, respectively. These phases are described using Redlich-Kister polynomials and the interpolation model of Muggianu.

These phases are formulated as:

Bcc: $(Fe,Cr,Ni)_1(C,O,Va)_3$

Fcc: $(Fe,Cr,Ni)_1(C,O,Va)_1$

## 4.4 Sigma phase

In the binary system iron-chromium there is an intermetallic solid phase known as the sigma phase. Nickel has significant solubility in this phase. The phase is described with three sublattices using site numbers 8:4:18. The phase is formulated as:

$(Fe,Ni)_8(Cr)_4(Cr,Fe,Ni)_{18}$

## 4.5 Wüstite and bunsenite

The wüstite and bunsenite phases are described with the compound energy model using two sublattices. The phase is formulated as:

$(Cr^{3+},Fe^{2+},Fe^{3+},Ni^{2+},Ni^{3+},Va)_1(O^{2-})_1$

In this work these phases are referred to as ‘halite’ according to its prototype phase.

## 4.6 Hematite and chromium oxide $Cr_2O_3$

The hematite and chromium oxide phases are described with the compound energy model using three sublattices. The phase is formulated as:

$(Cr^{3+},Cr^{2+},Fe^{3+})_2(Cr^{3+},Ni^{2+},Va)_1(O^{2-})_3$

In this work this phase is referred to as ‘corundum’ according to its prototype phase.

## 4.7 Spinel

The spinel phase is desciribed with the compound energy model using four sublattices. The phase is formulated as:

$(Cr^{3+},Cr^{2+},Fe^{3+},Fe^{2+},Ni^{2+})_1(Cr^{3+},Fe^{3+},Fe^{2+},Ni^{2+},Va)_2(Fe^{2+},Va)_2(O^{2-})_4$

This phase is magnetite $Fe_3O_4$, $Cr_3O_4$, chromite $FeCr_2O_4$, and nickel chromite $Cr_2NiO_4$.

The properties of the spinel phase are based on those of its component spinels $Fe_3O_4$, $Fe_2NiO_4$, $FeCr_2O_4$, and $Cr_2NiO_4$. Magnetite has been described by Sundman /18/ using four independent parameters, as presented earlier in Chapter 2.2.3. Taylor used the same model for magnetite and also enlarged the model to present chromite. Nickel ferrite is defined by Luoma /47/ using the same model. Combining these three descriptions, the final model will have ten independent parameters combined to the 50 parameters needed to describe this phase.

## 4.8 Graphite

The graphite phase is a stoichiometric pure carbon phase.

## 4.9 Carbide phases

The system chromium-carbon contains three carbides, described as $M_3C_2$, $M_7C_3$, and $M_{23}C_6$ in this work. The $M_3C_2$ phase is a stoichiometric chromium carbide phase with no solubility of iron or nickel and is described with two sublattices. The $M_7C_3$ phase has two sublattices and the $M_{23}C_6$ has three sublattices. The phases are formulated as:

$M_3C_2$: $(Cr)_3(C)_2$

$M_7C_3$: $(Cr,Fe,Ni)_7(C)_3$

$M_{23}C_6$: $(Cr,Fe,Ni)_{20}(Cr,Fe,Ni)_3(C)_6$

# 5 BINARY SYSTEMS

## 5.1 System Fe-Cr

The system iron-chromium has been assessed by Andersson and Sundman /33/. The assessed phase diagram is in very good agreement with the diagram published in /34/ except for the liquidus line at higher chromium contents. The reasons are the experimental difficulties and the high affinity of chromium to oxygen. The assessed phase diagram is shown in Figure 10.

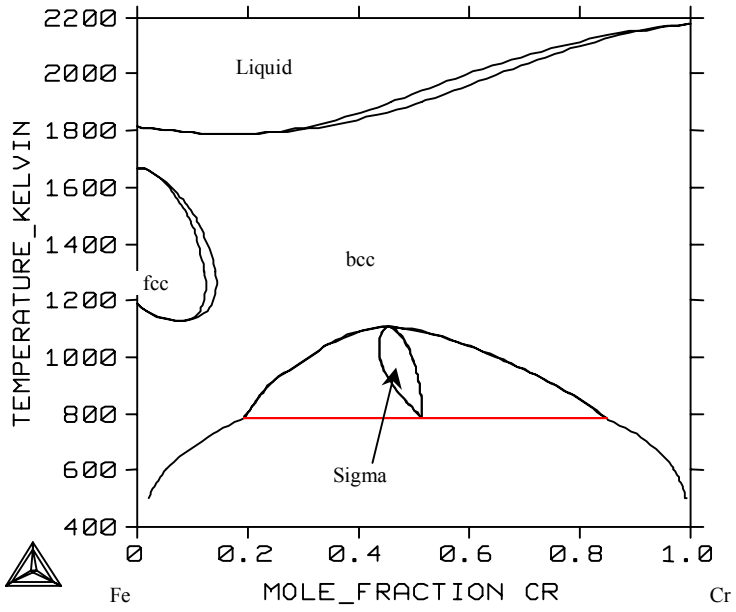


Figure 10. The assessed phase diagram for the system Fe-Cr /33/.

## 5.2 System Fe-Ni

At higher temperatures the system iron-nickel is rather well known. Publication /35/ presents a literature survey up to 1989 carried out by Swartzendruber. In the M version of the Thermo-Calc database system /36/ there is a set of thermodynamic parameters that are based on the unpublished work of Dinsdale /37/. These parameters give an assessed phase diagram shown in Figure 11. A remarkable difference between the present and the earlier assessed diagrams is that the intermetallic, low-temperature $FeNi_3$ phase, found by many authors, is ignored from the present diagram.

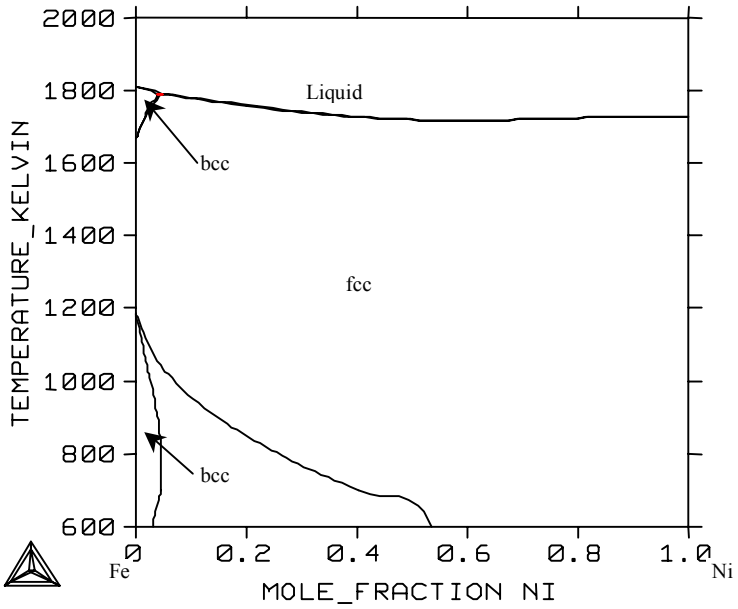


Figure 11. The assessed phase diagram for the system Fe-Ni.

## 5.3 System Fe-C

The system iron-carbon is very well known. Publication /35/ presents a literature survey conducted by Okamoto, which also includes the metastable phase diagram Fe-$Fe_3C$. The assessed parameters are given by Gustafson /38/. The calculated phase diagram shown in Figure 12 is in very good agreement with the experimental data.

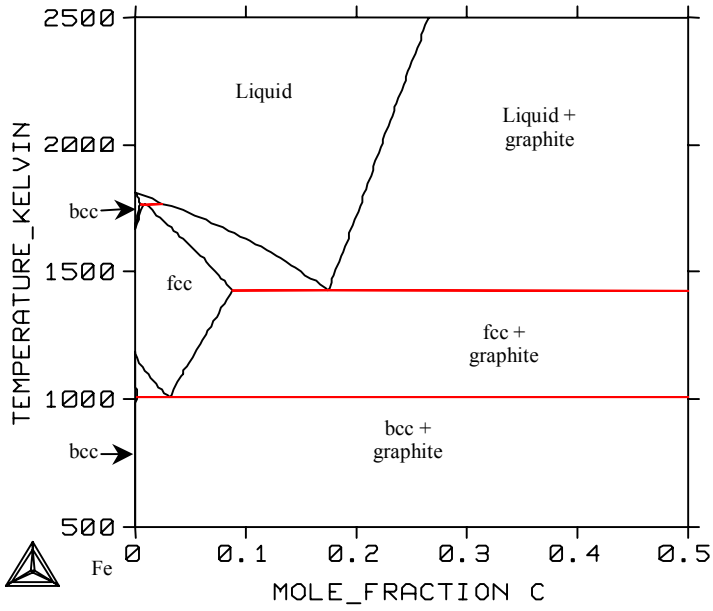


Figure 12. The assessed phase diagram for the system Fe-C.

## 5.4 System Fe-O

The iron-oxygen system has recently been optimised by three workers. Sundman /18/ made the first contribution, using an ionic sublattice model for the liquid phase and also a reassessment modifying the description of the liquid phase /13/. Kowalski et al. /16/ optimised this system using the associate model for the liquid phase. In this work Sundman's later description of the liquid /19/ was adopted. This description was converted to that of the associate model as shown in Section 2.2.5. The parameters obtained are given in Table 1. These parameters give very good agreement with the experimental data. The model for solid iron phases has been taken from Kowalski et al. /16/. In their model oxygen occupies the interstitial sublattice of both the bcc and fcc structures of iron. Also in this case the agreement with the experimental data is good as can be seen in Figure 14.

Table 1. Interaction parameters for the liquid phase of the system Fe-O.

| Parameter | Value (J) |
|---|---|
| $^0L(Fe - FeO)$ | 88340.5-8.184*T |
| $^1L(Fe - FeO)$ | 32827.5-15.4345*T |
| $^0L(Fe - FeO_{1.5})$ | 110000 |
| $^0L(FeO - FeO_{1.5})$ | -13181 |
| $^1L(FeO - FeO_{1.5})$ | 6676.5 |

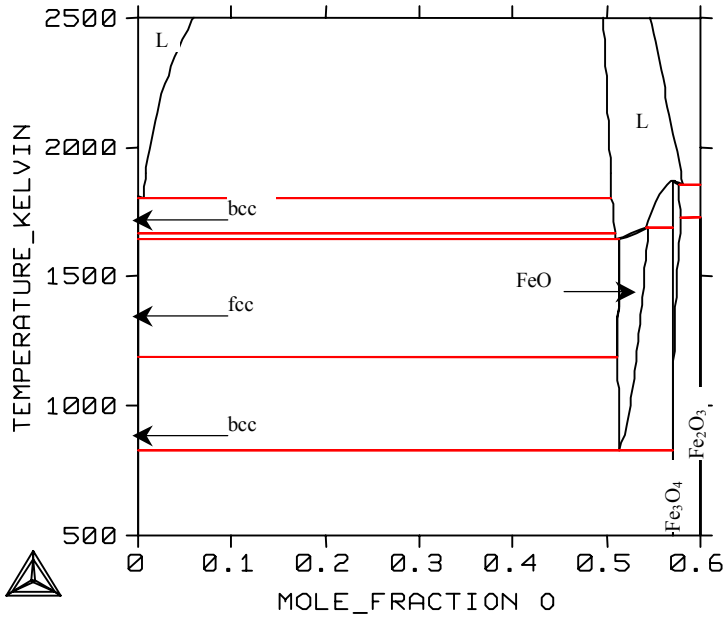


Figure 13. The assessed phase diagram for the system Fe-O.

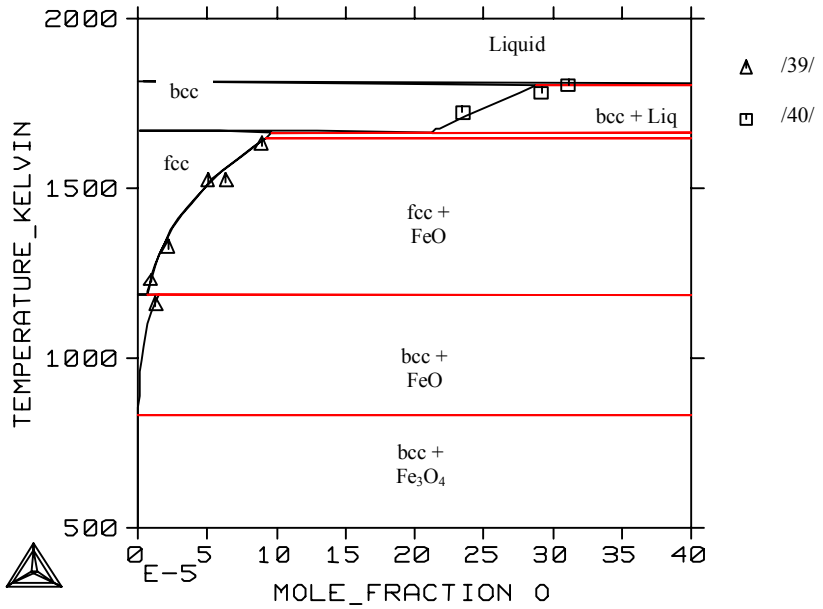


Figure 14. Oxygen solubility in solid iron.

## 5.5 System Cr-Ni

The system chromium-nickel has been optimised by Dinsdale /41/. The assessed phase diagram is shown in Figure 15. The calculated diagram is in very good agreement with the diagram expressed by Nash /42/, except for the intermetallic $Ni_2Cr$ phase which occurs at lower temperatures. This phase has a large stability region, 25 – 40 at-% of chromium, and it decomposes to nickel-rich fcc phase and chromium-rich bcc phase at 863 K.

Chromium has high solubility in solid nickel, up to 50 at-% at a eutectic temperature of 1618 K. The solubility of nickel in chromium is 32 at-% at eutectic temperature and it decreases dramatically at higher temperatures.

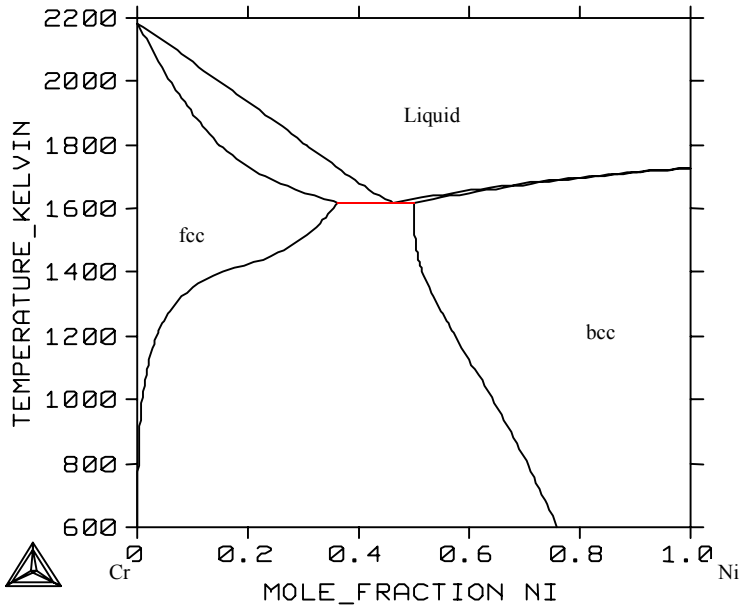


Figure 15. The assessed phase diagram for the system Cr-Ni.

## 5.6 System Cr-C

The optimised parameters for the system Cr-C have been taken from Andersson /43/. The calculated phase diagram has three stoichiometric phases with compositions $Cr_{23}C_6$, $Cr_7C_3$, and $Cr_3C_2$. In the literature these phases have been shown to have a remarkable deviation from stoichiometry. Also a metastable carbide formulated as $Cr_3C$ has been found. This phase has an orthorhombic crystal structure, isotypic with $Fe_3C$. Figure 16 shows the assessed phase diagram.

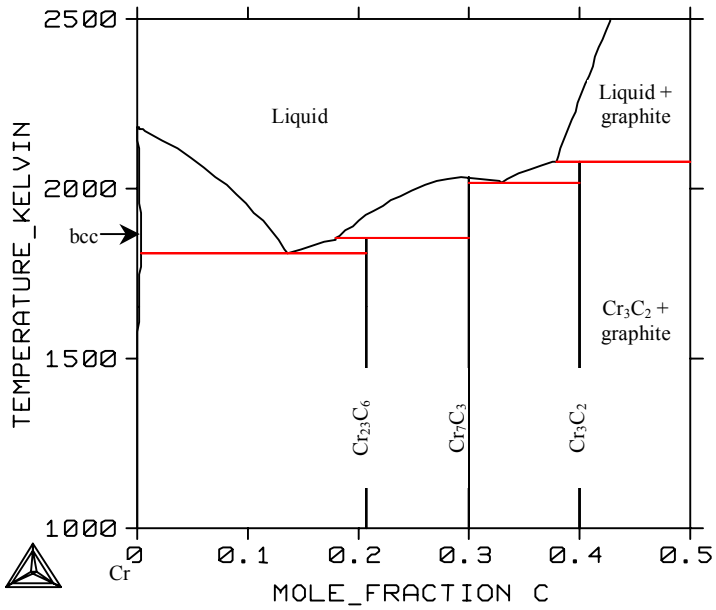


Figure 16. The assessed phase diagram for the system Cr-C.

## 5.7 System Cr-O

In the literature survey three different sets of parameters for the system Cr-O were found. Taylor et al. /12/ optimised this system using the ionic sublattice model for the liquid phase. The same workers made a new assessment /44/, only changing the description for the phase $Cr_3O_4$, which was described as a spinel phase with the compound energy model. Kowalski et al. /16/ optimised this system using the associate model for the liquid phase, but they used $CrO_{1.5}$ as the associate, which was not a good selection, as explained in Section 2.2.5. Therefore in this work the later optimisation of Taylor et al. has been used and its parameters for the liquid phase were transformed to those of the associate model, with associate $Cr_{2/3}O$. The interaction parameters for the liquid phase are shown in Table 2. The solubility of oxygen in solid chromium was described by Kowalski et al. /16/, using the sublattice model with oxygen on the interstitial sites. Their description correlating well with the experimental data was adopted as such.

Table 2. Interaction parameters for the liquid phase in the system Cr-O.

| Parameter | Value (J) |
|---|---|
| $^0L(Cr - Cr_{2/3}O)$ | 133892.3-54.1515*T |
| $^1L(Cr - Cr_{2/3}O)$ | 77153.7-15.4023*T |
| $^2L(Cr - Cr_{2/3}O)$ | -139752.9+60.2735*T |

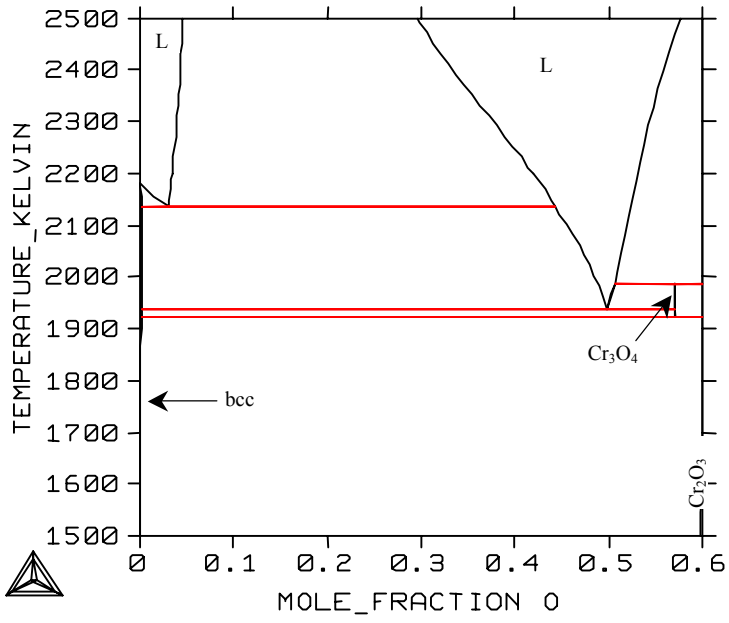


Figure 17. The assessed phase diagram for the system Cr-O.

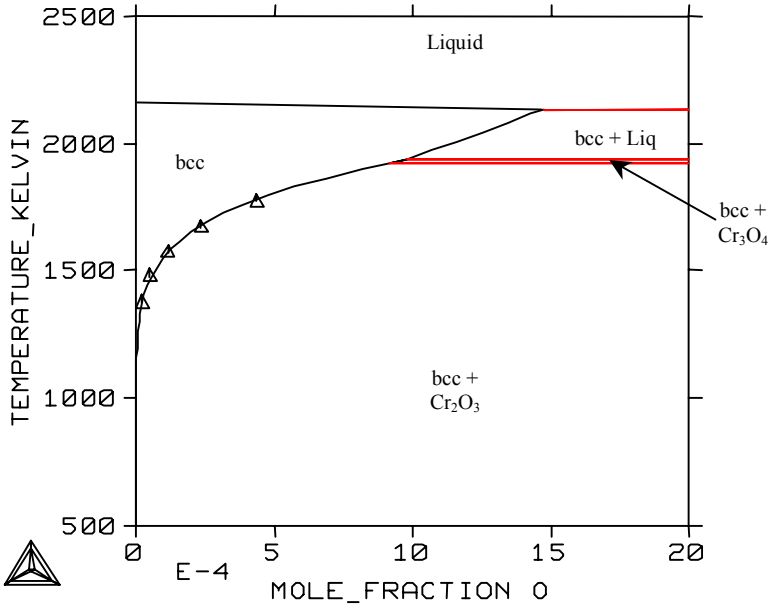


Figure 18. Oxygen solubility in solid chromium, experimental results taken from /45/.

## 5.8 System Ni-C

The binary system nickel-carbon has been optimised by Gabriel et al. /46/. These parameters give a phase diagram that is in very good agreement with the experimental diagram published in /35/. In this system there are no carbide phases. The solubility of carbon into the metallic nickel phase, as well as into the liquid phase, is shown in Figure 19.

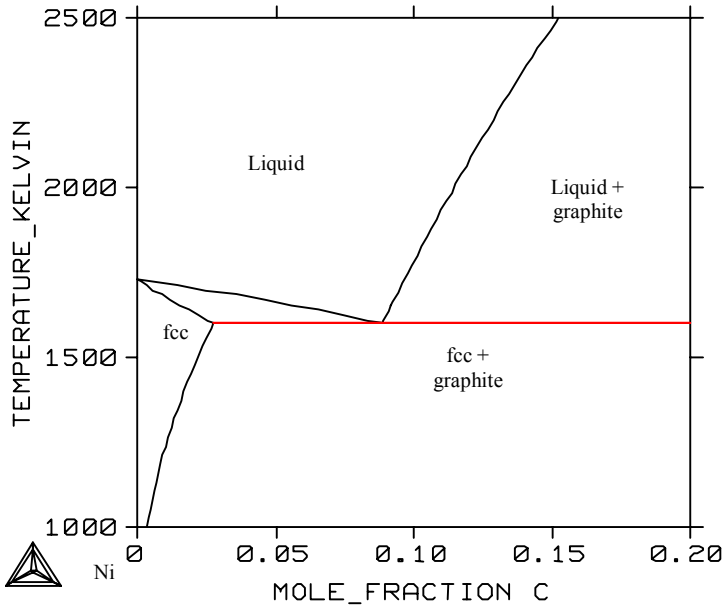


Figure 19. The assessed phase diagram for the system Ni-C.

## 5.9 System Ni-O

The most recent literature shows two sets of optimised parameters for the system Ni-O. Taylor et al. /12/ optimised this system using the ionic sublattice model for the liquid phase. Kowalski et al. /16/ used the associate model for the liquid phase. Luoma /47/ used the work by Taylor et al. optimising the ternary system Fe-Ni-O and therefore this work was used as the basis for the parameters for this system. The model parameters for the liquid phase were transformed to those of the associate model. The interaction parameters for the liquid phase are shown in Table 3. These parameters give good agreement with the experimental data. The solubility of oxygen in solid nickel was described by Kowalski et al. /16/, using the sublattice model with oxygen on the interstitial sites. Their description correlating well with the experimental data was adopted as such. Figure 20 shows the assessed phase diagram for the system Ni-O and Figure 21 the solubility of oxygen in solid metallic nickel.

Table 3. Interaction parameters for the liquid phase in the system Ni-O.

| Parameter | Value (J) |
|---|---|
| $^{0}$L(Ni – NiO) | 88355.5-25.1143*T |
| $^{1}$L(Ni – NiO) | -11457.4 |
| $^{2}$L(Ni – NiO) | 21039.8 |

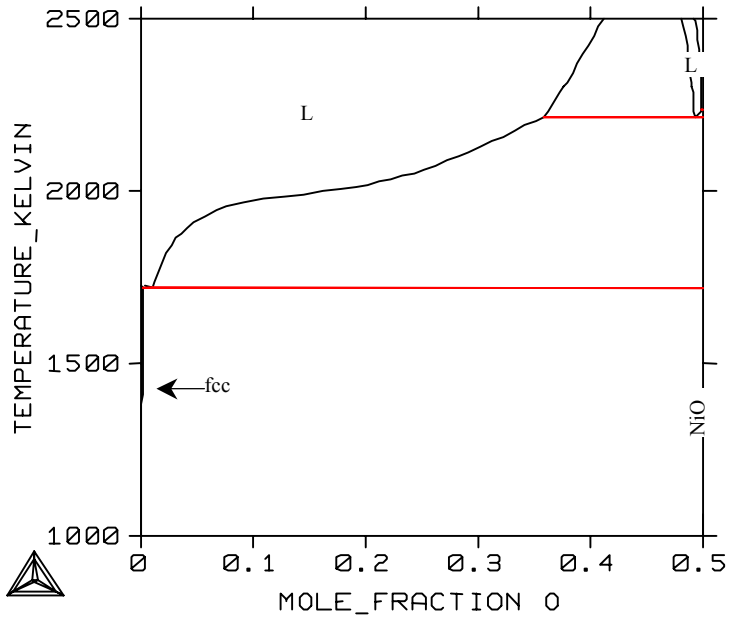


Figure 20. The assessed phase diagram for the system Ni-O.

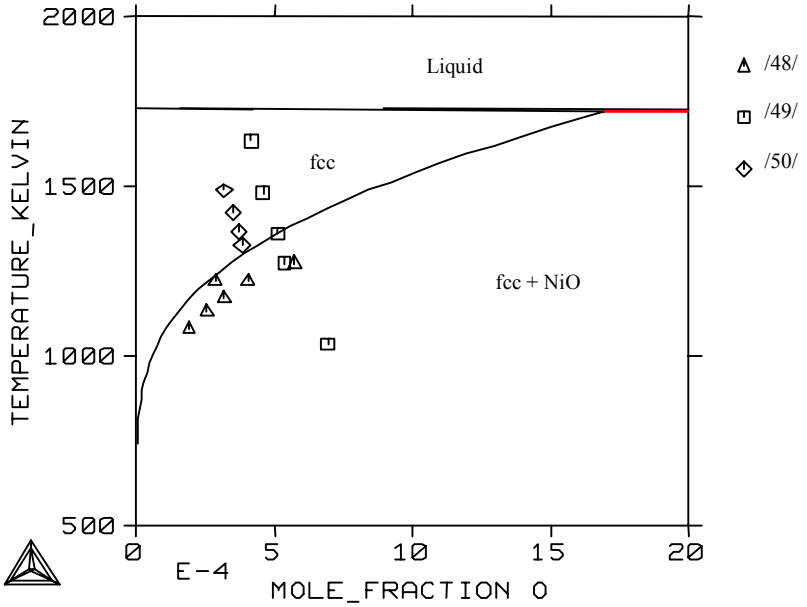


Figure 21. Oxygen solubility in solid nickel.

## 5.10 System C-O

In the system carbon-oxygen the only stable phases are gas and graphite. In this work oxygen is treated as insoluble in graphite. The gas phase is treated as an ideal gas mixture of $O_2$, CO, and $CO_2$. The thermodynamic data for these species are taken from the Thermo-Calc database, version M /36/. Other oxides of carbon are neglected.

# 6 TERNARY SYSTEMS

Most of the ternary systems have been taken from the Thermo-Calc database SSOL, version M /36/.

## 6.1 System Fe-Cr-Ni

In the Thermo-Calc database SSOL, version M contains optimised parameters for the system Fe-Cr-Ni, based on the study of Lee /51/. These parameters give a phase diagram at 1800 K, shown in Figure 22. This system is an almost ideal combination of its binary systems; the solid phases needed only one ternary parameter with temperature dependence and the liquid phase needed three parameters.

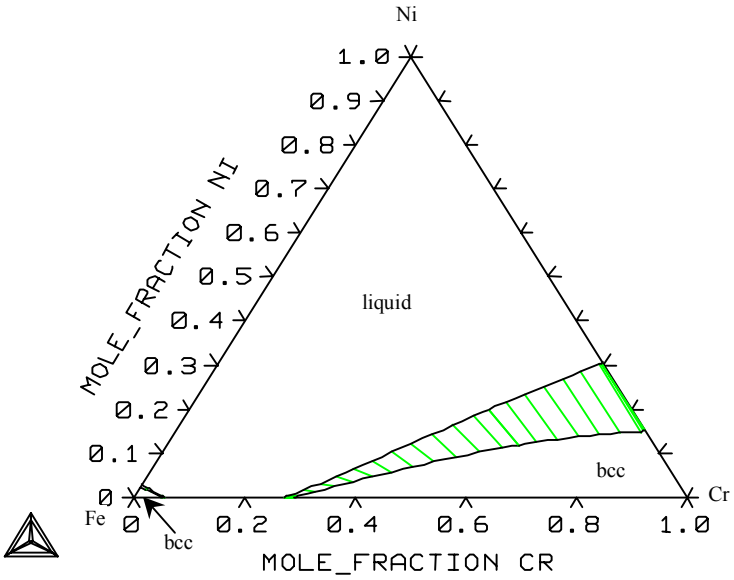


Figure 22. Isothermal section of the system Fe-Cr-Ni at 1800 K.

## 6.2 System Fe-Cr-C

The parameters for the system Fe-Cr-C have been taken from the Thermo-Calc database /36/, where the results from the study by Andersson /52/ are listed. Kowalski et al. made later modifications to the parameters of solid carbide phases. Figure 23 shows the isothermal section for this system at 1773 K, calculated with parameters given by Andersson.

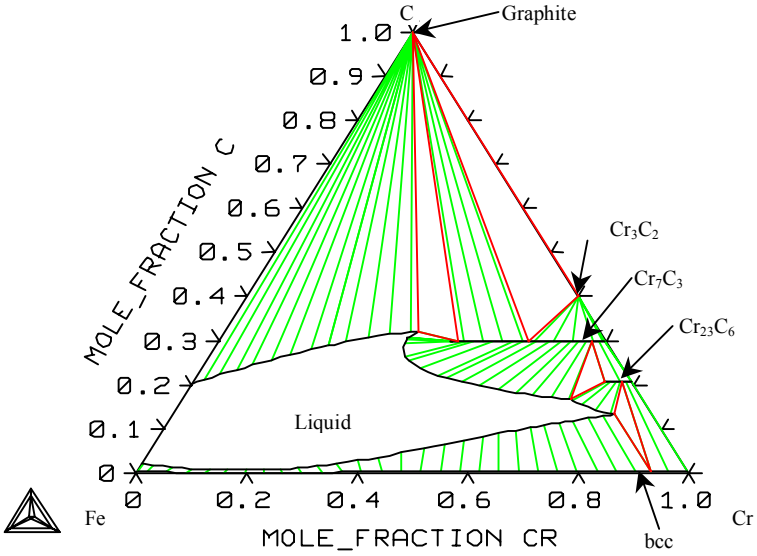


Figure 23. The assessed isothermal section for the system Fe-Cr-C at 1773 K.

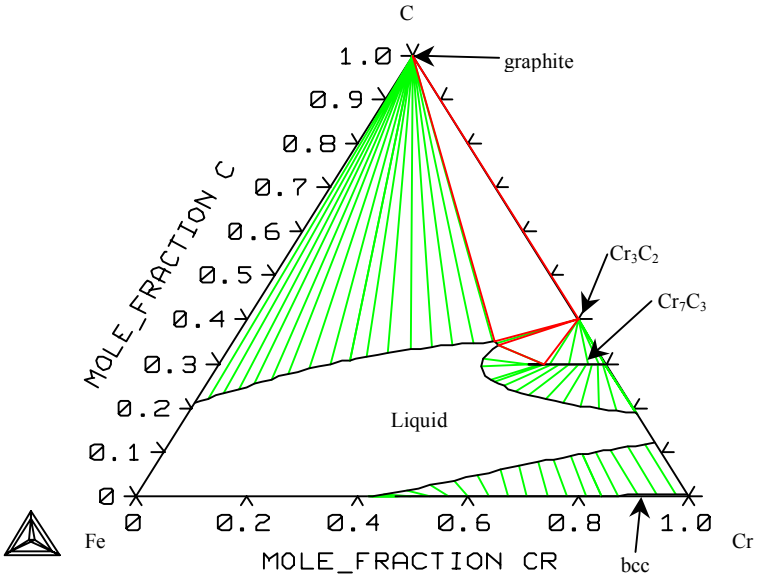


Figure 24. The assessed isothermal section of the system Fe-Cr-C at 1873 K.

## 6.3 System Fe-Cr-O

The ternary system Fe-Cr-O has been recently optimised by Luoma /53/ and Taylor et al. /44/ using the ionic liquid model for the liquid phase. The main difference between these two studies is the description of the spinel phase. Luoma did not include the divalent chromium in this phase and therefore the chromium oxide $Cr_3O_4$ had to be described as a stoichiometric oxide phase. Luoma also suggested that a distorted spinel does not exist. This phase was subsequently proved to exist later by Toker et al. /54/. In Taylor's study, the description of the spinel phase accounts for both a distorted spinel and chromium oxide $Cr_3O_4$. Therefore the assessed parameters for the spinel phase of Taylor et al. have been adopted for this work. The liquid phase was re-optimised because the model has been changed. The assessed interaction parameters for the liquid phase are shown in Table 4.

The solubility of oxygen in molten iron-chromium alloys has been measured by several authors /55-67/. The smallest solubility at 1600°C is 0.02 w-% at a composition of 7 w-% Cr /57/. The solubility is about the same according to other authors. The activity of oxygen in the liquid phase has also been measured by Janke et al. /68/, Geldenhuis et al./69/, Turkdogan /70/, Danilovich et al. /71/, and Sabirzyanov /72/. Adachi et al. /73/ and Iwamoto et al. /74/ measured the phase diagram at 1600°C.

A solid alloy in equilibrium with spinel and chromium oxide contains 2 w-% chromium at 1300°C. The chromium content will increase to 5-7 w-% at 1500-1700°C /75/. The melting point of the spinel phase was found to be 2100°C by Muan et al. /76/. Riboud et al. /77/ found a similar value, but they claim that it will melt congruently. They also found the solubility of $Cr_2O_3$ to wüstite to be 7 w-% at 1420°C, where the wüstite melts. Muan et al. /76/ also measured the stability regions of spinel and sesquioxide in air. Snethlage et al. /78/ measured the tielines between the solid oxides at 1000, 1095, and 1200°C. Webber /79/ measured the stabilities of solid oxides. Skala et al. /80/ studied the Gibbs energies of the formation of oxides by EMF technique.

Shaklin et al. /81, 82/ and Fujii et al. /83/ measured the activity of oxygen in wüstite. They found the solubility of chromium to be 1.9 w-% at 1000°C. Activities in the two-phase region have been measured by several authors /84-96/. Petric at al. /85/ also gave values for the preference energies of octahedral sites for trivalent cations. The Gibbs energy of the formation of chromite ($FeCr_2O_4$) has been measured by Shaklin et al. /81/, Kazin et al. /97/, Novokatshii et al. /98/, Linchevsky et al. /99/, and Zabeivorota et al. /100/.

Table 4. The assessed interaction parameters for the liquid phase in the system Fe-Cr-O.

| Parameter | Value (J) |
|---|---|
| ${}^0L(Cr - FeO)$ | -20345.551 |
| ${}^0L(Cr - FeO_{1.5})$ | 110000 |
| ${}^0L(Cr_{2/3}O - Fe)$ | 118897.9 |
| ${}^0L(Cr_{2/3}O - FeO)$ | 10000 |

In Figure 25 the calculated isothermal section at 1573 K is shown. The calculated section is in very good agreement with the experimental data. The only difference is in the solid metallic phases. Seybolt /91/ suggested that the spinel phase is also in equilibrium with the bcc phase, but in later studies /84,32/ the corundum phase was found to be in equilibrium with fcc iron. This difference can also be seen in an oxygen pressure diagram, which is shown in Figure 26. The oxygen pressures at the three phase equilibria are listed in Table 5 for comparison with the selected values from /32/.

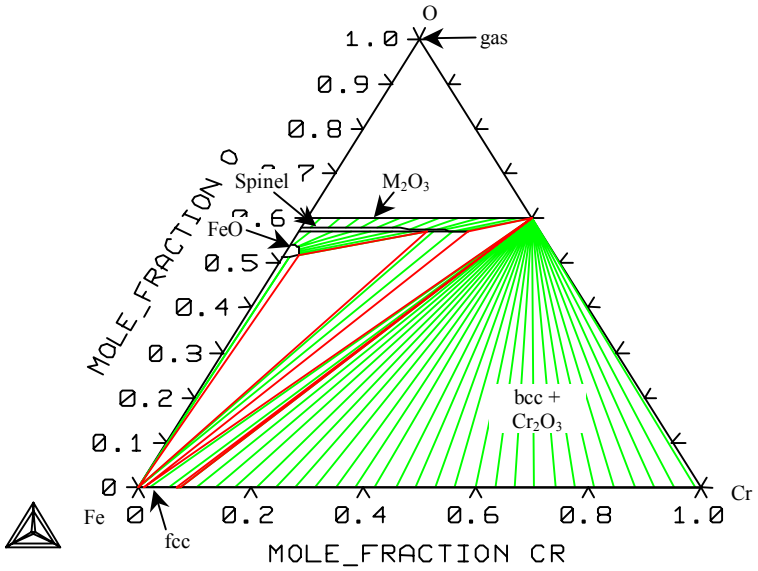


Figure 25. The isothermal section of the system Fe-Cr-O at 1573 K.

Table 5. Oxygen pressure at three phase equilibriums at 1573 K

| Phases in equilibrium | log $p_{O_2}$ | Log $p_{O_2}$ /32/ |
|---|---|---|
| fcc + FeO + Spinel | -10.81 | -10.7 |
| fcc + Spinel + $Cr_2O_3$ | -13.52 | -13.2 |
| fcc + bcc + $Cr_2O_3$ | -14.67 | -14.5 |

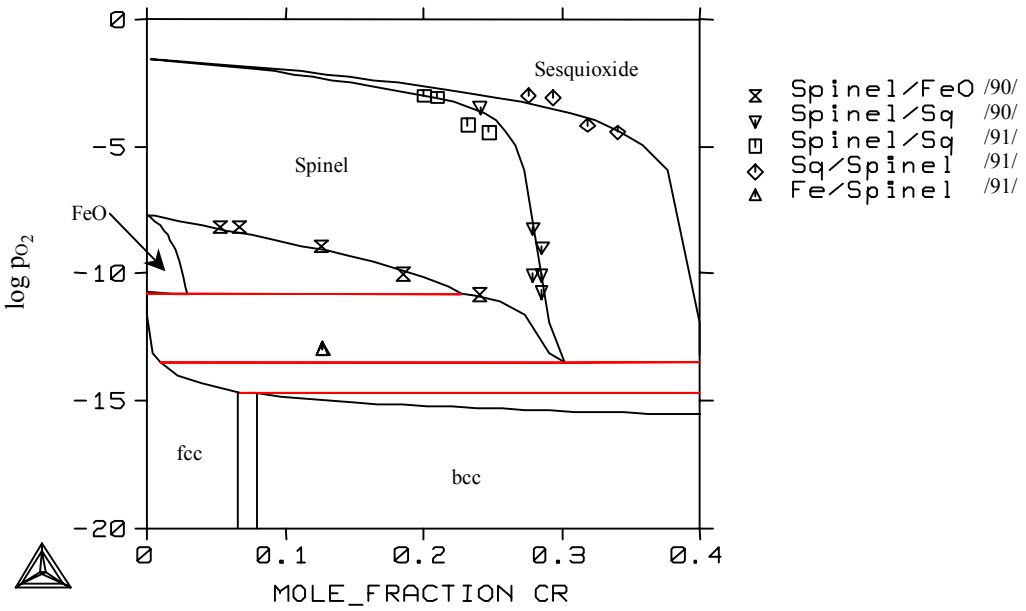


Figure 26. The oxygen pressure diagram of the system Fe-Cr-O at 1573 K.

The isothermal section at 1873 K is shown in Figure 27. The solubility of oxygen in metallic liquid at 1873 K is shown in Figure 28 and the activity of oxygen in equilibrium with solid oxides in Figure 29, with the experimental values. The calculated values are in good agreement with the experimental values. The minimum solubility of oxygen was calculated to be 0.03 w-% at 8 w-% of chromium.

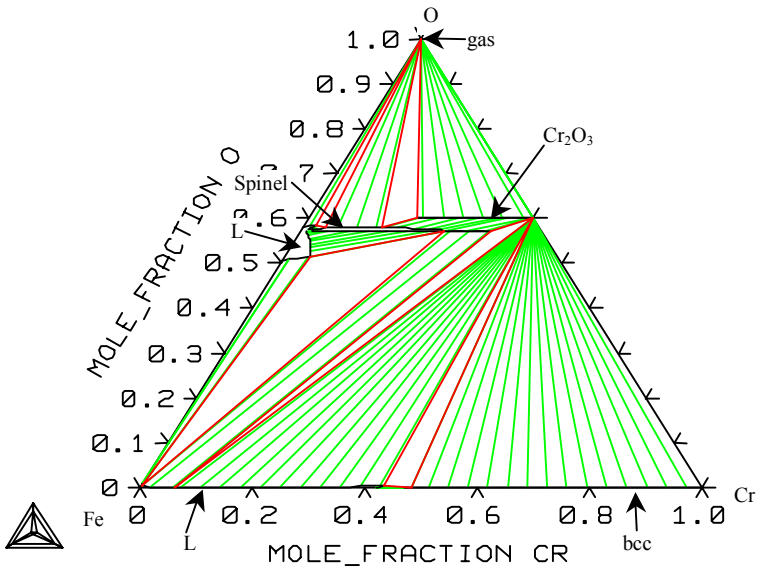


Figure 27. The isothermal section of the system Fe-Cr-O at 1873 K.

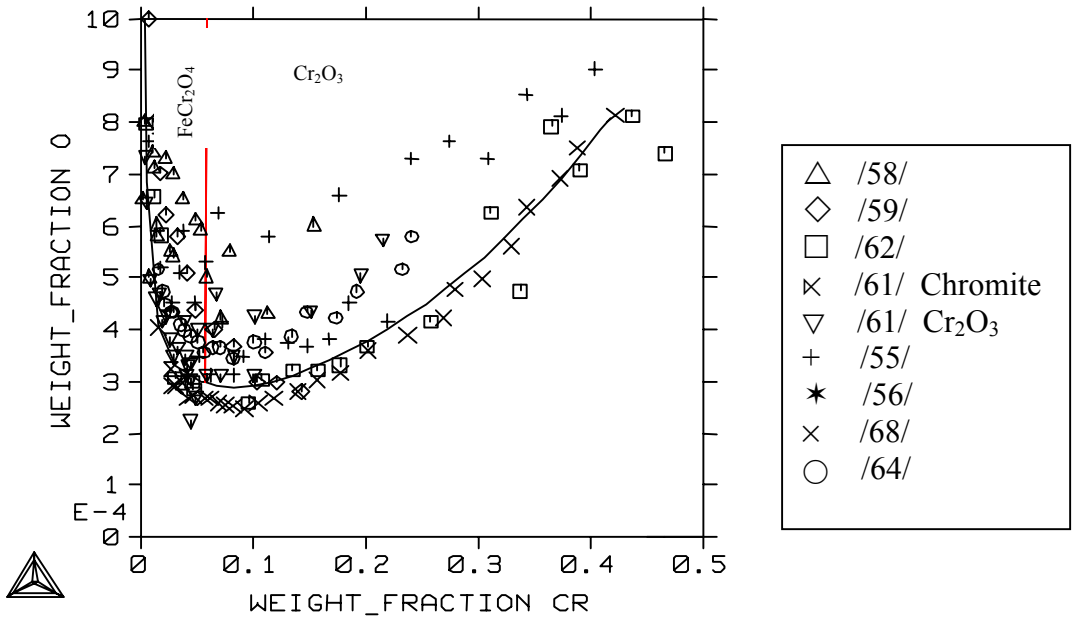


Figure 28. Solubility of oxygen in molten Fe-Cr alloys at 1873 K.

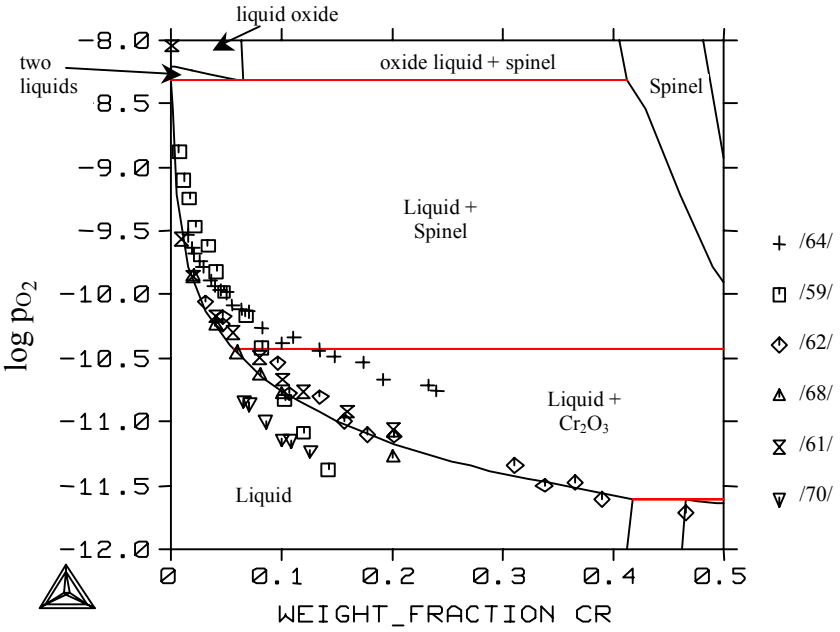


Figure 29. Oxygen pressure in liquid Fe-Cr alloys at equilibrium with solid oxides at 1873 K.

## 6.4 System Fe-C-O

The most recent large literature survey on the system Fe-C-O was carried out by Raghavan /32/. According to this work, most of the studies that have been made are on solid phase equilibria. In that area these binary systems define the whole system, because the solubility of the third component in the binary compounds is negligible.

The carbon-oxygen equilibrium in molten iron has also been studied by many authors /32/. Matoba /101/ and Schenck /102/ also review the results of other studies in this area. These studies show the solubility of oxygen to be at its minimum in at 2 w-% of carbon. To reproduce this behaviour ternary interaction parameters were assessed; they are shown in Table 6. Figure 31 shows the solubility of oxygen in molten iron-carbon alloys at temperatures of 1873 K and 2223 K, together with experimental values by /102, 103, 104/. The calculated values are in very good agreement with the experimental values.

Table 6. The assessed interaction parameters of the liquid phase in the system Fe-C-O.

| Parameter | Degree | Value (J) |
|---|---|---|
| $^{0}$L(C – FeO) | 0 | -338280.519 |
| $^{1}$L(C – FeO) | 1 | -274890.49 |

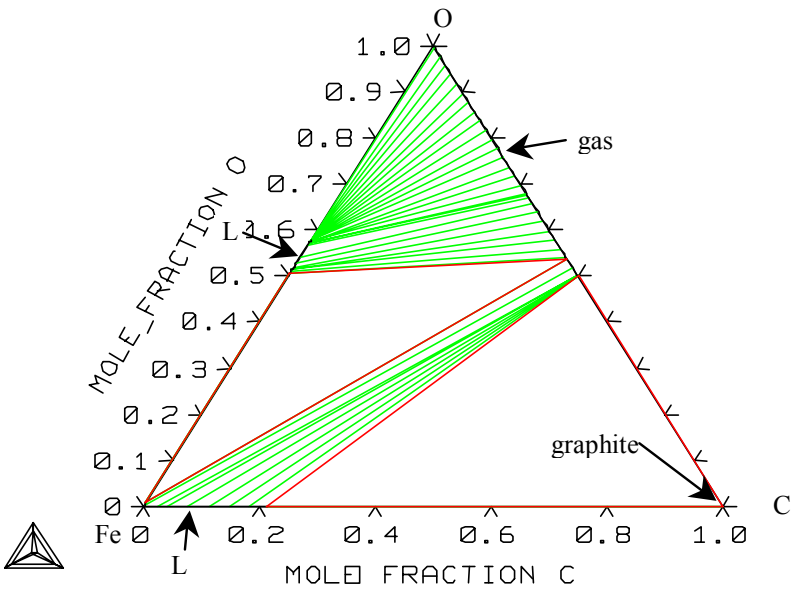


Figure 30. The assessed system Fe-C-O at 1873 K.

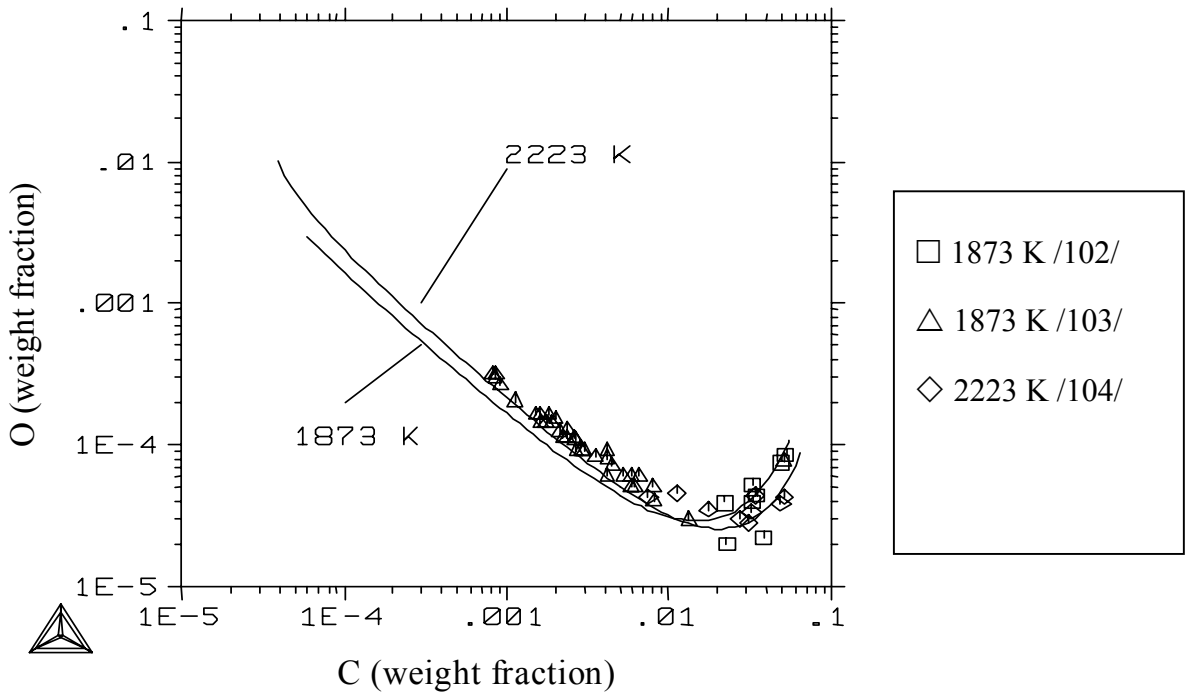


Figure 31. Solubility of oxygen in molten iron-carbon alloys at temperatures of 1873 and 2223K.

## 6.5 System Fe-Ni-C

The parameters for this system have been taken from the Thermo-Calc database /36/, based on the study of Gabriel et al. /105/. This system needed ternary parameters in all phases to reproduce the phase diagram shown in Figure 32. There are no carbide phases stable in the binary systems, nor in the ternary system.

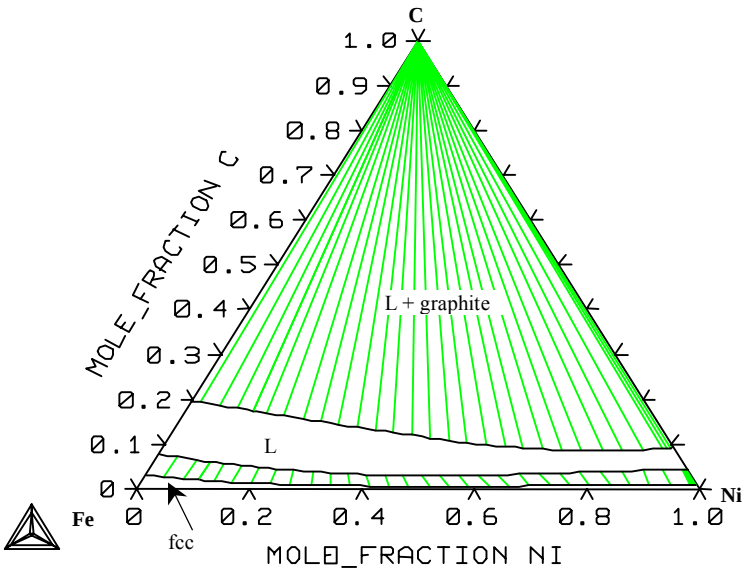


Figure 32. The assessed phase diagram of the system Fe-Ni-C at 1673 K.

## 6.6 System Fe-Ni-O

The topology of the ternary system Fe-Ni-O is not well known. Most of the experimental studies are limited to the temperature region near 1273 K and the liquid phase at 1773–1873 K. A good literature survey on the system has been carried out by Raghavan /32/. It has previously been assessed by Pelton et al. /106/ and Luoma /47/. Luoma used the ionic liquid model for the liquid phase and therefore this phase was reassessed using the associate model. The assessed parameters are shown in Table 7.

Liquidus lines have been measured by several authors in the metal-rich area at 1773–1873 K /107-113/. Koch /107/, von Bohlen u. Hallbach /114/, and Tsemekhman et al. /115/ measured the tielines between co-existing metallic and oxidic liquid phases in the temperature range 1773–1873 K. In the oxidic area the liquidus surface giving the melting point of the spinel phase has been measured by Shafer /116/. Fisher et al. /117, 118/ and Tankins et al. /119/ measured the activity coefficient in liquid Fe-Ni solutions.

Phase relationships in the wüstite region have been measured by many authors /120-127/. The maximum solubility of nickel in wüstite was found to be 0.07 at-% at 973 K /121/ and 1.2 at-% at 1373 K /126/. Trinel-Dufour /127/ reported a higher maximum value of 2.2 at-% at 1000°C. The solubility values of iron in nickel oxide in the literature are scattered, giving solubilities between 6.5 /124/ and 13.8 at-% /126/ at 1273 K /125, 128, 129/.

The spinel phase forms a continuous solid solution between magnetite ($Fe_3O_4$) and nickel ferrite ($NiFe_2O_4$) /32/. The melting point has been noted to increase linearly from that of magnetite (1870 K) to about 2013 K at a composition of $NiFe_2O_4$/116/. The homogeneity range on the oxygen-rich side decreases to a negligible width as the composition approaches nickel ferrite /116, 130/. Chachanidze /131/ measured the heat capacity and enthalpy for $NiFe_2O_4$. Similar values can be found from Brain et al. /132/. Many authors have measured the tie-lines between the spinel and other solid phases at 1273 K /125, 126, 129, 133-145/. The activity of magnetite and nickel ferrite in the solid solution was measured by Katayama et al. /146/, Paladino /142/, and Tretyakov /147/.

No solubility of nickel in hematite was reported /32 /.

Table 7. The assessed parameters for the liquid phase in the system Fe-Ni-O.

| Parameter | Value (J) |
|---|---|
| ${}^0L(Fe - NiO)$ | 123778.83 |
| ${}^0L(FeO - Ni)$ | 78655.777 |
| ${}^0L(FeO_{1.5} - Ni)$ | 110000 |

Figure 33 shows the isothermal section at 1273 K. The calculated section is in very good agreement with the experimental data. An oxygen pressure diagram is shown in Figure 34 and the spinel area is shown in Figure 35, including the activity of oxygen as log $p_{O_2}$ in the same area, together with the experimental points.

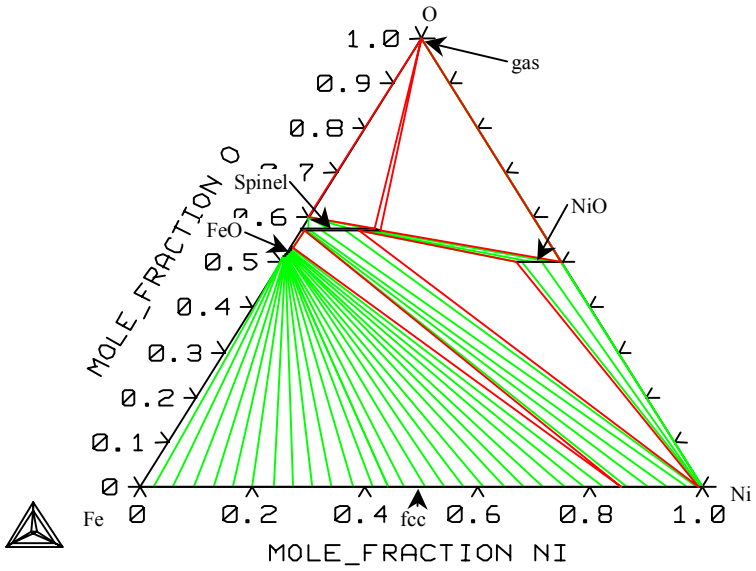


Figure 33. Isothermal section of the system Fe-Ni-O at 1273 K.

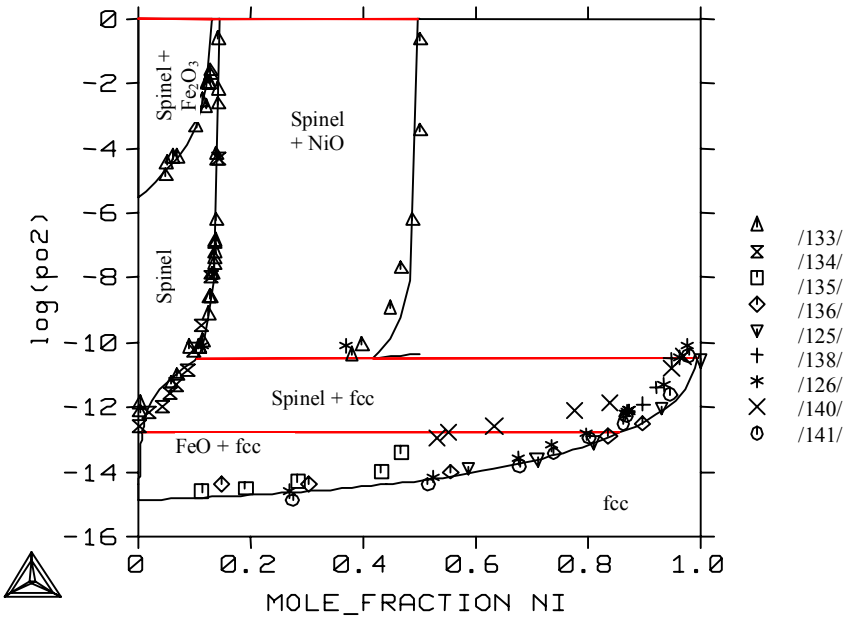


Figure 34. Oxygen pressure diagram of the system Fe-Ni-O at 1273 K.

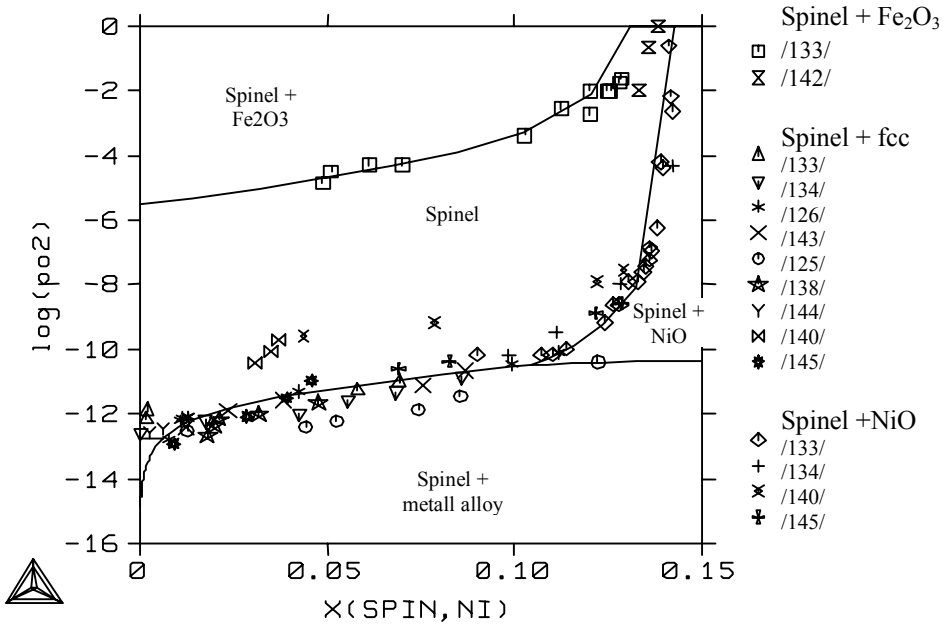


Figure 35. Spinel area of the system Fe-Ni-O at 1273 K.

Figure 36 shows the calculated solubility of nickel in wüstite with the experimental points and Figure 37 shows the solubility of iron in bunsenite with experimental values. As can be seen, the experimental values in Figure 37 are very scattered and show remarkable deviation from calculated values.

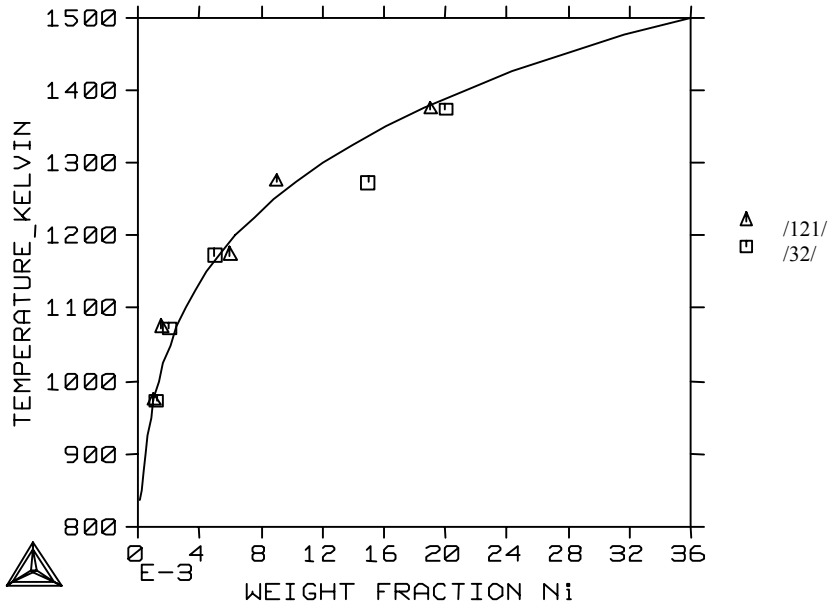


Figure 36. Solubility of nickel in wüstite in the system Fe-Ni-O.

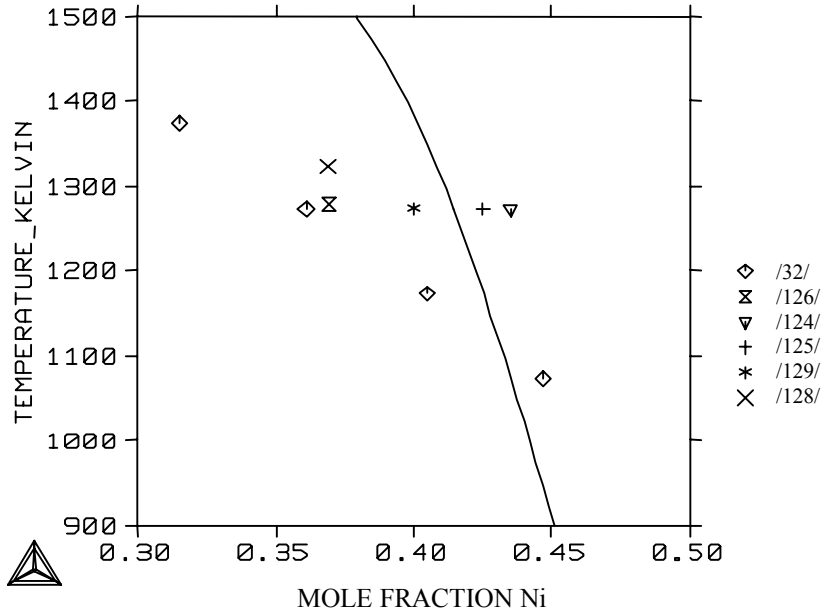


Figure 37. Solubility of iron in bunsenite in the system Fe-Ni-O.

Figure 38 shows an isothermal section at 1813 K and Figure 39 the solubility of oxygen in liquid metal alloys, together with the experimental values. The calculated values are in agreement with the experimental ones measured using an $Al_2O_3$-crucible. Values measured using a $SiO_2$ crucible gave lower solubility, due to the solubility of $SiO_2$. Figure 40 shows the activity coefficient $\gamma^0_O$ at 1873 K versus nickel content in the liquid alloys.

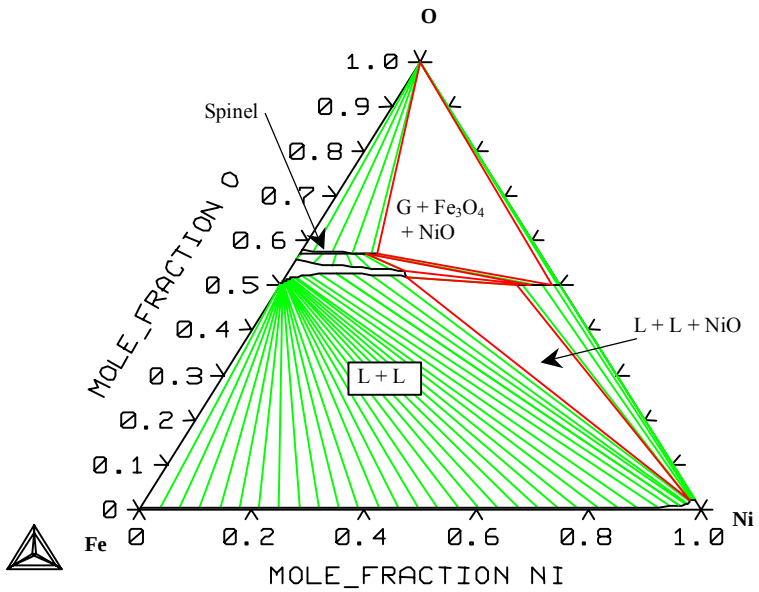


Figure 38. The isothermal section of the system Fe-Ni-O at 1813 K.

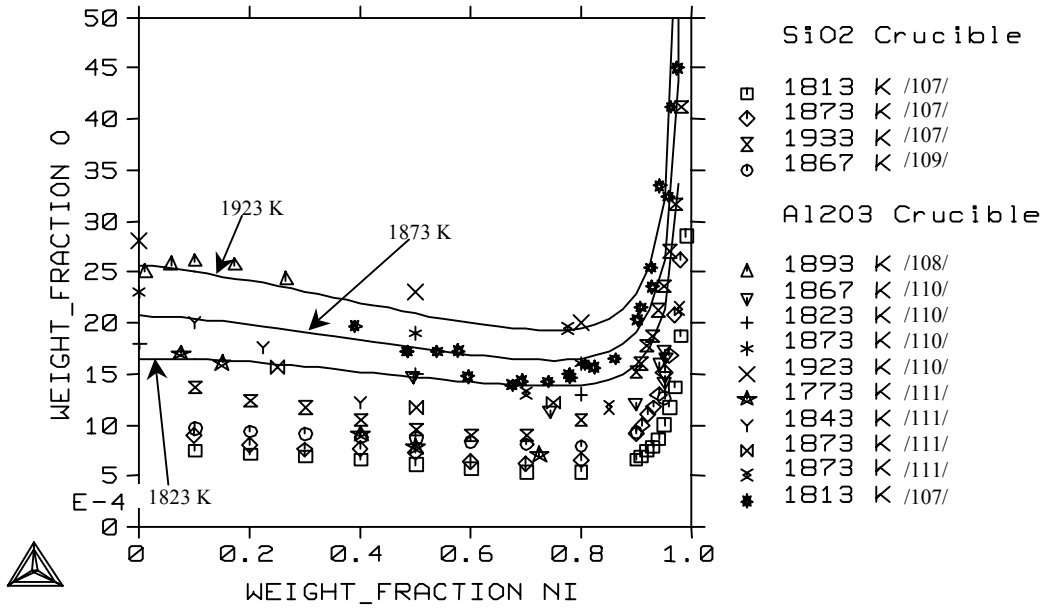


Figure 39. Solubility of oxygen in molten Fe-Ni alloys.

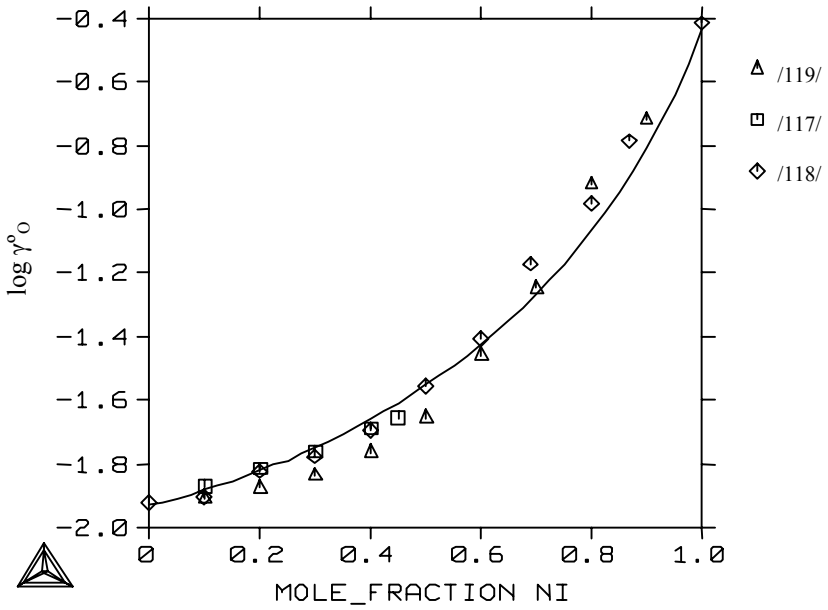


Figure 40. Activity coefficient $\gamma^0_O$ in liquid alloys of the system Fe-Ni-O at 1873 K.

The calculated phase diagrams and thermodynamic properties are in good agreement with the experimental ones, except for the bunsenite area, where the experimental values are very scattered. The high solubility of iron in bunsenite, as reported by Raghavan /32/, conflicts with measured liquid areas at higher temperatures and therefore the values given by Trinel-Dufour /129/ are more likely. Raghavan also suggested that there is no miscibility gap on the nickel-rich side in the liquid phase at temperature 1813 K and made no suggestions concerning the stability of bunsenite at that temperature. In the other publications this area has been reported as being similar to the calculated diagram.

The solubility of oxygen in liquid alloys was measured using three different crucibles. The lowest values were found using a $SiO_2$ crucible and the highest values using $Al_2O_3$-crucible. A CaO crucible gave values between these two. According to Koch /107/, the solubility of $SiO_2$ and CaO in oxide melt is very high, up to 40 w-%, at these temperatures, while the solubility of $Al_2O_3$ is much lower, less than 15 w-%. It is obvious, therefore, that the results obtained using an $Al_2O_3$ crucible are more reliable for the system Fe-Ni-O. However, this solubility gave rise to a considerable uncertainty regarding the measurements in this area of the phase diagram.

## 6.7 System Cr-Ni-C

The system chromium-nickel-carbon has been optimised at National Physical Laboratory (NPL) and published in the Thermo-Calc database, version M. The assessed phase diagram at 1800 K is shown in Figure 41. Nickel has a remarkable solubility in carbides $Cr_{23}C_6$ and $Cr_7C_3$.

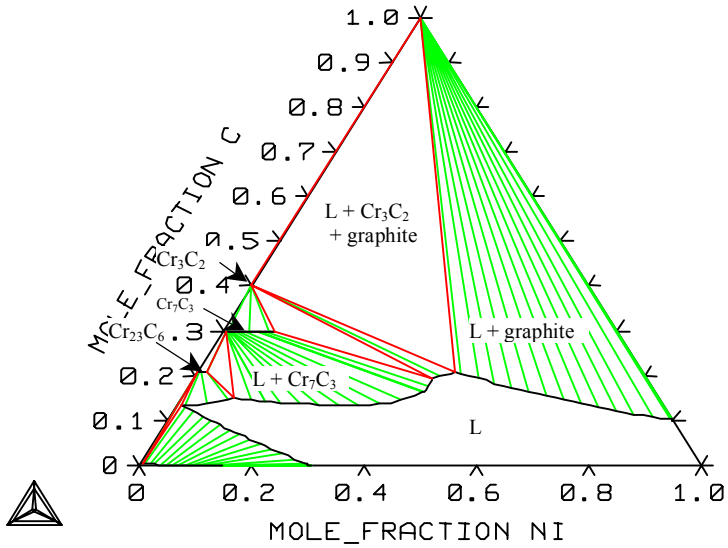


Figure 41. The assessed phase diagram for the system Cr-Ni-C at 1800 K.

## 6.8 System Cr-Ni-O

Taylor et al. /12/ have recently optimised the system Cr-Ni-O, using the partially ionic liquid model for the liquid phase. Therefore the liquid phase was reoptimised in this work using the associate model. The parameters of the solid phases were able to be used, as they were optimised.

Experimental information for the liquid phase was limited to the metal-rich area. Sakao et al. /148/ measured oxygen activities in melts by $H_2/H_2O$ equilibration at 1873K. They also measured oxygen activities and the solubility of oxygen at solid oxide phase saturation. Similar measurements were also made by Averin et al. /149/ at 1873 K, while Heinz et al. /64/ measured the solubility of oxygen and oxygen activity using the EMF method in a chromium oxide crucible at three temperatures. The results from all three groups are generally in good agreement. Belov et al. /150/ measured oxygen contents at saturation and investigated the solid phases present at equilibrium.

To reproduce these measurements only three new parameters were optimised, the binary interactions between metal and oxide associates and the ternary interaction between metals and chromium oxide in liquid. These parameters are listed in Table 8.

Table 8. The assessed interaction parameters for the liquid phase in the system Cr-Ni-O.

| Parameter | Value (J) |
|---|---|
| ${}^0L(Ni\text{-}Cr_{2/3}O)$ | 121951.851 |
| ${}^0L(Cr\text{-}NiO)$ | -141604.059 |
| ${}^0L(Cr\text{-}Ni\text{-}Cr_{2/3}O)$ | -164288.559 |

Figure 42 shows the calculated isothermal section at 1873 K. The calculated phase diagram is in very good agreement with the diagram given by Taylor et al. /12/. Only the solubility of oxygen at higher chromium content is higher.

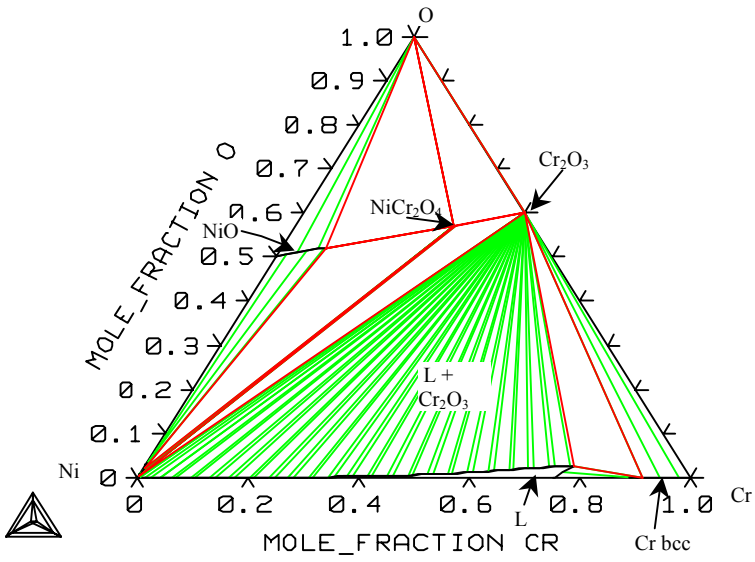


Figure 42. Isothermal section of the system Ni-Cr-O at 1873 K.

The solubility of oxygen in molten Ni-Cr alloys is shown in Figure 43 together with experimental points by Belov /150/, Averin /149/, and Heinz /64/. The calculated values of Sakao /148/ assume the $Cr_3O_4$ to be a stable oxide phase at that temperature and therefore their values are not strictly comparable. The assessed parameters reproduce quite well the values measured by Heinz. The measured solubility is very low at 2 at-% chromium and the assessed parameters give a solubility which is slightly higher than Averin's values.

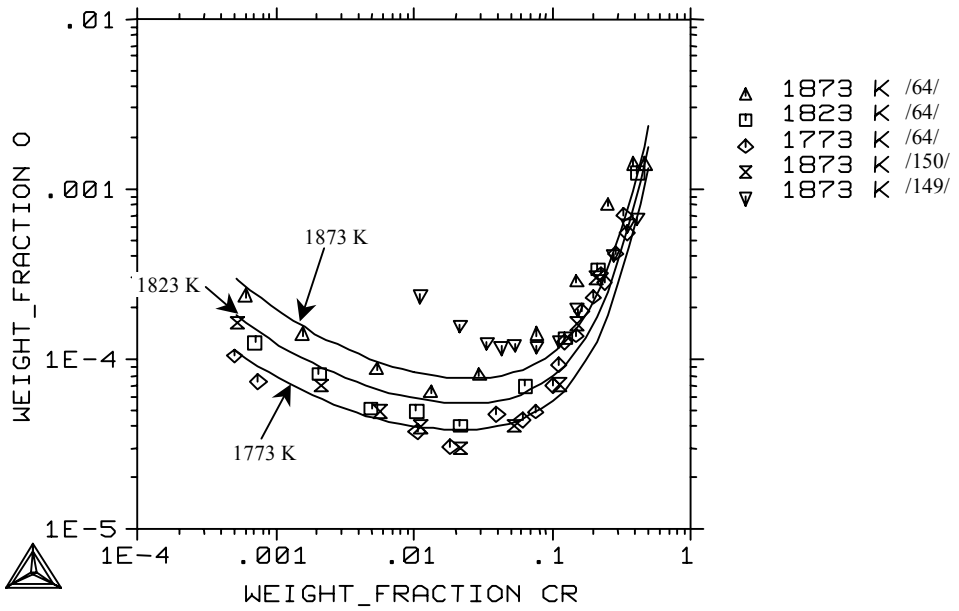


Figure 43. Calculated solubility of oxygen in molten Ni-Cr alloys in equilibrium with $Cr_2O_3$.

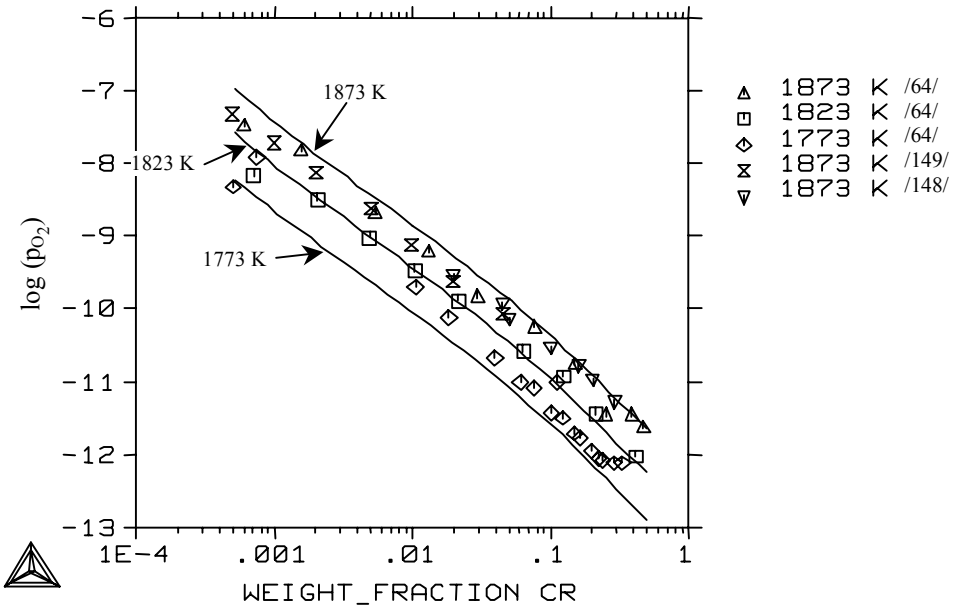


Figure 44. Calculated oxygen pressures in molten Ni-Cr alloys in equilibrium with $Cr_2O_3$.

The calculated oxygen pressure diagram of the system Cr-Ni-O at 1873 K is shown in Figure 45 together with experimental points. The calculated values are in very good agreement with the measured points.

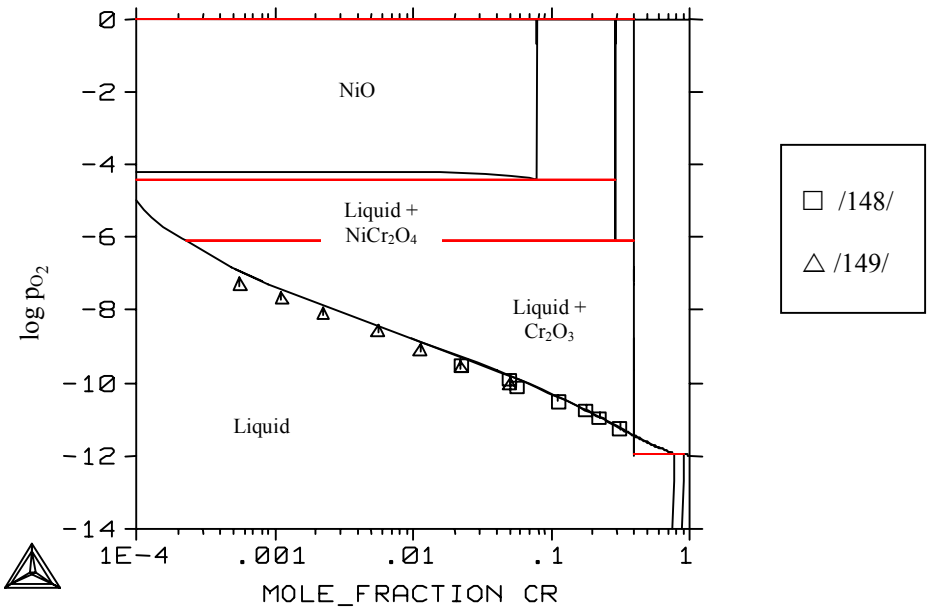


Figure 45. Calculated oxygen pressures in the system Ni-Cr-O at 1873 K.

Figure 46 shows the calculated activity coefficient of oxygen at infinite dilution in liquid Ni-Cr alloys at 1873 K together with points measured by Sakao et al. /148/. The assessed parameters do not reproduce the experimental points very well. At chromium content 15 – 30 at-% the calculated values are higher than the measured values.

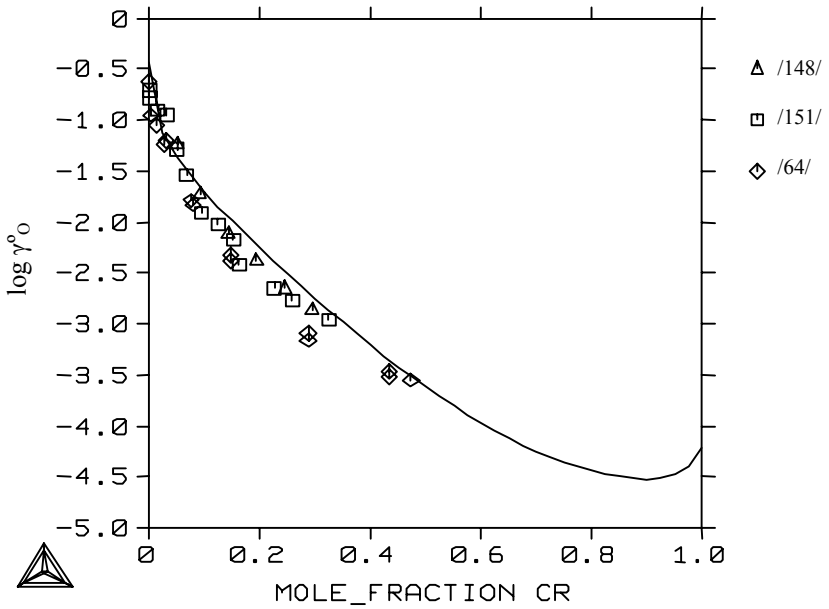


Figure 46. Calculated activity coefficient of oxygen at infinite dilution in liquid Ni-Cr alloys at 1873 K.

## 6.9 System Cr-C-O

All the experimental data for the system Cr-C-O are about the stoichiometric condensed phase. These are all consistent and present the same Ellingham diagram as published by Worrel /152/. The calculated diagram in Figure 48 is in very good agreement with this diagram.

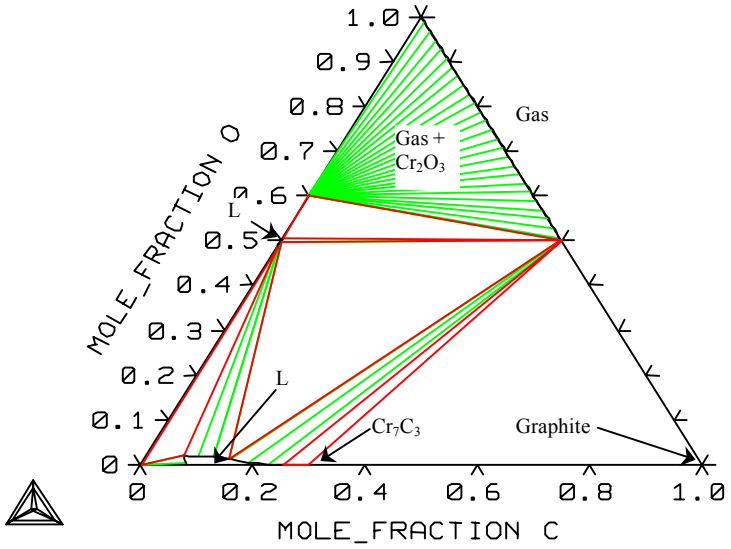


Figure 47. The assessed phase diagram for the system Cr-C-O at 2000K.

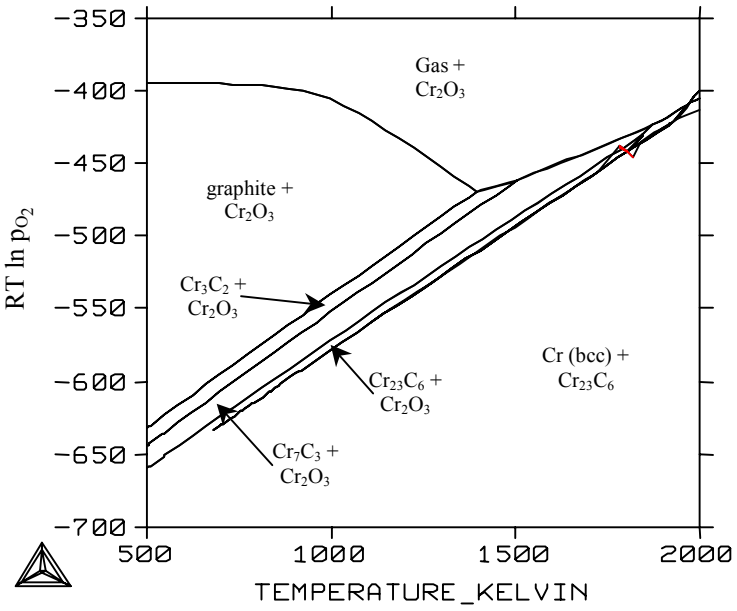


Figure 48. The diagram of carbides in the system Cr-O-C at pressure of 101325 Pa.

## 6.10 System Ni-C-O

The system nickel-carbon-oxygen is not well known. All the published data relate to a liquid phase in equilibrium with a gas phase. Artemov et al. /104/ have studied the solubility of oxygen in different carbon-containing melts at 2223 K. Artemov et al. /153/ have also measured solubility at temperatures of 1773 and 2193 K. Bochova et al. /154/ measured solubility at 1623 and 1803 K. In these studies the activity of components is also published. Bochova et al. reported the solubility at 1803 K to be much higher than did the other studies, which are in mutual agreement. These studies show that the solubility of oxygen rises when the carbon content is increased. To reproduce this behaviour five new parameters were optimised for the liquid phase, and these parameters are shown in Table 9. Figure 49 shows the calculated solubility of oxygen in melt together with experimental values. These calculated values are in good agreement, with the exception of Bochova's values at 1803 K. At a higher oxygen content there are no experimental data available.

Figure 50 shows the calculated phase diagrams at 1803 K.

Table 9. The assessed parameters for the liquid phase in the system Ni-C-O.

| Parameter | Value (J) |
|---|---|
| $^{0}$L(C-NiO) | 2481654.98 |
| $^{1}$L(C-NiO) | -1263008.08 |
| $^{0}$L(C-Ni-NiO) | -1520323.47 |
| $^{1}$L(C-Ni-NiO) | -4216172.34 |
| $^{2}$L(C-Ni-NiO) | 4130732.78 |

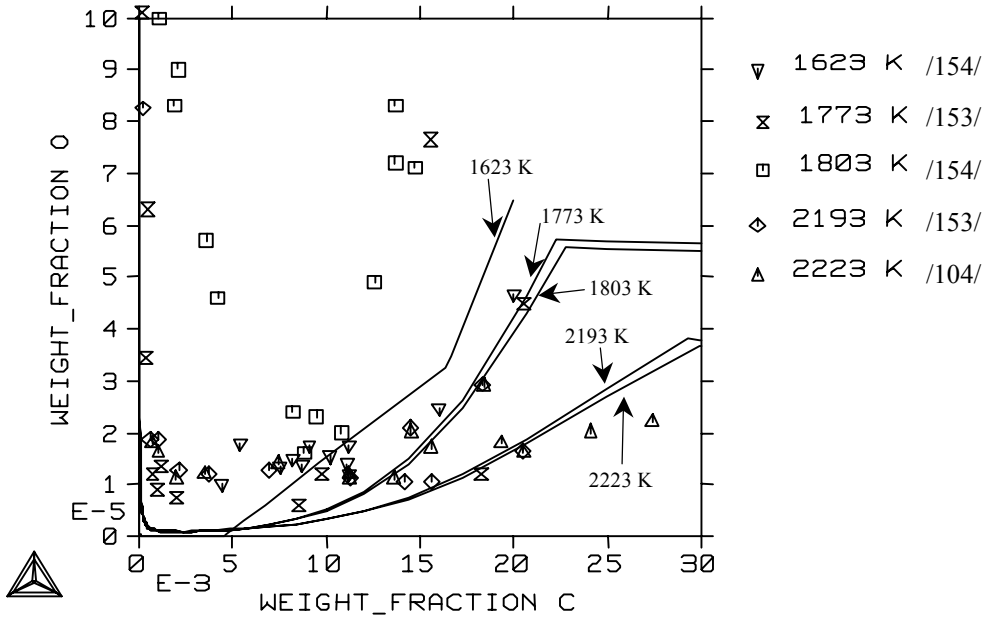


Figure 49. The solubility of oxygen to liquid Ni-C alloys in equilibrium with the gas phase.

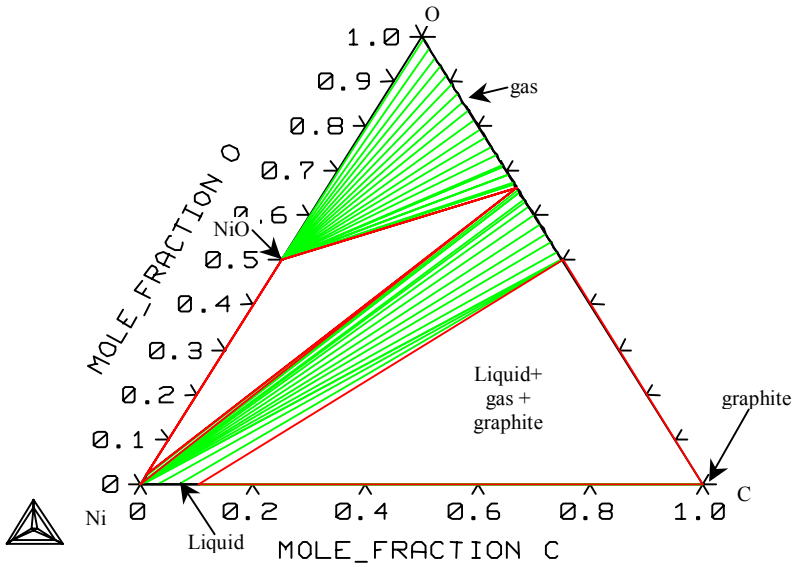


Figure 50. The assessed phase diagram for the system Ni-C-O at 1803 K.

# 7 QUATERNARY SYSTEMS

## 7.1 System Fe-Cr-Ni-C

The thermodynamic description of the quaternary system Fe-Cr-Ni-C has been taken from the Thermo-Calc database, based on the unpublished revision by Lee /51/. These parameters give a phase diagram agreeing well with the experimental data.

## 7.2 System Fe-Cr-Ni-O

There are only a few sources of experimental data for the quaternary system Fe-Cr-Ni-O. Shevtsov /155/ and Heinz /64/ measured the solubility of oxygen in molten iron-chromium alloys with different nickel contents at temperatures of 1873 K and 1823 K. These two studies gave very similar results. They found that increasing the amount of nickel decreases the solubility of oxygen. Ma /156/ calculated oxygen reactions in Fe-Cr-Ni melts and Laag /157/ studied oxygen activity in Fe-Cr-Ni melts without any experimental measurements. Laag used the Wagner formalism for the liquid phase, and suggested that there is a need for a quaternary interaction parameter. In this work no quaternary parameters were needed to reproduce the experimental data and therefore it is possible that the present model for the liquid phase describes the liquid phase better.

Figure 51 shows the solubility of oxygen in molten Fe-Ni-Cr alloys in equilibrium with $Cr_2O_3$ at 1873 K together with experimental points from /155/ and Figure 52 at 1823 K with experimental points from /64/.

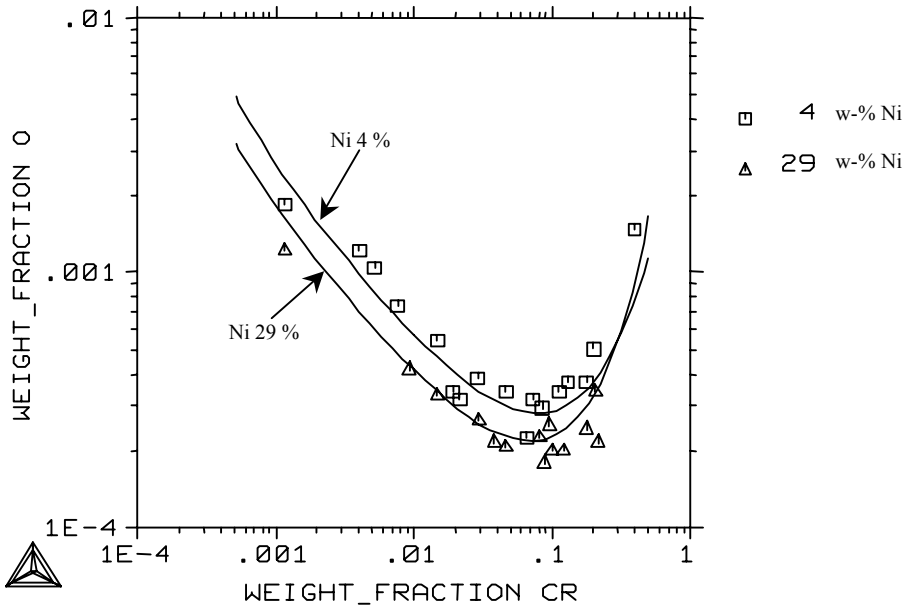


Figure 51. Solubility of oxygen in molten Fe-Cr-Ni alloys at 1873 K in equilibrium with $Cr_2O_3$ with different nickel content. Experimental values from /155/.

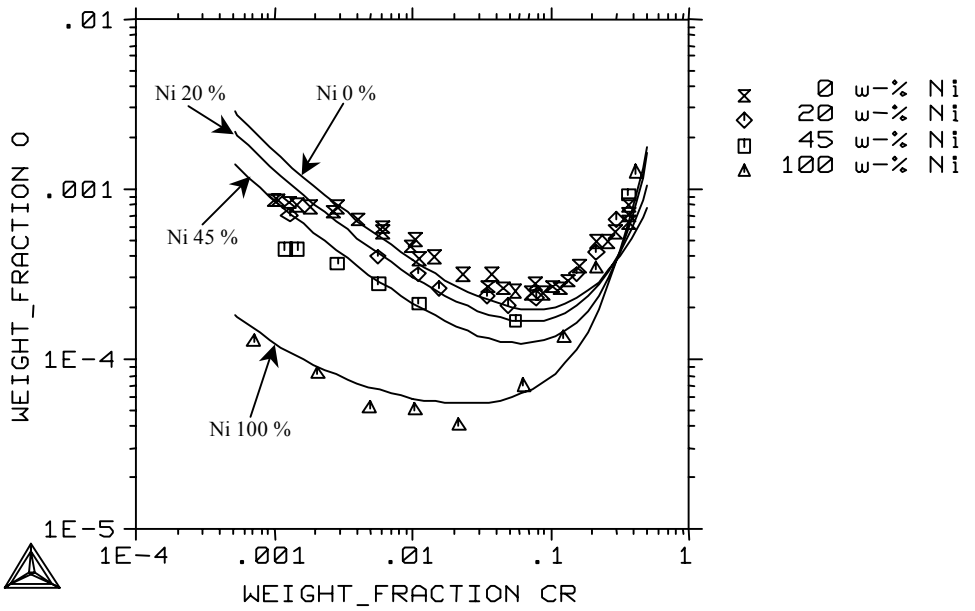


Figure 52. Solubility of oxygen in molten Fe-Cr-Ni alloys in equilibrium with $Cr_2O_3$ at 1823 K. Experimental points taken from /64/.

## 7.3 System Fe-Cr-C-O

The only experimental data from this system is given by Heinz et al. /64/. They measured the equilibrium relationship for the reaction

$$Cr_2O_3 + 3C \rightleftharpoons 3CO + 2\ Cr$$

in a carbon monoxide atmosphere in a $Cr_2O_3$ crucible.

Figure 53 shows the calculated equilibrium between molten Fe-Cr alloys and $Cr_2O_3$ with gas phase at 1 atm pressure at temperatures of 1823-1923 K. The calculated chromium content values are slightly higher than the values calculated by Heinz et al.

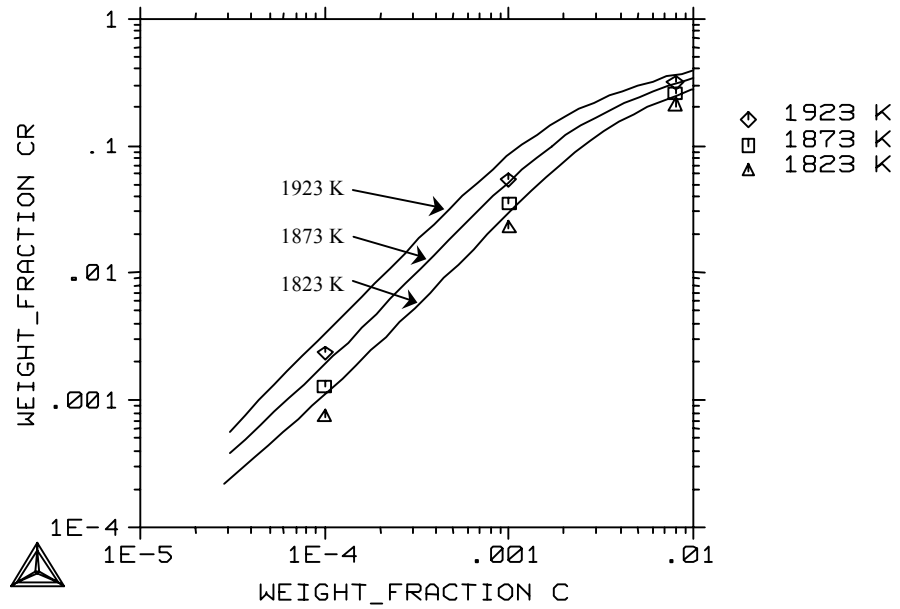


Figure 53. Equilibrium between molten Fe-Cr alloys, $Cr_2O_3$, and CO with calculated points from /64/.

The activity coefficient of carbon in molten Fe-Cr-O-C alloys is shown in Figure 54 for different chromium contents. Heinz /64/ noted that Cr-C interaction is very strong and affects this behaviour at higher carbon and chromium contents. All the calculated values show almost a linear behaviour versus carbon content. The effect of chromium content is very similar to thet of Heinz. Figure 55 shows the oxygen content of the melt under the same conditions.

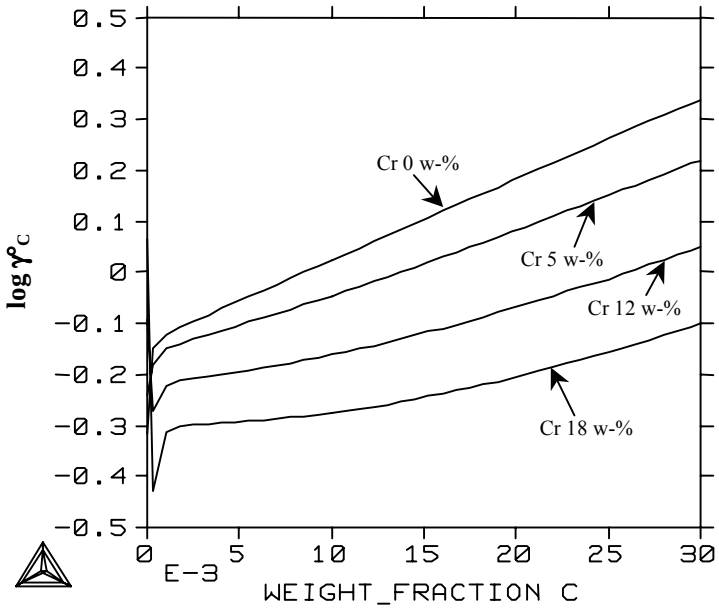


Figure 54. Activity coefficient of carbon in molten Fe-Cr-C-O alloys in equilibrium with gas phase at 1823 K.

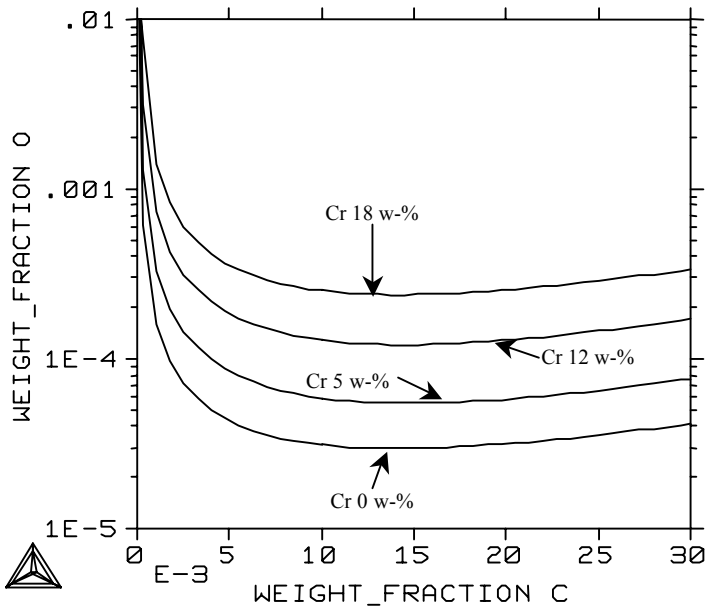


Figure 55. Solubility of oxygen to molten Fe-Cr-C alloys at equilibrium with gas phase at 1823 K.

## 7.4 System Fe-Ni-C-O

There are no experimental data available for the system Fe-Ni-C-O. Figure 56 presents the calculated solubility of oxygen in molten Fe-Ni-C alloys in equilibrium with a gas phase at 2223 K with varying nickel content. Experimental points for the systems Fe-C-O and Ni-C-O are taken from /104/. As can be seen, increasing the nickel content will decrease the solubility of oxygen. This can also be seen from Figure 57, which presents the same solubility as a function of nickel content with different carbon contents. The oxygen solubility has a minimum above the nickel contents of 80 w-% when the carbon content is high. With the carbon content of 0.01 w-% the solubility of oxygen will decrease continuously.

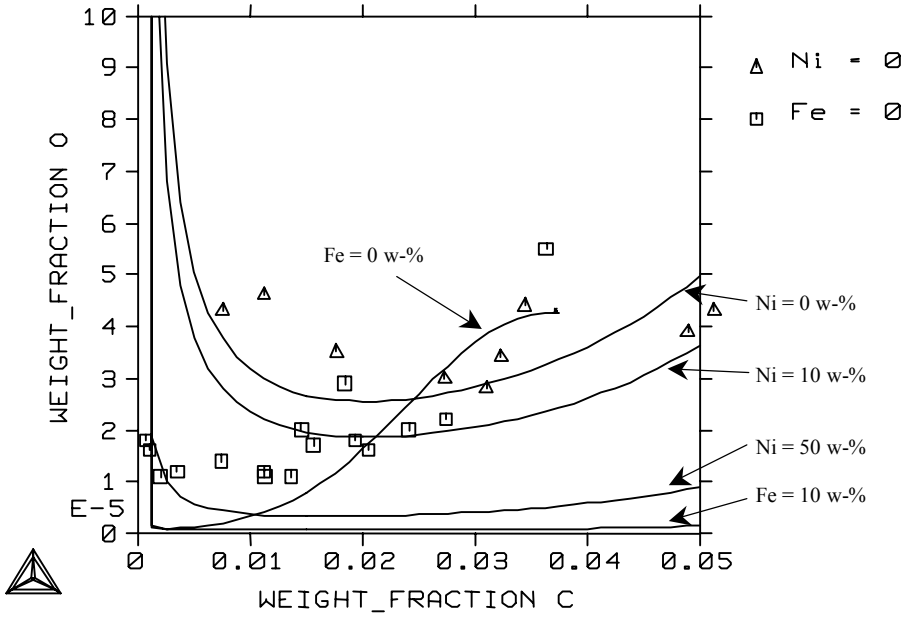


Figure 56. Solubility of oxygen in molten Fe-Ni-C alloys at 2223 K as a function of carbon content at different nickel contents. Experimental points for the systems Fe-C-O and Ni-C-O from /104/.

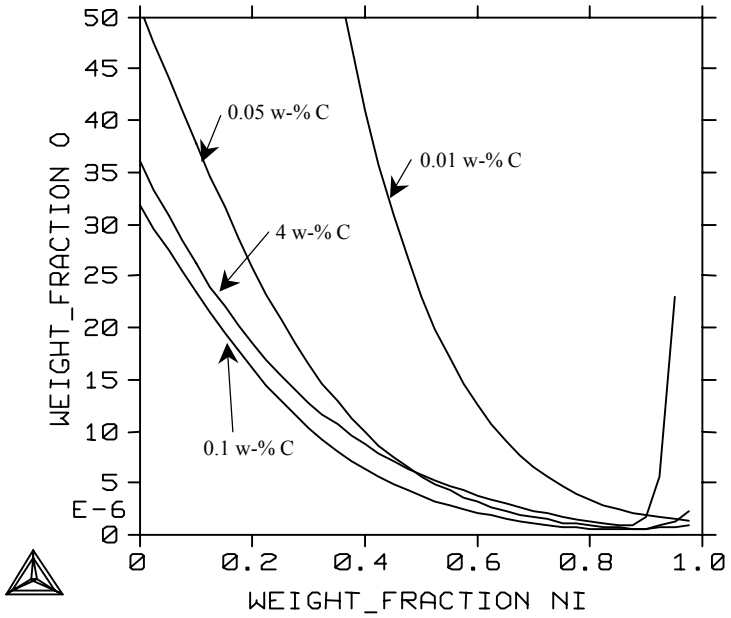


Figure 57. Solubility of oxygen in molten Fe-Ni-C alloys at 2223 K as a function of nickel content at different carbon contents.

## 7.5 System Cr-Ni-C-O

No experimental data are available in the literature from the system Cr-Ni-C-O. Figure 58 shows the calculated oxygen solubility in molten Cr-Ni-C alloys at 1823 K in equilibrium with a gas phase with different chromium contents. At low chromium contents the solubility curve is similar to that of the system Ni-C-O, i.e. the solubility has a minimum at a low carbon content. A higher chromium content will give a continuously decreasing solubility curve. Figure 59 shows the same equilibrium as a function of chromium content with different carbon contents. As can be seen, a small amount of chromium (less that 10 w-%) in the liquid alloy with more than 1 w-% carbon will decrease the solubility of oxygen and increasing the chromium content from this value will increase the solubility. With lower carbon content the solubility of oxygen will increase continuously until chromium oxide is stabilized. This behaviour could not be proven experimentally but a similar effect can be seen in the system Cr-Ni-O.

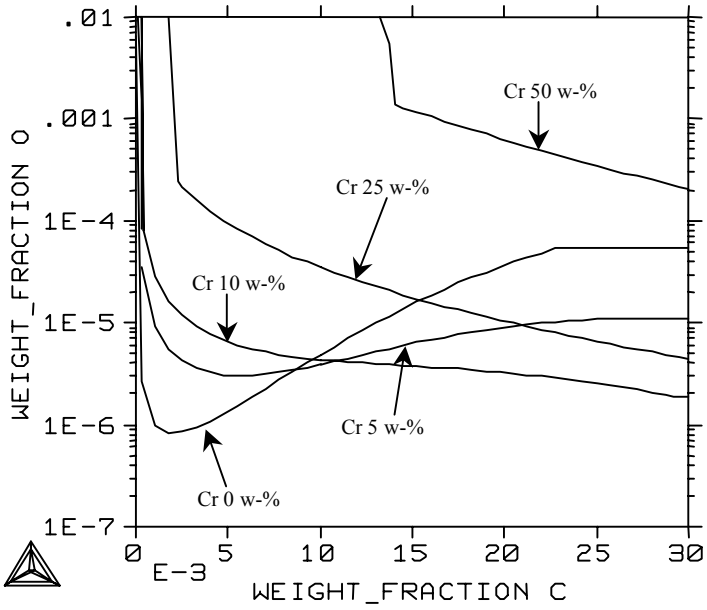


Figure 58. Solubility of oxygen in molten nickel-chromium alloys at 2223 K as a function of carbon content with different chromium content.

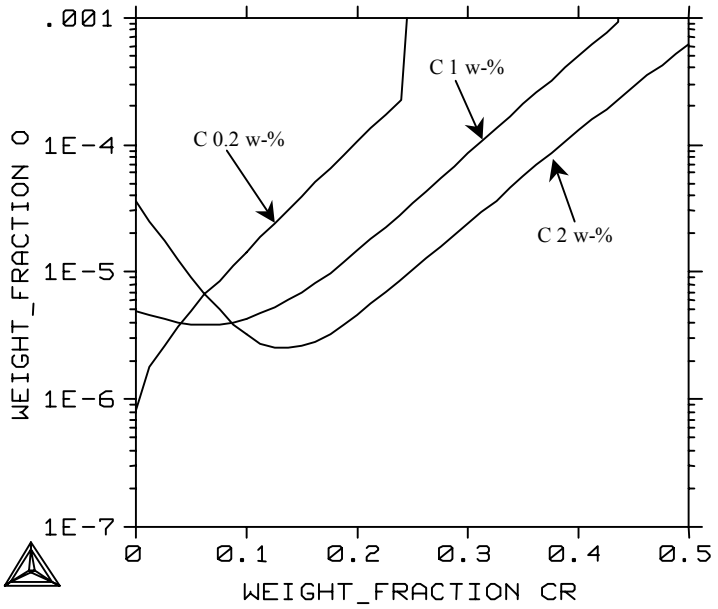


Figure 59. Solubility of oxygen in molten Ni-Cr alloys at 1823 K with different carbon contents as a function of chromium content.

# 8 SYSTEM Fe-Cr-Ni-C-O

No experimental data are available in the literature from the system Fe-Cr-Ni-C-O. Therefore the properties of system are illustrated by showing the calculated oxygen solubilities in the liquid phase.

Figure 60 shows the solubility of oxygen in molten iron alloys at 1873 K in equilibrium with the gas phase. As can be seen, increasing the chromium content increases the solubility of oxygen, while increasing the nickel content decreases the solubility. It should be noted that the nickel content does not affect the chromium oxide saturation limits, as can be seen from Figure 61 but the graphite saturation occurs at a lower carbon content when the nickel content is higher. The gas phase in these calculations was almost pure carbon monoxide.

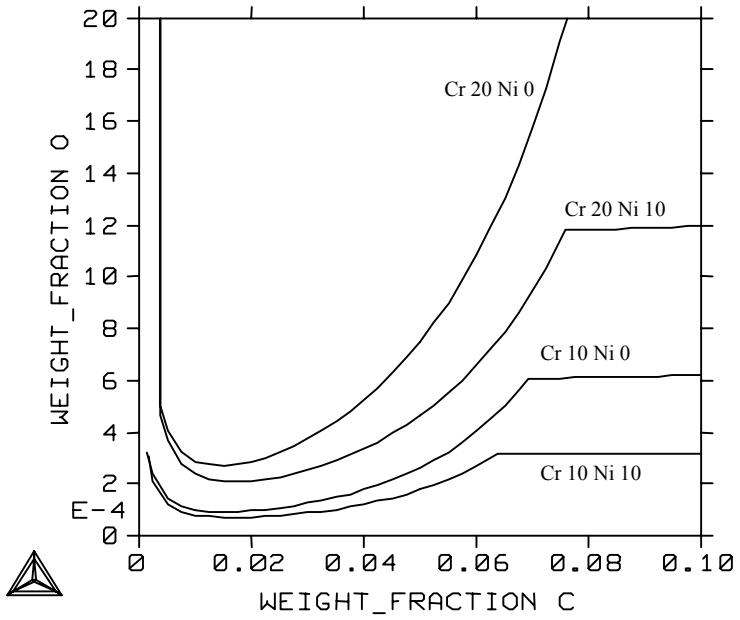


Figure 60. Solubility of oxygen in molten iron as a function of carbon content with different chromium and nickel contents at 1873 K. Chromium and nickel contents in weight percent.

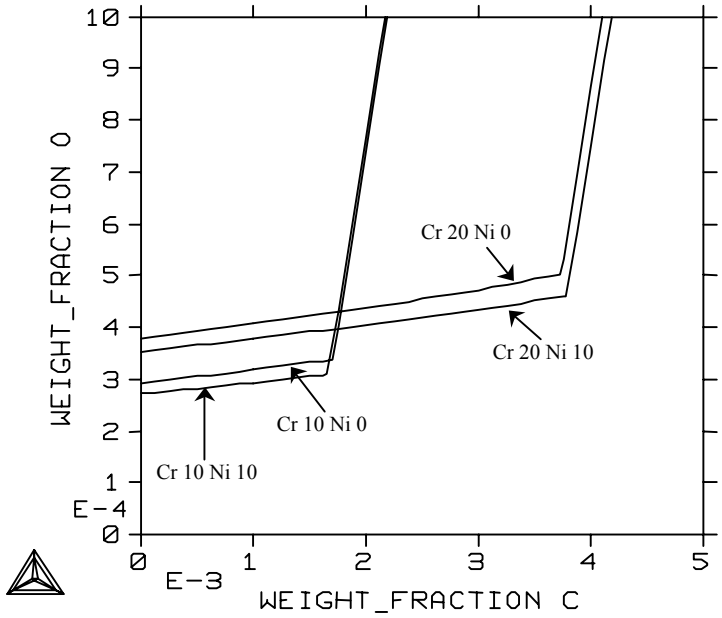


Figure 61. Solubility of oxygen in molten iron at 1873 K in equilibrium with chromium oxide with different chromium and nickel contents. Chromium and nickel contents in weight percent.

At higher temperatures the shape of the solubility line is similar and the effect of nickel is the same, as can be seen in Figure 62. The solubility of oxygen is lower but the saturation limit of graphite is higher. The oxide phase that is stable at 2073 K is the chromium oxide.

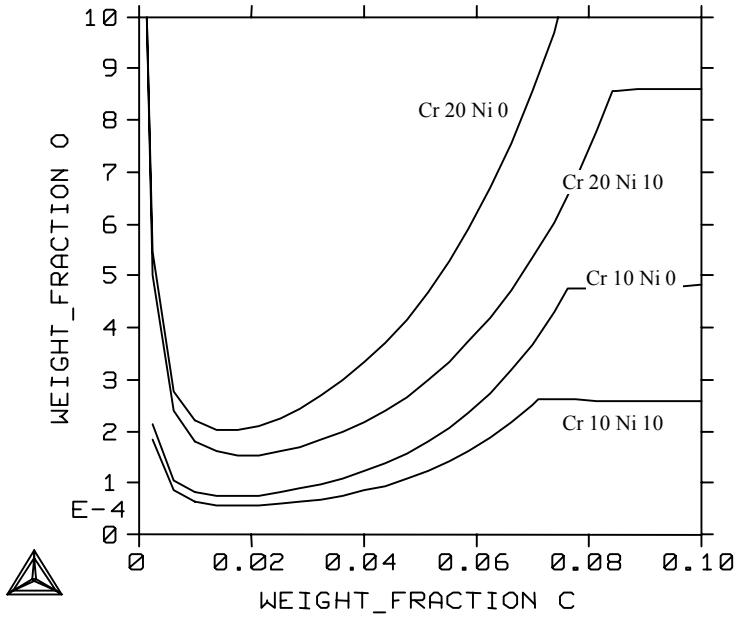


Figure 62. Solubility of oxygen in molten iron at 2073 K as a function of carbon content with different nickel and chromium contents. Carbon and nickel contents in weight percent.

Figure 63 shows the solubility of oxygen in molten iron alloys in equilibrium with the gas phase at 1873 K as a function of chromium content with different carbon and nickel contents. With these calculated carbon contents adding the nickel content with 10 w-% will decrease the solubility of oxygen. The gas phase mainly consists of the carbon monoxide.

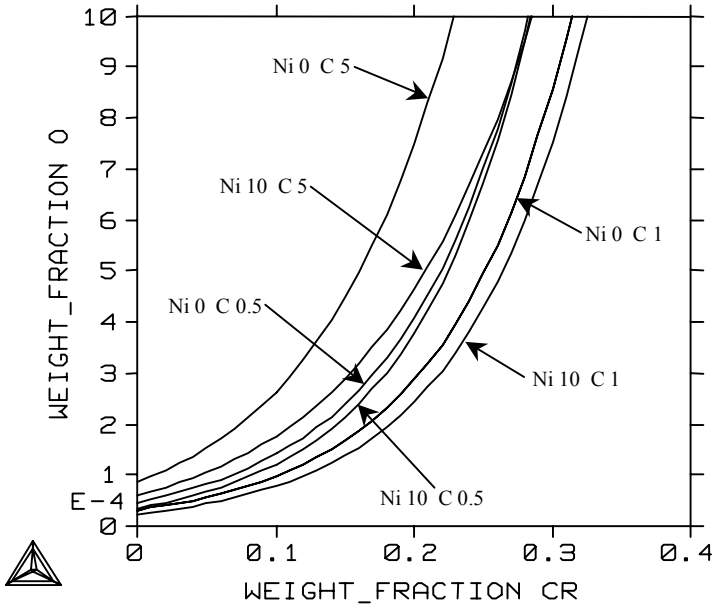


Figure 63. Solubility of oxygen in molten iron alloys at 1873 K as a function of chromium content with different carbon and nickel contents. Carbon and nickel contents in weight percent.

# 9 DISCUSSION

In this work the binary systems are based on earlier assessments. Those systems including oxygen are generated by converting the parameters of the ionic liquid model to those of the associate model. This can be done easily, because these models are numerically the same for binary systems. The selection of the associates was made in such a way that the activity coefficient for the one atomic oxygen in infinite dilution gained a defined value. The solubility of oxygen in solid metallic phases was modelled introducing oxygen to the second sublattice, which represents the interstitial sites in a cubic structure. The parameters for the solid metallic phases were taken from another study and they gave solubility that correlated well with the experimental data. All the other systems were found from the Thermo-Calc database, in which all systems use the same standard state and are consistent with each other.

Ternary systems that do not include oxygen were taken from the same Thermo-Calc database. These systems are quite well known and have previously been carefully studied by other authors.

The liquid phase in the system Fe-Cr-O was re-optimised using the associate model. The assessed parameters gave phase diagrams which were in very good agreement with the experimental data. At a temperature of 1573 K the spinel and $Cr_2O_3$ phases are in equilibrium with the bcc phase, although some workers have suggested that in this equilibrium the solid metallic phase is fcc. All the other three-phase equilibria are similar in all studies. The oxygen pressures at this temperature are very close to the measured values. At higher temperatures the phase diagram and thermodynamic measurements are more scattered. For the solubility of oxygen in molten Fe-Cr alloy the assessed parameters gave values that fit quite well with the latest measurements.

In the system Fe-C-O ternary assessing was made only for the liquid phase. At lower temperatures the binary systems define the behaviour of the ternary system. At higher temperatures there are only a few experimental measurements of the solubility of oxygen in the liquid phase. The assessed parameters gave solubility that was in very good agreement with these measurements.

The system Fe-Ni-O was optimised earlier using the ionic liquid model for the liquid phase. Therefore, this phase was re-optimised. The assessed parameters gave a phase diagram which was in general agreement with the experimental data. The solubility of oxygen in molten Fe-Ni alloys in equilibrium with the oxide melt has been measured by several authors using three different crucibles. The solubility of $SiO_2$ and CaO in oxide melt is very high at these temperatures, while the solubility of $Al_2O_3$ is much lower. It is obvious, therefore, that the results found using an $Al_2O_3$ crucible are more reliable in the system Fe-Ni-O. Another difference in this system was in the area of bunsenite. Raghavan /32/ gave high solubility values for iron in bunsenite on the basis of study by two authors /124, 121/ and also the temperature dependence for the solubility. Other authors /125, 126, 128, 129/ reported solubility at one temperature to be much lower. The assessed parameters could not reproduce the temperature dependence given by Raghavan /32/.

The liquid phase in the system Cr-Ni-O was reassessed because the earlier work was made with the ionic liquid model. Only three parameters were needed to reproduce all the experimental phase diagrams and the thermodynamic data. The solubility of oxygen in molten Cr-Ni alloys over a small temperature range has been measured by several authors. The calculated solubility was in very good agreement with all the data except for the oldest measurements. Oxygen activities have also been measured by two authors and the optimised parameters gave very similar values. The activity coefficient of oxygen at infinite dilution has been measured by three authors. The calculated values are in quite good agreement with these experimental works.

Only a limited amount of experimental data are available for the system Cr-C-O and these are all represented by the same Ellingham diagram. Because this kind of diagram is defined by the thermodynamic functions of solid binary phases it is obvious that the calculated diagram is in very good agreement with the experimental diagrams. The solubility of oxygen in molten Cr-C alloys was not reported in the literature. This can also be because of the high melting point of chromium, which will make experimental work very difficult.

Oxygen solubility in liquid Ni-C alloys in equilibrium with CO has been measured by several authors. One of these measurements disagreed with other measurements and gave unreliably high values. Other studies gave a consistent set of values. In this work it was not possible to find a set of parameters that could reproduce the solubility. The optimised parameters gave a solubility that was one decade lower than the measured values at lower carbon contents. At higher carbon contents, i.e. over 1.5 w-%, the calculated solubility is in agreement with the experimental data. All possible parameter configurations were tested and the set of parameters used gave the best possible values. Another possibility is that the problem lies in binary systems. This was also tested by optimising the system Ni-O again, together with the system Ni-O-C. This however, did not give a good result. The problem was finally traced to the solubility of oxygen, which became too high in the binary system. This will invariably cause significant uncertainty in higher order systems where this system is included.

The system Fe-Cr-Ni-C was taken from the Thermo-Calc database, based on the study of Lee /51 /.

The solubility of oxygen in molten Fe-Cr-Ni alloys has been measured by two authors at two temperatures. Interpolation from the optimised sub-systems gave results that were in quite good agreement with these experimental data. Therefore there was no need to optimise any quaternary interaction parameters. The calculated solubilities show that increasing the nickel amount in molten alloys will decrease the solubility of oxygen when there is less than 50 w-% chromium. At higher chromium contents the solubility of oxygen will increase slightly with increasing nickel content. From the experimental data this cannot be seen very clearly, but there are some points that demonstrate this affect.

The description of the system Fe-Cr-C-O is presented by two kinds of diagrams. The first diagram shows the chromium and carbon contents in molten alloys in equilibrium with chromium oxide and CO at different temperatures. According to this diagram, increasing the amount of carbon in molten alloy will destabilise the chromium oxide. The other diagrams are calculated at one temperature and with lower chromium contents so as to avoid the stabilisation of chromium oxide. These diagrams show that increasing the chromium content in the melt will decrease the activity coefficient of carbon and oxygen solubility will increase. These results are in agreement with those of other authors, who noted that Cr-C interaction is very strong and will have an effect at higher chromium contents.

There were no experimental data available for the system Fe-Ni-C-O and therefore it was described using only interpolation models from its sub-systems. The solubility of oxygen in molten Fe-Ni-C alloys was calculated with different nickel contents. The problem found with the system Ni-C-O is that the solubility of oxygen is very low at lower carbon and iron contents. At higher carbon contents the calculated solubility curve will show a minimum at approximately 85 w-% of nickel. Similar behaviour can be seen in the system Fe-Ni-O, particularly at higher temperatures, when nickel and carbon have a strong interaction in the melt. Therefore it is obvious that this effect can be even stronger when carbon is present in the melt.

The system Cr-Ni-C-O was calculated from its sub-systems using only interpolation models because there were no experimental data available. The solubility of oxygen in molten Cr-Ni-C alloys was calculated at different nickel contents. From these diagrams it can be seen that the effect of increasing carbon content will be very different at different nickel contents. At higher nickel contents the solubility of oxygen is at its minimum; when the chromium content is more than 10 w-% the solubility of oxygen will decrease continuously. This is quite obvious, because in the system Ni-C-O there is a minimum, but in the system Cr-C-O there is not. It should certainly be noted that the solubility of oxygen is greatly affected at lower chromium content by the ternary system Ni-C-O, which was not in agreement with the experimental data at lower carbon contents.

The system Fe-Cr-Ni-C-O was presented by the solubility of oxygen in molten alloys with different metal compositions typical for stainless steels production. The solubility of oxygen in equilibrium with CO as a function of carbon content with different chromium and nickel contents is shown at two different temperatures. At these selected compositions there is a minimum solubility at approximately 1.5 w-% of carbon. The chromium content has a greater effect on the solubility of oxygen than does the nickel content and the effect is reversed. Increasing chromium content will increase the solubility of oxygen, while increasing nickel content will decrease it. This solubility was also calculated as a function of chromium content with selected carbon and nickel contents. According to these calculations, the solubility of oxygen will increase continuously along with increasing chromium content.

It should be noted that in these calculations there is no slag model and therefore these calculated diagrams do not represent such situation, where there is present slag forming components.

Systems of present work are collected in Table 10 including references to assessments and validation with experimental data.

Table 10. Systems of present work

| System | Assessment | Verification with experimental data | Agreement |
|---|---|---|---|
| Fe-Cr | Andersson et al. /33/ | Yes /33/ | Good |
| Fe-Ni | Dinsdale et al. /37/ | Unpublished work | - |
| Fe-C | Gustafson /38/ | Yes /38/ | Good |
| Fe-O | Kowalski et al. /16/<br>Sundman et al. /18/<br>Data conversion | Yes /16, 18/ | Good |
| Cr-Ni | Dinsdale et al. /37/ | Unpublished work | - |
| Cr-C | Andersson /43/ | Yes /43/ | Good |
| Cr-O | Kowalski et al. /16/<br>Taylor et al. /44/<br>Data conversion | Yes /44,16/ | Good |
| Ni-C | Gabriel et al. /46/ | Yes /46/ | Good |
| Ni-O | Taylor et al. /12/<br>Kowalski et al. /16/<br>Data conversion | Yes /12, 16/ | Good |
| C-O | Ideal mixture | None | - |

Table 10 continues.

| System | Assessment | Verification with experimental data | Agreement |
|---|---|---|---|
| Fe-Cr-Ni | Lee /51/ | Unpublished work | - |
| Fe-Cr-C | Andersson /52/ | Yes /52/ | Good |
| Fe-Cr-O | This work | Yes / This work | Good |
| Fe-C-O | This work | Yes / This work | Good |
| Fe-Ni-C | Gabriel et al. /105/ | Yes /105/ | Good |
| Fe-Ni-O | This work | Yes / This work | Reasonable |
| Cr-Ni-C | NPL /36/ | Unpublished work | - |
| Cr-Ni-O | This work | Yes / This work | Good |
| Cr-C-O | Interpolation, this work | Yes / This work | Reasonable |
| Ni-C-O | This work | Yes / This work | Moderate |
| Fe-Cr-Ni-C | Interpolation, Lee /51/ | Unpublished work | - |
| Fe-Cr-Ni-O | Interpolation, this work | Yes / This work | Good |
| Fe-Cr-C-O | Interpolation, this work | Yes / This work | Reasonable |
| Fe-Ni-C-O | Interpolation, this work | No | - |
| Cr-Ni-C-O | Interpolation, this work | No | - |
| Fe-Cr-Ni-C-O | Interpolation, this work | No | - |

# 10 CONCLUSIONS

In this work a thermodynamic database for the system Fe-Cr-Ni-O-C has been built using previously assessed binary, ternary, and quaternary systems. Six ternary systems, Fe-Cr-O, Fe-C-O, Fe-Ni-O, Cr-Ni-O, Cr-C-O, and Ni-C-O, have been assessed. Quaternary and quinary systems were calculated using only interpolation models. This method of building a database is known as the Calphad method and it is widely used in modern thermodynamics. A result of this work is an internally consistent database, which, in combination with suitable calculation software, facilitates predictive phase equilibrium calculations for solid and liquid compositions of relevance to many industrial applications.

A thermodynamic assessment of a system is performed by using a model for the Gibbs energy of all phases in the system. The model parameters are evaluated on the basis of the available experimental data. The applied optimisation routine, Parrot, allows both phase diagrams and thermodynamic data to be used. The strength of the assessment procedure lies in its ability to detect systematic errors and conflicts between different data sets as measured by different authors. A thermodynamically consistent data set can be obtained by careful evaluation of the experimental data. Another selection must be made to choose an appropriate model and a suitable set and number of interaction parameters to fit all the experimental data with reasonable accuracy. In selecting the models used it is important to consider all the sub-systems in the database in order that the description of the phase is the same in all systems. The final model is usually a compromise between the general fit, the number of optimised parameters, and safe extrapolations to higher order systems.

In this work the metal-oxygen binary systems were calculated using the associate model for the liquid phase. This model allows the combination of metal-metal binary systems optimised using a random substitutional solution model in the same database. The model parameters were transformed from the parameters optimised for the ionic liquid model by other authors. The phase diagrams calculated are in very good agreement with the experimental data. Because of the new assessments of the binary systems, all the ternary systems that include oxygen were optimised. Only in the Ni-C-O system the parameters were unable to reproduce the experimental data.

The quaternary systems calculated are in good agreement with the experimental data without using any quaternary parameters. The amount of experimental data for these higher order systems is, in general, very small. For the quinary system no experimental data were found in the literature.

The model parameters assessed in this work describe the system Fe-Cr-Ni-C-O well according to the experimental information from its sub-systems. Therefore, the database can be treated as an adequate description of the system. The only way to validate the model is to do experimental work.

The main application of this database is in the area of stainless steel processes. Therefore, the quinary system was presented only for metal-rich melts with a low nickel concentration. Nevertheless, this database is a full description of the five-component system and can be used at any concentrations, though at high nickel contents and low carbon contents the model is less accurate. While using this database in other areas, one should notice that the uncertainty of the description is much greater in the areas where no experimental information is available.

# 11 REFERENCES


1 Haase, R., Thermodynamik der Mischphasen. Berlin, Springer Verlag, 1956

2 Leidler, K.J. & Meiser, J.H., Physical Chemistry. Menlo Park, California, The Benjamin/Cummings Publishing Company Inc., 1982

3 Inden, G., Calphad Meeting V. 21-25th June 1976, Max-Planck-Institut, Düsseldorf, Germany, 1114-1

4 Hillert, M. & Jarl, M., *CALPHAD*, **2**(1978)3, 227-238

5 Margules, M., Mathem. *Naturwiss. Cl.*, **104**(1895), 1243-78

6 Redlich, O. & Kister, A., *Ind. Eng. Chem.*, **40**(1948), 345-8

7 Hillert, M., *Thermochim. Acta*, **12**9(1988), 71-5

8 Sundman, B. & Ågren, J., *J.Phys.Chem.Solids*, **42**(1981), 297-301

9 Saunders, N. & Miodownik, A.P., CALPHAD (Calculation of Phase Diagrams): A Comprehensive Guide, Exeter, Pergamon Materials Series vol. 1, 1998

10 Barry, T.I., Dinsdale, A.T., Gibsy, J.A., Hallstedt, B., Hillert, M., Jansson, B., Jonsson, S., Sundman, B. & Taylor, J.R., Petten Symposium on Phase Diagrams, Institute of Metals, 1990

11 Hillert, M., Jansson, B., Sundman, B. & Ågren, J., *Met. Trans. A*, **16A**, (1985), 261

12 Taylor, J.R. & Dinsdale, A.T., *Z. Metallkde.*, **81**(1990)5, 354-66

13 Selleby, M., unpublished research. **Ref: 9**

14 Sommer, F., *Z.Metallkde.*, **73**(1982), 72

15 Rannikko, H., A Thermodynamic Assessment of the Cu-O-CaO-$SiO_2$ System, Ph.D. Thesis. Helsinki University of Technology, Helsinki, 1995

16 Kowalski, M. & Spencer, P.J., *CALPHAD*, **19**(1995)3, 229-243

17 Taylor, J.R. & Dinsdale, A.T., *Z.Metallkde.* **81**(1990)5, 354-66

18 Sundman, B., *J.Phase Equil.*, **22**(1991)1, 127-40

19 Selleby, M., Thermodynamic Modelling and Evaluation of the Ca-Fe-O-Si System, Thesis, RIT, Stockholm, 1993

20 Chartrand, P. & Pelton, A.D., *J. Phase Equil.*, **21**(2000)2, 141-7

21 Toop, G.W., *Trans AIME*, **233**(1965), 850-4

22 Hillert, M., *CALPHAD*, **4**(1980), 1

23 Kohler, F., *Monatsh. Chemie,* **91**(1960), 738

24 Muggianu, Y.-M., Gambino, M. & Bros, J.-P., *J.Chem.Phys.*, **72**(1975), 83

25 Sundman, B., Jansson, B. & Andersson, J.-O., *CALPHAD*, **9**(1985)2, 153-90

26 Andersson, J.-O., Höglund, L., Jönsson, B. & Ågren, J., Fundamentals and Applications of Ternary Diffusion, G.R. Purdy Ed., NY USA, Pergamon Press, 1990, pp 153-63

27 Lukas, H.L., Henig, E.Th. & Zimmermann, B., *CALPHAD*, **1**(1977), 225

28 Davies, R.H., Dinsdale, A.T., Hodson, S.M., Gisby, J.A., Pugh, N.J., Barry, T.L. & Chart, T.G., in User Aspects of Phase Diagrams, ed. Hayes, F.H., Inst.Metals, London, 1991

29 Thompson, W.T., Eriksson, G., Pelton, A.D. & Bale, C.W., *Proc.Met.Soc.CIM*, **11**(1988), 87

30 Eriksson, G, & Hack, K., *Met.Trans. B*, **21B**(1990), 1013

31 Kaysser, W.A., *Int.J. Powder Met.*, **25**(1989), 157-65

32 Raghavan, V., Phase Diagrams of Ternary Iron Alloys, Part 5: Ternary Systems Containing Iron and Oxygen, Calcutta, Indian Institute of Metals, 1989

33 Andersson, J-O. & Sundman, B., *CALPHAD* **11**, (1987), 83-92

34 Kubaschewski, O., Iron-Chromium, Iron Binary Phase Diagrams, Berlin, Springer Verlag, 1982

35 Massalski, T.B., Binary Alloy Phase Diagrams, Ohio, American Society for Metals, Metals Park, 1986

36 Thermo-Calc database, version M

37 Dinsdale, A. & Chart, T., MTDS NPL, unpublished work (1986): **ref 36**

38 Gustafson, P., *Scan. J. Metall.* **14**(1985)5, 259-267

39 Swisher, J.H. & Turkdogan, E.T., *Trans. AIME*, **239**(1967), 426 **ref: 16**

40 Hepworth, M.T., Smith, R.P. & Turkdogan, E.T., *Trans. AIME,* **136**(1966), 1278 **ref: 16**

41 Dinsdale, A. & Chart, T., MTDS NPL, Unpublished work (1986) **ref: 36**

42 Nash, P., *Phase Diagrams of Binary Nickel Alloys*, 1991 **ref:35**

43 Andersson, J.-O-. *CALPHAD,* **11**(1987), 271-6

44 Taylor, J.R. & Dinsdale, A.T., *Z.Metallkde*, **84**(1992)5, 335-45

45 Caplan, D., Fraser, M.J. & Burr, A.A., Ductile Chromium , *ASM* (1957) 196-215, **ref: 16**

46 Gabriel, A., Chatillon, C. & Ansara, I., *CALPHAD,* **11**(1987), 203-218 **ref:36**

47 Luoma, R., *CALPHAD*, **19**(1995)3, 279-95

48 Park, J.-W. & Alister, J., *Metall. Trans. A.*, **18A** (1987), 43 **ref: 16**

49 Seybolt, A.U. & Follman, R.L., *Trans. AIME*, **200** (1954), 548 **ref: 16**

50 Alcock, C.B. & Brown, P.B., *Metals. Sci. J*., **3** (1969), 116 **ref: 16**

51 Lee, B-J., Unpublished Revision (1991), **ref:36**

52 Andersson, J-O., *Met. Trans A*, **19A**(1988), 627-636

53 Luoma, R., A Thermodynamic Analysis of the System Iron-Chromium-Oxygen, Licenciate's Thesis. Helsinki University of Technology, Espoo, 1992

54 Toker, N.Y., Darken, L.S. & Muan, A., *Met. Trans. B*, **22B**(1991)10, 689-703

55 Hilty, D.C., Forgeng, W.D. & Folman, R.L., *Trans. AIME*, **203**(1955), 253-68

56 Koch, W., Bruch, J. & Rohde, H., *Arch. Eisenhüttenw*., **31**(1960), 279-86

57 StPierre, G.R. & Blackburn, R.D., *Trans. AIME*, **242**(1968), 2-4

58 Wentrup, H. & Knapp, B., *Techn.Mitt.Krupp.Forschung*, **4**(1951)11, 237-56

59 Petrov, B.S., Viskarev, A.F., Tyurin, E.I. & Yavoiskii, V.I., *Sb.Mosk.Inst.Stali Splavov*, **61**(1970), 198-201

60 Omori, Y. & Sanbongi, K., *Tohoku Daigaku Seiko Seiren Kenkyoshi Iho*, **23**(1967)2, 129

61 Chen, H-M. & Chipman, J., *Trans.Amer.Soc.Metals*, **38**(1947), 70-113

62 Fruehan, R.J., *Trans.AIME*, **245**(1969), 1215-8

63 Schenck, H. & Steinmezt, E., *Arch.Eisenhüttenw*., **38**(1967)12, 871-3

64 Heinz, M., Koch, K. & Janke, D., *Steel Research*, **60**(1989)6, 246-54

65 Nakamura, Y. & Uchimura, M., *Trans.Iron Steel Inst.Japan*, **13**(1973), 343-9

66 Shevtsov, V.E., *Izv.Vyssh.Ucheb.Zaved., Chern.Metall*., (1979)7, 5-7

67 Shevtsov, V.E., Lekthemetz, U.L. & Shtraukh, V.P., *Metallurgiya Chern.Met., Alma-Ata*, (1979), 117-21

68 Janke, D. & Fischer, W.A., *Arch.Eisenhüttenw***. 47**(1976)3, 147-51

69 Geldenhuis, J.M.A. & Dieppenaar, R.J., *Met.Trans.B*, **22B**(1991), 915-8

70 Turkdogan, E.T., *J.Iron Steel Inst*., **178**(1954), 278-83

71 Danilovich, Yu.A. & Morozov, A.N., *Sborn.Nauch.-Techn.Trud.Nauchn.-Issled.Inst.Met. Chelyab.Sovnarkhoza*, (1961)4, 19-25

72 Sabirzyanov, T.G., *Izv.Akad.Nauk.SSSR, Metally*, (1985)5, 40-3

73 Adachi, A., Iwamoto, N. & Kitamura, M., *Tetsu to Hagane,* **52**(1966)2, 204-5

74 Iwamoto, N., Takano, M., Kanayama, H. & Adachi, A., *Tetsu to Hagane*, **56**(1970)6, 727-33

75 Evans, L.G. & Muan, A., *Amer.Ceramic Soc.Bull*., **49**(1970)4, 491

76 Muan, A. & Somiya, S., *J.Amer.Ceram.Soc*., **43**(1960)4, 204-9

77 Riboud, P.V. & Muan, A., *Trans.AIME*, **230**(1964), 88-90

78 Shnetlage, R. & Klemm, D.D., *N.Jb.Miner.Abh*., **125**(1975)3, 227-42

79 Webber, J., *Corr.Sci*., **16**(1976), 499-506

80 Skala, J., Lansky, V., Macoszek, M., Maderic, R. & Bury, P., *Kovove Mater*., **20**(1982)3, 359-71

81 Shaklin, A.L., Mikhailov, G.G. & Lykasov, A.A., *Sb.Nauch.Tr.Chelyabinsk Politechn.In-T*., (1975)163, 21-31

82 Shaklin, E.L. & Mikhailov, G.G., *Izv.Vyssh.Ucbec.Zaved.Cher.Metall*., (1976)10, 15-6

83 Fujii, C.T. & Meussner, R.A., *Tans.AIME*, **242**(1968), 1259-65

84 Katsura, T., Wakihara, M., Hara, S-I. & Sugihara, T., *J.Solid State Chem*., **13**(1975), 107-13

85 Petric, A. & Jacob, K.T., *J.Am.Ceram.Soc*., **65**(1982)2, 17-23

86 Jacob, K.T. & Alcock, B., *Met.Trans. B*., **6B**(1975), 215-21

87 Snethlage, R. & Schröcke, H., *N.Jb.Mineral.Monatsh*.,(1976)5, 214-28

88 Yamazaki, T., Terashima, K. & Yahiro, T., *Netsu Shori*, **28**(1988)6, 389-95

89 Kay, D.A.R., *Rev.Int.hautes Temper.Refract*., **16**(1976), 21-32

90 Katsura, T. & Muan, A., *Trans.AIME*, **230**(1964), 77-84

91 Seybolt, A.U., *J.Electr.Chem.Soc*., **107**(1960), 147-56

92 Th.Laheij, M.A.J., van Loo, F.J.J. & Metselaar, R., *Oxid.Metals*, **14**(1980)3, 207-15

93 Marhabi, L., Trinel-Dufour, M.C., Perrot, P., Lazouni, H.A. & Derriche, Z., *Ann.Chim. (Paris),* **12**(1987)3, 223-35

94 Richards, R.G. & White, J., *Trans.Britt.Ceram.Soc*., **53**(1954), 422-59

95 Schmal, N.G. & Dillenburg, H., *Z.Physikal.Chem*., **65**(1969), 119-38

96 Viktorovich, G.S., Lisovskii, D.I., Zhalov, V.S. & Gutin, V.A., *Russ.J.Phys.Chem*., **46**(1972)6,882

97 Kazin, I.V., Kyskin, V.I., Petrova, S.M. & Kaganyuk, D.S., *Zh.Fiz.Khim*., **58**(1984)1, 37-41

98 Novokatshii, I.A. & Lemer, L.M., *Zh.Neorg.Khim*., **11**(1969)9, 2014-20

99 Linchevsky, B.V. & Samarin, A.M., *Izv.Akad.Nauk. SSSR Tekhn*., (1953)5, 691-704

100 Zabeivorota, N.S., Lykasov, A.A. & Mikhailov, G.G., *Izvest.Akad.Nauk. SSSR, Neorg.Mater*., **16**(1980)1, 181-3

101 Matoba, S. & Ban-Ya, S., *Tetsu to Hagane*, **66**(1980)9, 1406-22

102 Schenck, H., Steinmezt, E. & Gloz, M., *Arch. Eisenhüttenw*., **39**(1968)1, 69-71

103 Schenck, H & Hinze, H., *Arch. Eisenhüttenw*. **37**(1966), 545-50

104 Artemov, V.I., Burtsev, V.T., Kashin, V.I. & Saksonova, L.N., *Vzaimodeistvie Gazov Metal, Tr.Sov.-Yaponskogo Simp.Fiz.-Khim.Osn.Met. Protessov,* (1971)3 (pub 1973), 76-82

105 Gabriel, A., Gustafson, P. & Ansara, I., *CALPHAD* , **11**(1987), 203-218

106 Pelton, A.D., Schmalzried, H. & Sticher, J., *J.PhysChem.Solids*, **40**(1979), 1103-22

107 Koch, F., Die Gleichgewichte zwishcen Eisen und Sauerstoff in Nickelschmelzen unter eisenoxidhaltigen Schlacken, Thesis, Technische Universität Clausthal, 1985, Also as: Kuxmann U. & Koch F., Metall., 40(1986)5, 479-85

108 Petrov, B.S., Vishkarev, A.F., Tyurin, E.I. & Yavoiskii, V.I., *Sb.Mosk.Inst.Stali.Splavov*, **61**(1970)2, 198-201

109 Bardenheuer, P. & Brauns, E., *Mitteilungen Kaiser-Wilhelm-Institut für Eisenf.*, **17**(1935), 127

110 Wriedt, H.A. & Chipman, J., *J.Metals*, **203**(1955)3, 477-9

111 Fedotov, V.P. & Samarin, A.M., *Polska Akad.Nauk.Arch.Hutnic.*, **1**(1956)3, 183-93

112 Averin, V.V., Polyakov, A.Yu. & Samarin, A.M., *Izv.Akad.Nauk.SSSR, Otdel.Tekh.Nauk.Met. i Toplivo*, (1959)1, 13-21

113 Shevtsov, V.E., Lekhmetz, V.L. & Brovkev, V.A., *Metallurgiya Chern,Met.*, (1977)3, 41-6

114 von Bohlen und Hallbach, C. & Leitgebel, W., *Techn.Mitt.Krupp.Forschungsber.*, **4**(1941)4, 37-44

115 Tsemekhman, L.Sh. & Vaisburd, S.E., *Russ.J.Phys.Chem.*, **43**(1969)12, 1777-80

116 Shafer, M.W., *J.Phys.Chem.*, **65**(1961), 2055-62

117 Fischer, A.W. & Hausmann, M., *Arch.Eisenhüttenw.*, **37**(1966)12, 959-61

118 Fischer, A.W., Janke, D. & Ackermann, W., *Arch.Eisenhüttenw.*, **41**(1970)4, 361-7

119 Tankins, E.S. & Gocken, N.A., *Met.Trans.*, **2**(1971)6, 1605-11

120 Victorovich, G.S. & Lisovskii, D.I., *Tsvet.Met.*, (1966)11, 43-8

121 Victorovich, G.S., Gutin, V.A. & Lisovskii, D.I., *Tsvet.Met.,* (1966)12, 47-9

122 Victorovich, G.S., Lisovskii, D.I. & Gutin, V.A., *Russ.J.Phys.Chem.*, **43**(1969)12, 1709-11

123 Victorovich, G.S., Dobrovinskii, R.Yu., Zhalov, V.S., Lisovskii, D.I., Men, A.N. & Chufarov, G.I., *Russ.J.Phys.Chem.*, **44**(1970)1, 116-8

124 Dalvi, A.D. & Smeltzer, W.W., *J.Electrochem.Soc.*, **117**(1970)11, 1431-6

125 Davies, H. & Smeltzer, W.W., *J.Electrochem.Soc.*, **119**(1972)10, 1362-8

126 Dalvi, A.D. & Sridhar, R., *Can.Met.Quart.*, **15**(1976)4, 349-57

127 Trinel-Dufour, M-C., Pouillard, G. & Perrot, P., *J.Chem.Research (M)*, (1981)3, 901-19

128 Ono, K., Yokogawa, K., Yamaguchi, A. & Moriyama, J., *J.Japan Inst.Met*., **35**(1971)8, 750-6

129 Trinel-Dufour, M-C., Derriche, Z. & Perrot, C.R., *Acad.Sc.Paris*, **287**(1978), 273-5

130 O'Bryan, H.M., Monforte, F.R. & Blair, R., *J.Am.Ceram.Soc*., **48**(1965)11, 577-80

131 Chachanidze, G.D., *Izvest.Akad.Nauk.SSSR, Neorg.Mater.*, **26**(1970)2, 376-9

132 Barin, I., Knacke, O. & Kubaschewski, O., Thermodynamic Properties of Inorganic Substances, New York, Springer Verlag, 1973, Supplement 1977

133 Schneider, F. & Schmalzried, H., *Z.Phys.Chem.Neue Folge*, **166**(1990), 1-18

134 Schmalzried, H. & Tretjakov, J.D., *Ber.Bunsenges.Phys.Chem*., **70**(1966), 180-9

135 Roeder, G.A. & Schmalzried, H., *J.Electrochem.Soc*., **117**(1964), 1074-8

136 Gatellier, C., Henriet, D. & Olette, M., *Compt.Rend*., **271C**(1970), 453-6

137 Trinel-Dufour, M-C. & Perrot, P., *Compt.Rend*., **281C**(1975), 589-92

138 Trinel-Dufour, M-C., Pouillard, G. & Perrot, P., *J.Chem.Research (M)*, (1979)6, 2401-23

139 Trinel-Dufour, M-C., Pouillard, G. & Perrot, P., *J.Chem.Research (M),* (1979)9,3174-94

140 Zlazinskii, A.G., Balakirev, V.F. & Chufarov, G.I., *Russ.J.Phys.Chem*., **47**(1973)2, 259-61

141 Steinmetz, E. & Sibum, H., *Techn.Mitt.Krupp.Forsch.Ber*., **37**(1979)2, 45-68

142 Paladino, A.E. Jr., *J.Am.Ceram.Soc*., **42**(1959)4, 168-75

143 Kuznetsov, Yu.S., *Nauch.Tr.Mosk.In-T., Stali i Splavov*, (1983)149,68-77

144 Gries, B., Diplomarbeit, Universität Hannover, 1985, **ref:133**

145 Kushko, M.T., Balakierev, V.F., Popov, G.P., Panfilov, N.N., Chufarov, G.I., Bogachenko, V.V. & Komarova, L.V., *Khimiya I Teknol.Oksidn.Magnit.Materialov, (Volgograd)*, (1978)4, 54-7

146 Katayama, I., Watanabe, Y. & Kozuka, Z., *Trans.JIM*, **20**(1979), 593-6

147 Tretyakov, Yu.D., Thermodynamics of Ferrites, Chem.Publ.Leningrad, (1967), Ch VI., p 164, **ref: 146**

148 Sakao, H. & Sano, K., *J.Japan Inst.Metals*, **26**(1962), 240-4

149 Averin, V.V., Cherkasov, P.A. & Samarin, A.M., *Issled po Zharaprochn. Splavam, Akad.Nauk. SSSR Inst.Met*., **9**(1962), 204-18

150 Belov, B.F. & Novokhatskiy, I.A., *Russ.Met*., **5**(1970), 52-5

151 Janke, D. & Fischer, W.A., *Arc. Eisenhüttenw*., **46**(1975, 297-302 **ref:64**

152 Worrel, W.L., *Trans. Met. Soc. AIME*, **233**(1965), 1173-7

153 Artemov, V.I., *Metally*, (1974)1, 3 **ref:154**

154 Bochova, L.V., Tsemekhman, L.Sh., Burylev, B.P., Pavlinova, L.A. & Morozova, L.F., *Izvest Akad. Nauk. SSSR*, *Metally*, (1986)2, 17-22

155 Shevtsov, V.E., *Izvest.Akad.Nauk.SSSR, Metally*, (1979)2, 71-4

156 Ma, Z. & Janke, D., *Steel research*, **70**(1999)10, 395-402

157 Laag, T., Ohser, J. & Janke, D., *Steel research*, **68**(1997)8, 341-4

# 12 APPENDIX. THERMODYNAMIC DATA

```
GAS
     G(GAS,CO;0) = +F2598T+R*T*LN(1E-05*P)
     G(GAS,CO2;0) = +F2608T+R*T*LN(1E-05*P)
     G(GAS,O2;0) = +GHSEROO+RTLNP


LIQUID
     G(LIQUID,C;0) = +117369-24.63*T+GHSERCC
     G(LIQUID,CR;0) = +GCRLIQ
     G(LIQUID,CR2/3O;0) = -349024.67+86.92567*T-1.3237067*T*LN(T)
          +.66666667*GCRLIQ+.5*GHSEROO
     G(LIQUID,FE;0) = +GFELIQ
     G(LIQUID,FEO;0) = -274550.4+449.282*T-74.363*T*LN(T)
     G(LIQUID,FEO3/2;0) = -433945+603.837*T-93.18525*T*LN(T)
     G(LIQUID,NI;0) = +GNILIQ
     G(LIQUID,NIO;0) = -201172.8+88.303*T-2.17898*T*LN(T)+GNILIQ+.5*GHSEROO
     L(LIQUID,C,CR;0) = -90526-25.9116*T
     L(LIQUID,C,CR;1) = 80000
     L(LIQUID,C,CR;2) = 80000
     L(LIQUID,C,CR,FE;0) = -496063
     L(LIQUID,C,CR,FE;1) = 57990
     L(LIQUID,C,CR,FE;2) = 61404
     L(LIQUID,C,FE;0) = -124320+28.5*T
     L(LIQUID,C,FE;1) = 19300
     L(LIQUID,C,FE;2) = +49260-19*T
     L(LIQUID,C,FE,NI;0) = +122200-58.8*T
     L(LIQUID,C,FE,NI;1) = +92200-58.8*T
     L(LIQUID,C,FE,NI;2) = +152200-58.8*T
     L(LIQUID,C,NI;0) = -111479+35.2685*T
     L(LIQUID,C,NI,NIO;0) = -1520323.47
     L(LIQUID,C,NI,NIO;1) = -4216172.34
     L(LIQUID,C,NI,NIO;2) = 4130732.78
     L(LIQUID,C,NIO;0) = 2481654.98
     L(LIQUID,C,NIO;1) = -1263008.08
     L(LIQUID,C,FEO;0) = -338280.519
     L(LIQUID,C,FEO;1) = -274890.49
     L(LIQUID,CR,FEO3/2;0) = 110000
     L(LIQUID,CR,CR2/3O;0) = +133892.3-54.1515*T
     L(LIQUID,CR,CR2/3O;1) = +77153.7-15.4023*T
     L(LIQUID,CR,CR2/3O;2) = -139752.9+60.2735*T
     L(LIQUID,CR,CR2/3O,NI;0) = -164288.559
     L(LIQUID,CR,FE;0) = -14550+6.65*T
     L(LIQUID,CR,FE,NI;0) = 14510
     L(LIQUID,CR,FE,NI;1) = 11977
     L(LIQUID,CR,FE,NI;2) = 5147
     L(LIQUID,CR,NI;0) = +318-7.3318*T
     L(LIQUID,CR,NI;1) = +16941-6.3696*T
     L(LIQUID,CR,NIO;0) = -141604.059
     L(LIQUID,CR,FEO;0) = -20345.551
     L(LIQUID,CR2/3O,FE;0) = 118897.9
     L(LIQUID,CR2/3O,NI;0) = 121951.851
     L(LIQUID,CR2/3O,FEO;0) = 10000
     L(LIQUID,FE,FEO;0) = +88340.5-8.184*T
     L(LIQUID,FE,FEO;1) = +32827.5-15.4345*T
     L(LIQUID,FE,FEO3/2;0) = 110000
```

```
      L(LIQUID,FE,NI;0) = -18378.86+6.03912*T
      L(LIQUID,FE,NI;1) = +9228.1-3.54642*T
      L(LIQUID,FE,NIO;0) = 123778.83
      L(LIQUID,FEO,FEO3/2;0) = -13181
      L(LIQUID,FEO,FEO3/2;1) = 6676.5
      L(LIQUID,FEO,NI;0) = 78655.777
      L(LIQUID,FEO3/2,NI;0) = 110000
      L(LIQUID,NI,NIO;0) = +88355.5-25.1143*T
      L(LIQUID,NI,NIO;1) = -11457.4
      L(LIQUID,NI,NIO;2) = 21039.8


 BCC_A2
      G(BCC_A2,CR:C;0) = +GHSERCR+3*GHSERCC+GPCRBCC +416000
      G(BCC_A2,FE:C;0)= +322050+75.667*T+GHSERFE+GPFEBCC+3*GHSERCC
      G(BCC_A2,NI:C;0) = +400000-100*T+GHSERNI+3*GHSERCC
      G(BCC_A2,CR:O;0) = +GHSERCR+3*GOSOL
      G(BCC_A2,FE:O;0) = +GHSERFE+3*GOSOL
      G(BCC_A2,NI:O;0) = +GNIBCC+3*GOSOL
      G(BCC_A2,CR:VA;0) = +GHSERCR+GPCRBCC
      G(BCC_A2,FE:VA;0)= +GHSERFE+GPFEBCC
      G(BCC_A2,NI:VA;0) =    +GNIBCC
      L(BCC_A2,CR,FE:C;0) = -1250000+667.7*T
      TC(BCC_A2,CR:C;0) = -311.5
      TC(BCC_A2,CR,FE:C;0) = 1650
      TC(BCC_A2,CR,FE:C;1) = 550
      TC(BCC_A2,CR,NI:C;0) =    2373
      TC(BCC_A2,CR,NI:C;1) =    617
      TC(BCC_A2,FE:C;0) = 1043
      TC(BCC_A2,NI:C;0) = 575
      TC(BCC_A2,CR:VA;0) = -311.5
      TC(BCC_A2,FE:VA;0) = 1043
      TC(BCC_A2,NI:VA;0) =   575
      BMAGN(BCC_A2,FE:C;0) = 2.22
      BMAGN(BCC_A2,CR,NI:C;0) = 4
      BMAGN(BCC_A2,CR:C;0) = -.008
      BMAGN(BCC_A2,NI:C;0) = .85
      BMAGN(BCC_A2,CR:VA;0) = -.01
      BMAGN(BCC_A2,FE:VA;0) = 2.22
      BMAGN(BCC_A2,NI:VA;0) =   .85
      BMAGN(BCC_A2,CR,FE:C;0) = -.85
      L(BCC_A2,CR:C,VA;0) = -190*T
      L(BCC_A2,FE,NI:C;0) = -956.63-1.28726*T
      L(BCC_A2,FE,NI:C;1) = +1789.03-1.92912*T
      L(BCC_A2,FE:C,VA;0) = -190*T
      L(BCC_A2,CR:O,VA;0) = -673435+27.86*T
      L(BCC_A2,FE:O,VA;0) = -517549+71.83*T
      L(BCC_A2,CR,NI:VA;0) = +17170-11.8199*T
      L(BCC_A2,CR,NI:VA;1) = +34418-11.8577*T
      TC(BCC_A2,CR,NI:VA;0) = 2373
      TC(BCC_A2,CR,NI:VA;1) = 617
      BMAGN(BCC_A2,CR,NI:VA;0) = 4
      L(BCC_A2,CR,FE:VA;0) = +20500-9.68*T
      BMAGN(BCC_A2,CR,FE:VA;0) = -.85
      TC(BCC_A2,CR,FE:VA;0) = 1650
      TC(BCC_A2,CR,FE:VA;1) = 550
      L(BCC_A2,FE,NI:VA;0) = -956.63-1.28726*T
      L(BCC_A2,FE,NI:VA;1) = +1789.03-1.92912*T
```

```
 CEMENTITE
      G(CEMENTITE,CR:C;0) = +3*GHSERCR+GHSERCC-48000-9.2888*T
      G(CEMENTITE,FE:C;0) = +GFECEM
      G(CEMENTITE,NI:C;0) = +3*GHSERNI+GHSERCC+34700-20*T
      L(CEMENTITE,CR,FE:C;0) = +25278-17.5*T
      L(CEMENTITE,CR,FE,NI:C;0) = 60000
      L(CEMENTITE,CR,NI:C;0) = 27898
      L(CEMENTITE,FE,NI:C;0) = 29400


 CORUNDUM
      G(CORUNDUM,CR+2:CR+3:O-2;0) = +665910+GCR2O3
      G(CORUNDUM,CR+3:CR+3:O-2;0) = +GCR2O3-232227.2+241.3793*T
      G(CORUNDUM,FE+3:CR+3:O-2;0) = -232227.2+241.3793*T+.33333*GCR2O3
           +.66666*GFE2O3
      G(CORUNDUM,CR+2:NI+2:O-2;0) = +665910+GCR2O3
      G(CORUNDUM,CR+3:NI+2:O-2;0) = +GCR2O3+28048.1+54.4*T
      G(CORUNDUM,FE+3:NI+2:O-2;0)= 0.0
      G(CORUNDUM,CR+2:VA:O-2;0)= +GCR2O3
      G(CORUNDUM,CR+3:VA:O-2;0) = +GCR2O3
      G(CORUNDUM,FE+3:VA:O-2;0)= +GFE2O3
      TC(CORUNDUM,CR+3:VA:O-2;0) = -918
      TC(CORUNDUM,CR+2:VA:O-2;0) = -918
      TC(CORUNDUM,CR+3:NI+2:O-2;0) = 306
      TC(CORUNDUM,CR+2:NI+2:O-2;0) = 306
      TC(CORUNDUM,CR+3:CR+3:O-2;0) = -918
      TC(CORUNDUM,CR+2:CR+3:O-2;0) = -918
      TC(CORUNDUM,FE+3:VA:O-2;0) = -2867
      BMAGN(CORUNDUM,CR+3:VA:O-2;0) = -5.814
      BMAGN(CORUNDUM,CR+2:VA:O-2;0) = -5.814
      BMAGN(CORUNDUM,CR+3:NI+2:O-2;0) = .237
      BMAGN(CORUNDUM,CR+2:NI+2:O-2;0) = .237
      BMAGN(CORUNDUM,CR+3:CR+3:O-2;0) = -5.814
      BMAGN(CORUNDUM,CR+2:CR+3:O-2;0) = -5.814
      BMAGN(CORUNDUM,FE+3:VA:O-2;0) = -25.1

FCC_A1
      G(FCC_A1,CR:C;0) = +GHSERCR+GHSERCC+1200-1.94*T
      G(FCC_A1,FE:C;0) = +77207-15.877*T+GFEFCC+GHSERCC
      G(FCC_A1,NI:C;0) = +GHSERNI+GHSERCC+62000-7.6*T
      G(FCC_A1,CR:O;0) = +GPCRBCC+GCRFCC+GOSOL
      G(FCC_A1,FE:O;0) = +GFEFCC+GOSOL
      G(FCC_A1,NI:O;0) = +GHSERNI+GOSOL
      G(FCC_A1,CR:VA;0) = +GCRFCC+GPCRBCC
      G(FCC_A1,FE:VA;0) = +GFEFCC+GPFEFCC
      G(FCC_A1,NI:VA;0) = +GHSERNI
      TC(FCC_A1,FE:VA;0) = -201
      TC(FCC_A1,CR:VA;0) = -1109
      TC(FCC_A1,NI:C;0) = 633
      TC(FCC_A1,FE:C;0) = -201
      TC(FCC_A1,NI:VA;0) =    633
      BMAGN(FCC_A1,FE:VA;0) = -2.1
      BMAGN(FCC_A1,CR:VA;0) = -2.46
      BMAGN(FCC_A1,NI:C;0) = .52
      BMAGN(FCC_A1,FE:C;0) = -2.1
      BMAGN(FCC_A1,NI:VA;0) =    .52
      L(FCC_A1,CR,FE:C;0) = -74319+3.2353*T
      L(FCC_A1,CR,NI:C;0) = -125935+95*T
```

```
      L(FCC_A1,CR:C,VA;0) = -11977+6.8194*T
      L(FCC_A1,FE,NI:C;0) = +49074-7.32*T
      L(FCC_A1,FE,NI:C;1) = -25800
      L(FCC_A1,FE:C,VA;0) = -34671
      L(FCC_A1,NI:C,VA;0) = -14902+7.5*T
      L(FCC_A1,FE:O,VA;0) = -168758+19.17*T
      L(FCC_A1,NI:O,VA;0) = -165608+32.24*T
      L(FCC_A1,CR,NI:VA;0) = +8030-12.8801*T
      L(FCC_A1,CR,NI:VA;1) = +33080-16.0362*T
      L(FCC_A1,CR,FE:VA;0) = +10833-7.477*T
      L(FCC_A1,CR,FE:VA;1) = 1410
      L(FCC_A1,FE,NI:VA;0) = -12054.355+3.27413*T
      L(FCC_A1,FE,NI:VA;1) = +11082.1315-4.45077*T
      L(FCC_A1,FE,NI:VA;2) = -725.805174
      TC(FCC_A1,FE,NI:VA;0) = 2133
      TC(FCC_A1,FE,NI:VA;1) = -682
      TC(FCC_A1,CR,NI:C;0) =    3605
      TC(FCC_A1,CR,NI:VA;0) = -3605
      BMAGN(FCC_A1,CR,NI:VA;0) = -1.91
      BMAGN(FCC_A1,CR,NI:C;0) =    -1.91
      BMAGN(FCC_A1,FE,NI:VA;0) = 9.55
      BMAGN(FCC_A1,FE,NI:VA;1) = 7.23
      BMAGN(FCC_A1,FE,NI:VA;2) = 5.93
      BMAGN(FCC_A1,FE,NI:VA;3) = 6.18


 GRAPHITE
      G(GRAPHITE,C;0) = +GHSERCC


 HALITE
      G(HALITE,CR+3:O-2;0) = -140288.1-519.3911*T+57.1626*T*LN(T)+GNIO
      G(HALITE,FE+2:O-2;0) = +GWUSTITE
      G(HALITE,FE+3:O-2;0) = +1.25*AWUSTITE+1.25*GWUSTITE
      G(HALITE,NI+2:O-2;0) = +GNIO
      G(HALITE,NI+3:O-2;0) = +132919.5-64.8855*T+GNIO
      G(HALITE,VA:O-2;0) = 0.0
      TC(HALITE,CR+3:O-2;0) = 519
      TC(HALITE,NI+2:O-2;0) = 519
      TC(HALITE,NI+3:O-2;0) = 519
      BMAGN(HALITE,CR+3:O-2;0) = .9873
      BMAGN(HALITE,NI+2:O-2;0) = .9873
      BMAGN(HALITE,NI+3:O-2;0) = .9873
      L(HALITE,CR+3,FE+2:O-2;0) = -106261.25+64.162113*T
      L(HALITE,CR+3,FE+3:O-2;0) = -283545.67+151.647*T
      L(HALITE,FE+2,FE+3:O-2;0) = -12324.4
      L(HALITE,FE+2,FE+3:O-2;1) = 20070
      L(HALITE,FE+2,NI+2:O-2;0) = -21995.7281+19.7411922*T
      L(HALITE,FE+2,NI+2:O-2;1) = -3335.37286
      L(HALITE,FE+3,NI+2:O-2;0) = 64792.4377


M23C6
      G(M23C6,CR:CR:C;0) = +GCRM23C6
      G(M23C6,FE:CR:C;0)= +.1304348*GCRM23C6+.8695652*GFEM23C6
      G(M23C6,NI:CR:C;0) = +.8695652*GNIM23C6+.1304348*GCRM23C6
      G(M23C6,CR:FE:C;0) = +.8695652*GCRM23C6+.1304348*GFEM23C6
      G(M23C6,FE:FE:C;0) = +GFEM23C6
      G(M23C6,NI:FE:C;0) = +.8695652*GNIM23C6+.1304348*GFEM23C6
      G(M23C6,CR:NI:C;0) = +.8695652*GCRM23C6+.1304348*GNIM23C6
      G(M23C6,FE:NI:C;0) = +.8695652*GFEM23C6+.1304348*GNIM23C6
```

```
     G(M23C6,NI:NI:C;0) = +GNIM23C6
     L(M23C6,CR,FE:CR:C;0) = -205342+141.6667*T
     L(M23C6,CR,FE,NI:CR:C;0) = -460000
     L(M23C6,CR,NI:CR:C;0) = 100000
     L(M23C6,FE,NI:CR:C;0) = 196000
     L(M23C6,CR,FE:FE:C;0) = -205342+141.6667*T
     L(M23C6,CR,FE,NI:FE:C;0) = -460000
     L(M23C6,CR,NI:FE:C;0) = 100000
     L(M23C6,FE,NI:FE:C;0) = 196000
     L(M23C6,CR,FE:NI:C;0) = -205342+141.6667*T
     L(M23C6,CR,FE,NI:NI:C;0) = -460000
     L(M23C6,CR,NI:NI:C;0) = 100000
     L(M23C6,FE,NI:NI:C;0) = 196000


M3C2
     G(M3C2,CR:C;0) = +GCRM3C2


M5C2
     G(M5C2,FE:C;0) = +5*GHSERFE+2*GHSERCC+54852-33.7518*T


M7C3
     G(M7C3,CR:C;0) = +GCRM7C3
     G(M7C3,FE:C;0) = +7*GHSERFE+3*GHSERCC+75000-48.2168*T
     G(M7C3,NI:C;0) = +7*GHSERNI+3*GHSERCC+107130-36.605*T
     L(M7C3,CR,FE:C;0) = -4520-10*T
     L(M7C3,CR,NI:C;0) = 100000
     L(M7C3,FE,NI:C;0) = 68600


SIGMA
     G(SIGMA,FE:CR:CR;0) = +8*GFEFCC+22*GHSERCR+92300-95.96*T+GPSIG1
     G(SIGMA,NI:CR:CR;0) = +8*GHSERNI+22*GHSERCR+221157-227*T
     G(SIGMA,FE:CR:FE;0) = +8*GFEFCC+4*GHSERCR+18*GHSERFE+117300-95.96*T+GPSIG2
     G(SIGMA,NI:CR:FE;0) = +8*GHSERNI+4*GHSERCR+18*GHSERFE
     G(SIGMA,FE:CR:NI;0) = +8*GFEFCC+4*GHSERCR+18*GNIBCC
     G(SIGMA,NI:CR:NI;0) = +8*GHSERNI+4*GHSERCR+18*GNIBCC+175400


SPINEL
     G(SPINEL,CR+2:CR+3:FE+2:O-2;0) = +10.5*FSPIN-3.5*GFE3O4-1.5*BFE3O4+RSPIN
               +SSPIN+DFE3O4
     G(SPINEL,CR+3:CR+3:FE+2:O-2;0) = +10.5*FSPIN-1.5*GFE3O4+DFE3O4
          -1.5*BFE3O4+RSPIN
     G(SPINEL,FE+2:CR+3:FE+2:O-2;0) = +7*FSPIN+2*GFE3O4+DFE3O4-BFE3O4
     G(SPINEL,FE+3:CR+3:FE+2:O-2;0) = +7*FSPIN+2*GFE3O4+DFE3O4-2*BFE3O4
     G(SPINEL,NI+2:CR+3:FE+2:O-2;0) = +10.5*GCR2FEO4+21*GNISP-15.5*GFE3O4
             -7*GNICR2O4-BNISP-.5*BCR2FEO4+.5*BFE3O4+DFE3O4
     G(SPINEL,CR+2:FE+2:FE+2:O-2;0)= +3.5*FSPIN+5.5*GFE3O4-.5*BFE3O4
          +RSPIN+SSPIN+DFE3O4
     G(SPINEL,CR+3:FE+2:FE+2:O-2;0) = +3.5*FSPIN+5.5*GFE3O4+RSPIN
          -.5*BFE3O4+DFE3O4
     G(SPINEL,FE+2:FE+2:FE+2:O-2;0) = +9*GFE3O4+DFE3O4
     G(SPINEL,FE+3:FE+2:FE+2:O-2;0) = +9*GFE3O4+DFE3O4-BFE3O4
     G(SPINEL,NI+2:FE+2:FE+2:O-2;0) = +7*GNISP+2*GFE3O4+DFE3O4
     G(SPINEL,CR+2:FE+3:FE+2:O-2;0) = +3.5*FSPIN+5.5*GFE3O4-1.5*BFE3O4
          +RSPIN+SSPIN+DFE3O4
     G(SPINEL,CR+3:FE+3:FE+2:O-2;0) = +3.5*FSPIN+5.5*GFE3O4+RSPIN
          -1.5*BFE3O4+DFE3O4
```

```
G(SPINEL,FE+2:FE+3:FE+2:O-2;0) = +9*GFE3O4+DFE3O4-BFE3O4
G(SPINEL,FE+3:FE+3:FE+2:O-2;0) = +9*GFE3O4+DFE3O4-2*BFE3O4
G(SPINEL,NI+2:FE+3:FE+2:O-2;0) = +7*GNISP+2*GFE3O4+DFE3O4-BFE3O4
G(SPINEL,CR+3:NI+2:FE+2:O-2;0) = +7*GNICR2O4+2*GFE3O4+DFE3O4-BFE3O4
G(SPINEL,FE+2:NI+2:FE+2:O-2;0) = +14*GNISP-BNISP-5*GFE3O4+BFE3O4+DFE3O4
G(SPINEL,FE+3:NI+2:FE+2:O-2;0) = +14*GNISP-BNISP-5*GFE3O4+DFE3O4
G(SPINEL,NI+2:NI+2:FE+2:O-2;0) = +21*GNISP-BNISP-12*GFE3O4+DFE3O4
G(SPINEL,CR+2:VA:FE+2:O-2;0)= +3.5*FSPIN+3.5*GFE3O4-1.5*BFE3O4+RSPIN
     +SSPIN+CFE3O4+DFE3O4
G(SPINEL,CR+3:VA:FE+2:O-2;0)= +3.5*FSPIN+3.5*GFE3O4+RSPIN-1.5*BFE3O4
     +DFE3O4+CFE3O4
G(SPINEL,FE+2:VA:FE+2:O-2;0) = +7*GFE3O4+DFE3O4+CFE3O4-BFE3O4
G(SPINEL,FE+3:VA:FE+2:O-2;0) = +7*GFE3O4+DFE3O4+CFE3O4-2*BFE3O4
G(SPINEL,NI+2:VA:FE+2:O-2;0) = +7*GNISP+DFE3O4+CFE3O4-BFE3O4
G(SPINEL,CR+2:CR+3:VA:O-2;0) = +10.5*FSPIN-3.5*GFE3O4-.5*BFE3O4+RSPIN
     +SSPIN
G(SPINEL,CR+3:CR+3:VA:O-2;0) = +10.5*FSPIN-3.5*GFE3O4+RSPIN-.5*BFE3O4
G(SPINEL,FE+2:CR+3:VA:O-2;0) = +7*FSPIN
G(SPINEL,FE+3:CR+3:VA:O-2;0) = +7*FSPIN-BFE3O4
G(SPINEL,NI+2:CR+3:VA:O-2;0) = +GNICR2O4
G(SPINEL,CR+2:FE+2:VA:O-2;0) = +3.5*FSPIN+3.5*GFE3O4+.5*BFE3O4+RSPIN
     +SSPIN
G(SPINEL,CR+3:FE+2:VA:O-2;0) = +3.5*FSPIN+3.5*GFE3O4+RSPIN+.5*BFE3O4
G(SPINEL,FE+2:FE+2:VA:O-2;0) = +7*GFE3O4+BFE3O4
G(SPINEL,FE+3:FE+2:VA:O-2;0)= +7*GFE3O4
G(SPINEL,NI+2:FE+2:VA:O-2;0) = +7*GNISP+BFE3O4
G(SPINEL,CR+2:FE+3:VA:O-2;0) = +3.5*FSPIN+3.5*GFE3O4-.5*BFE3O4+RSPIN+SSPIN
G(SPINEL,CR+3:FE+3:VA:O-2;0) = +3.5*FSPIN+3.5*GFE3O4+RSPIN-.5*BFE3O4
G(SPINEL,FE+2:FE+3:VA:O-2;0) = +7*GFE3O4
G(SPINEL,FE+3:FE+3:VA:O-2;0) = +7*GFE3O4-BFE3O4
G(SPINEL,NI+2:FE+3:VA:O-2;0) = +7*GNISP
G(SPINEL,CR+2:NI+2:VA:O-2;0) = +10.5*FSPIN+21*GFE2NIO4-17*GFE3O4
     -GNICR2O4-BFE2NIO4-.5*RSPIN+1.5*BFE3O4+SSPIN
G(SPINEL,CR+3:NI+2:VA:O-2;0) = +10.5*GCR2FEO4+21*GFE2NIO4-17*GFE3O4
     -GNICR2O4-BFE2NIO4-.5*BCR2FEO4+1.5*BFE3O4
G(SPINEL,FE+2:NI+2:VA:O-2;0) = +14*GNISP-BNISP-7*GFE3O4+2*BFE3O4
G(SPINEL,FE+3:NI+2:VA:O-2;0) = +14*GNISP-BNISP-7*GFE3O4+BFE3O4
G(SPINEL,NI+2:NI+2:VA:O-2;0) = +21*GFE2NIO4-14*GFE3O4-BFE2NIO4+2*BFE3O4
G(SPINEL,CR+2:VA:VA:O-2;0)= +3.5*FSPIN+1.5*GFE3O4-.5*BFE3O4+RSPIN+SSPIN
       +CFE3O4
G(SPINEL,CR+3:VA:VA:O-2;0)= +3.5*FSPIN+1.5*GFE3O4+RSPIN-.5*BFE3O4+CFE3O4
G(SPINEL,FE+2:VA:VA:O-2;0) = +5*GFE3O4+CFE3O4
G(SPINEL,FE+3:VA:VA:O-2;0)= +5*GFE3O4+CFE3O4-BFE3O4
G(SPINEL,NI+2:VA:VA:O-2;0)= +7*GFE2NIO4-2*GFE3O4+CFE3O4
L(SPINEL,CR+2,NI+2:CR+3:VA:O-2;0) = 100000
L(SPINEL,CR+2:CR+3,NI+2:VA:O-2;0) = 1000000
L(SPINEL,CR+3,FE+2:CR+3:VA:O-2;0) = 20000
L(SPINEL,FE+2:CR+3,FE+2:VA:O-2;0) = +152380-60*T
L(SPINEL,FE+2:CR+3,FE+3:VA:O-2;0) = -24942+28.5714*T
L(SPINEL,FE+2:CR+3,VA:VA:O-2;0) = 5000
L(SPINEL,FE+2:CR+3,VA:VA:O-2;1) = 150000
L(SPINEL,FE+3:CR+3,FE+2:VA:O-2;0) = +152380-60*T
L(SPINEL,FE+3:CR+3,VA:VA:O-2;0) = 5000
L(SPINEL,FE+3:CR+3,VA:VA:O-2;1) = 150000
L(SPINEL,CR+3,FE+2:FE+2:VA:O-2;0) = 20000
L(SPINEL,FE+3:FE+2,NI+2:VA:O-2;0) = 29422.554
L(SPINEL,FE+3:FE+2,NI+2:VA:O-2;1) = -63932.452
L(SPINEL,CR+3,FE+2:FE+3:VA:O-2;0) = 20000
L(SPINEL,FE+2,NI+2:FE+3:VA:O-2;0) = 29422.554
L(SPINEL,FE+2,NI+2:FE+3:VA:O-2;1) = -63932.452
L(SPINEL,CR+3,FE+2:VA:VA:O-2;0) = 20000
```

```
For compounds containing only Fe as metal specie
      TC(SPINEL,X:X:X:O;0) = 848
      BMAGN(SPINEL,X:X:X:O:0) = 44.54
For compounds containing only Fe and Cr as metal specie
      TC(SPINEL,X:X:X:O;0) = 100
      BMAGN(SPINEL,X:X:X:O:0) = 0.9
For all other compounds
      TC(SPINEL,X:X:X:O;0) = 0
      BMAGN(SPINEL,X:X:X:O:0) =  0


Symbols defined for the system:
GHSEROO
       298.14<T< 1000.00: -6961.74451-76729.7484*T**(-1)-51.0057202*T
     -22.2710136*T*LN(T)-.0101977469*T**2+1.32369208E-06*T**3
       1000.00<T< 3300.00: -13137.5203+525809.556*T**(-1)+25.3200332*T
     -33.627603*T*LN(T)-.00119159274*T**2+1.35611111E-08*T**3
       3300.00<T< 6000.00: -27973.4908+8766421.4*T**(-1)+62.5195726*T
     -37.9072074*T*LN(T)-8.50483772E-04*T**2+2.14409777E-08*T**3
GHSERCR
       298.14<T< 2180.00: -8851.93+157.48*T-26.908*T*LN(T)+.00189435*T**2
     -1.47721E-06*T**3+139250*T**(-1)
       2180.00<T< 6000.00: -34864+344.18*T-50*T*LN(T)-2.88526E+32*T**(-9)
GPCRLIQ  = 0.0
GCRLIQ
       298.13<T< 2180.00: +24335.93-11.42*T+GHSERCR+2.37615E-21*T**7
       2180.00<T< 6000.00: +18405-8.562*T+GHSERCR+2.88526E+32*T**(-9)
GHSERNI
       298.14<T< 1728.00: -5179.159+117.854*T-22.096*T*LN(T)-.0048407*T**2
       1728.00<T< 3000.00: -27840.655+279.135*T-43.1*T*LN(T)
     +1.12754E+31*T**(-9)
GNILIQ
       298.14<T< 1728.00: +16414.686-9.397*T+GHSERNI-3.82318E-21*T**7
       1728.00<T< 3000.00: +18290.88-10.537*T+GHSERNI-1.12754E+31*T**(-9)
GPCRBCC   = 0.0
GNIBCC   =  +8715.084-3.556*T+GHSERNI
GCRFCC  = +7284+.163*T+GHSERCR
GHSERFE
       298.14<T< 1811.00: +1224.83+124.134*T-23.5143*T*LN(T)-.00439752*T**2
     -5.8927E-08*T**3+77359*T**(-1)
       1811.00<T< 6000.00: -25384.451+299.31255*T-46*T*LN(T)
     +2.29603E+31*T**(-9)
GPFELIQ   =  0.0
GFEOLIQ
       298.13<T< 3000.00: -137387+225.42*T-37.2741*T*LN(T)
GFELIQ
       298.13<T< 1811.00: +12040.17-6.55843*T-3.6751551E-21*T**7+GHSERFE
       1811.00<T< 6000.00: -10839.7+291.302*T-46*T*LN(T)
GPFEBCC   =  0.0
GFEFCC
       298.14<T< 1811.00: -1462.4+8.282*T-1.15*T*LN(T)+6.4E-04*T**2+GHSERFE
       1811.00<T< 6000.00: -27098.266+300.25256*T-46*T*LN(T)
     +2.78854E+31*T**(-9)
GPFEFCC  =  0.0
GNIO
       298.14<T< 1000.00: -254927.2+276.208*T-46.0391*T*LN(T)-.00931454*T**2
     +1.29092E-06*T**3+382916*T**(-1)
       1000.00<T< 1800.00: -256835.2+340.043*T-56.36068*T*LN(T)
     +.00254106*T**2-8.11809E-07*T**3+1270*T**(-1)
       1800.00<T< 2600.00: -259131.4+337.305*T-55.75758*T*LN(T)
     +.00220246*T**2-7.80093E-07*T**3
```

```
GCR2O3
       298.14<T< 1000.00: -1177233+809.1578*T-131.164*T*LN(T)+.00446534*T**2
     -1.25132E-06*T**3+1436443*T**(-1)
      1000.00<T< 2600.00: -1165910.7+692.4532*T-114.2843*T*LN(T)
     -.00671862*T**2+1.3801E-07*T**3+12489.5*T**(-1)
GNICR2O4
       298.14<T< 2600.00: -1442728.78+1005.1*T-167.1508*T*LN(T)
     -.00893284*T**2+1052276*T**(-1)
GWUSTITE
       298.13<T< 3000.00: -279318+252.848*T-46.12826*T*LN(T)-.0057402984*T**2
AWUSTITE
       298.13<T< 3000.00: -55384+27.888*T

GFE3O4
       298.13<T< 3000.00: -161731+144.873*T-24.9879*T*LN(T)-.0011952256*T**2
     +206520*T**(-1)
DFE3O4
       298.13<T< 3000.00: +402520-30.529*T
BFE3O4
       298.13<T< 3000.00: +46826-27.266*T
CFE3O4
       298.13<T< 3000.00: +120730-20.102*T
GFE2O3    = -858683+827.946*T-137.0089*T*LN(T)+1453810*T**(-1)
DSPIN   = +803771.23-4.0007951*T
CSPIN   = +80332958+16.289507*T
BSPIN   = -24566.924-12.308445*T
GFNISP  = -147220.123-16.6910152*T
GFE2NIO4
       298.14<T<  855.00: +GFNISP-20467.2552+400.448186*T-62.3120472*T*LN(T)
     +.0503445214*T**2+839636.684*T**(-1)-1.38076596E-05*T**3
       855.00<T< 6000.00: +GFNISP-10502.2653+201.453166*T-29.8108703*T*LN(T)
     +1.8807775E-04*T**2+210885.222*T**(-1)
BFE2NIO4  = +77674.4601+7.6682004*T
GFCRSPIN  = -194495.65-26.740014*T
GCR2FEO4  = +GFCRSPIN-8609.63051+159.470785*T-23.287*T*LN(T)
     -.00159592857*T**2+227728.571*T**(-1)
BCR2FEO4  = -315480
GNISP
       298.14<T<  855.00: +GFNISP-20467.2552+400.448186*T-62.3120472*T*LN(T)
     +.0503445214*T**2+839636.684*T**(-1)-1.38076596E-05*T**3
       855.00<T< 6000.00: +GFNISP-10502.2653+201.453166*T-29.8108703*T*LN(T)
     +1.8807775E-04*T**2+210885.222*T**(-1)
BNISP     = +77674.4601+7.6682004*T
F2598T
       298.14<T<  800.00: -118162.143-23.1823998*T-25.84624*T*LN(T)
     -.003281553*T**2-1.63612533E-07*T**3-55604.1*T**(-1)
       800.00<T< 2200.00: -122211.037+7.61017725*T-29.9366*T*LN(T)
     -.0027053115*T**2+1.75559167E-07*T**3+541480.5*T**(-1)
      2200.00<T< 6000.00: -131274.213+62.1198839*T-37.17593*T*LN(T)
     -1.020237E-04*T**2-6.44914833E-10*T**3+2724014*T**(-1)
F2608T
       298.14<T<  800.00: -404174.703-15.7853122*T-27.539*T*LN(T)
     -.02231934*T**2+3.00075833E-06*T**3+93853*T**(-1)
       800.00<T< 1800.00: -415639.498+121.517247*T-47.95575*T*LN(T)
     -.005779695*T**2+4.24028167E-07*T**3+1325131.5*T**(-1)
      1800.00<T< 4000.00: -430260.3+219.465874*T-61.1864*T*LN(T)
     -3.6174865E-04*T**2+2.80415833E-09*T**3+4427090.5*T**(-1)
      4000.00<T< 6000.00: -442257.546+259.307421*T-66.02645*T*LN(T)
     +4.887686E-04*T**2-2.47381833E-08*T**3+9866895*T**(-1)
GHSERCC  = -17368.441+170.73*T-24.3*T*LN(T)-4.723E-04*T**2
     +2562600*T**(-1)-2.643E+08*T**(-2)+1.2E+10*T**(-3)
```

```
GCRM23C6  = -521983+3622.24*T-620.965*T*LN(T)-.126431*T**2
GFECEM    = -10745+706.04*T-120.6*T*LN(T)
GFEM23C6  = +7.666667*GFECEM-1.666667*GHSERCC+66920-40*T
GNIM23C6  = +23*GHSERNI+6*GHSERCC+210000-84.71*T
GCRM3C2   = -100823.8+530.66989*T-89.6694*T*LN(T)-.0301188*T**2
GCRM7C3   = -201690+1103.128*T-190.177*T*LN(T)-.0578207*T**2
GPSIG1    = +1.09E-04*P
GPSIG2    = +1.117E-04*P
FSPIN     = -214607.7+138.83*T-23.28714*T*LN(T)-.001595929*T**2+227729.3*T**(-1)
RSPIN     20000000 +156000-3.37*T
SSPIN     = +46028.95+38.73173*T-11.58574*T*LN(T)+.006411774*T**2
GOSOL     = +.5*GHSEROO+65*T
```